



## Deliverable D4.1.5 – Innovations on component level for coming 20MW turbines

Agreement n.:	308974
Duration	November 2012 – October 2017
Co-ordinator:	DTU Wind

The research leading to these results has received funding from the European Community's Seventh Framework Programme FP7-ENERGY-2012-1-2STAGE under grant agreement No. 308974 (INNWIND.EU).



---

#### PROPRIETARY RIGHTS STATEMENT

This document contains information, which is proprietary to the "INNWIND.EU" Consortium. Neither this document nor the information contained herein shall be used, duplicated or communicated by any means to any third party, in whole or in parts, except with prior written consent of the "INNWIND.EU" consortium.

---

# Document information

Document Name:	<b>Deliverable D4.1.5. – Innovations on component level for coming 20MW turbines (final report)</b>
Document Number:	<b>Deliverable D 4.1.5 – Revision 0</b>
Author:	<b>Rogier Nijssen, Francisco Lahuerta (WMC) Wilfried Njomo Wandji, Anand Natarajan (DTU) Lars Bo Ibsen (AAU) Niklas Scholle, Luka Radulović (LUH) Martin Kohlmeier, Aligi Foglia (FhG-H) R. Shirzadeh, Martin Kühn (ForWind-UOL) S. Tiedemann, T. Fischer, D. Kaufer (RAW)</b>
Document Type	Report
Dissemination level	PU
Review:	<b>WP Leader</b>
Date:	<b>2016-09-30</b>
WP:	<b>4 Offshore Foundations and Support Structures</b>
Task:	<b>4.1 Innovations on component level for bottom-based structures</b>
Approval:	Approved by Author

## 1 TABLE OF CONTENTS

<b>1</b>	<b>TABLE OF CONTENTS .....</b>	<b>3</b>
<b>2</b>	<b>INTRODUCTION .....</b>	<b>6</b>
<b>2.1</b>	<b>References .....</b>	<b>7</b>
<b>3</b>	<b>INNOVATIVE MATERIALS (LUH, WMC).....</b>	<b>8</b>
<b>3.1</b>	<b>Sandwich material for tubes (LUH) .....</b>	<b>8</b>
3.1.1	Summary of main developments on component level for Task 4.1.3 and 4.1.4 .....	8
3.1.2	Applicability of developments on 20MW turbines.....	10
	Monopile support structure – Hybride tower .....	11
3.1.3	Technology Readiness Level and Recommendations.....	14
<b>3.2</b>	<b>Adhesives for tubular joints and sandwiches (WMC) .....</b>	<b>15</b>
3.2.1	Summary of main developments on component level from task 4.1.3 and 4.1.4 .....	15
	Test load direction .....	17
	Scale effects .....	17
	Bondline quality .....	17
	Quality of pre-treatment .....	19
	Test set-up effects .....	19
3.2.2	Applicability of developments on 20MW turbines .....	19
3.2.3	Main challenges and bottlenecks for the upscaling to 20 MW .....	20
3.2.4	Conclusion and impact of innovations for 20MW turbines .....	20
	Conclusions.....	20
3.2.5	Recommendations and further development needs .....	20
	Detailed finite element modeling of the hybrid joint tests .....	20
	More accurate and extensive fatigue data required .....	21
	Geometrical details .....	21
	Large thicknesses.....	21
	Development of monitoring techniques .....	21
	Mixed mode loading, fracture energy, including humidity .....	21
	Effect of voids .....	22
	Potential of different adhesive types, and preparation- and application methods .....	22
<b>3.3</b>	<b>References .....</b>	<b>23</b>
<b>4</b>	<b>Soil &amp; foundation (AAU, FHG-H).....</b>	<b>24</b>
<b>4.1</b>	<b>Soil pile interaction / axial pile loading (FHG-H).....</b>	<b>24</b>
4.1.1	Combining experiments and CPT methods to assess required geometry of vibro-driven piles	24
	Description of the experimental works.....	24
4.1.2	Presentation of the experimental results .....	26
	Interpretation of the ultimate resistance by means of the CPT methods .....	27
	Dimensions of the pile, vibro-driven vs. impact-driven.....	28
4.1.3	Numerical model for axially loaded piles in tension.....	29
4.1.4	Description of the model.....	29
4.1.5	Numerical analyses to assess the plausibility of the model.....	31
4.1.6	Conclusions .....	33

<b>4.2</b>	<b>References</b> .....	<b>35</b>
<b>5</b>	<b>LOAD MITIGATION (UOL, DTU)</b> .....	<b>36</b>
<b>5.1</b>	<b>LOAD MITIGATION (Forwind-UOL)</b> .....	<b>36</b>
5.1.1	Semi-active damping devices .....	36
	Magnetorheological damper .....	37
	Dynamic modeling of a MR damper .....	37
5.1.2	Description of the performed studies of the innovation .....	39
	Boundary conditions.....	39
	Mechanism to calculate the MR damper forces.....	39
5.1.3	Conclusion .....	41
<b>5.2</b>	<b>Development of magneto-rheological damper for jacket substructure for 20 MW wind turbines at 50 m water depths (DTU)</b> .....	<b>42</b>
5.2.1	Summary of main developments on component level from task 4.1.3: applicability of developments, main challenges, and bottlenecks for the upscaling to 20 MW .....	42
5.2.2	Reference 20MW wind turbine, jacket substructure, and environmental conditions .....	42
	Environmental conditions and aero-hydro-servo-elastic simulations .....	42
	20 MW reference wind turbine .....	43
	Jacket substructure .....	43
5.2.3	Magneto-rheological damper device .....	44
	Physical description and mathematical modeling.....	44
	Operational conditions and control strategy .....	46
	Application on jacket and installation process .....	46
5.2.4	Simulations and results .....	47
	Fatigue calculations .....	47
	Reference case and brace selection .....	49
	Efficiency of a double MR damper inserted in one brace .....	50
	Efficiency of four pairs MR dampers .....	51
	Energy balance .....	52
5.2.5	Conclusion and impact of innovations for 20 MW turbines .....	53
<b>5.3</b>	<b>References</b> .....	<b>54</b>
<b>6</b>	<b>MANUFACTURING (RAW)</b> .....	<b>56</b>
<b>6.1</b>	<b>Introduction</b> .....	<b>56</b>
<b>6.2</b>	<b>Manufacturing</b> .....	<b>56</b>
6.2.1	Jacket assembly strategies and manufacturing costs .....	56
6.2.2	Current jacket design .....	56
6.2.3	Modular jacket design.....	57
<b>6.3</b>	<b>Assumptions for Transportation and Installation</b> .....	<b>58</b>
6.3.1	Dimensions of the Jacket.....	58
6.3.2	Environmental Conditions.....	58
6.3.3	Port and harbor requirements .....	60
6.3.4	Installation cost model.....	60
6.3.5	Vessel costs .....	61
	Transportation costs.....	61
	Installation costs.....	61
	Downtime costs .....	61

<b>6.4</b>	<b>Assessment of installation concepts.....</b>	<b>62</b>
6.4.1	Sheerleg crane .....	63
	Transportation and installation procedure.....	63
	Assumed maximum sea state.....	64
	Time consumption .....	65
6.4.2	Heavy lift vessel.....	65
	Transportation and installation procedure.....	66
	Assumed maximum sea state.....	66
	Time consumption .....	67
6.4.3	Jack-up vessel .....	67
	Transportation and installation procedure.....	68
	Assumed maximum sea state.....	68
	Time consumption .....	69
6.4.4	U-barge.....	69
	Transportation and installation procedure.....	70
	Assumed maximum sea state.....	71
	Time consumption .....	72
6.4.5	Additional concepts.....	72
<b>6.5</b>	<b>Analysis of time consumption and installation costs .....</b>	<b>73</b>
6.5.1	Analysis of time consumption.....	73
6.5.2	Analysis of installation costs.....	74
<b>6.6</b>	<b>Evaluation and conclusion .....</b>	<b>75</b>
6.6.1	Evaluation matrix.....	75
6.6.2	Conclusion .....	76
<b>6.7</b>	<b>References.....</b>	<b>77</b>
	<b>Appendix A.....</b>	<b>78</b>

## 2 INTRODUCTION

Levelised cost of energy (LCOE) is one of the main decision drivers for or against offshore wind exploitation. Recent projects indicated actual LCOEs of around 165 € per MWh [2-01]. A reduction is highly desired, if not even necessary, for a further deployment of offshore wind energy. A study by the Crown Estate [2-01] indicates possible reduction up to under 100 € per MWh until 2020, which would be a reduction of 37.5%. Various fields were identified, which might contribute achieving this goal. Innovations regarding the support structure were one of those. Therefore, a reduction of investment costs of approximately 20% is aimed for the support structures during the course of this project [2-02] to significantly contribute to the realisation of the goal in LCOE reduction. Furthermore, risks and possibilities will be assessed.

The prospects of completely new concepts are expected to be minor, therefore the focus in Task 4.1. is on “Innovations on component level”. Relevant topics for future cost-effective, mass-producible designs were identified, such as new foundation types (without grout and/or piling), soil-structure-interaction of large piles or suction buckets, innovative transition piece designs or designs using hybrid materials never employed in wind energy before. In addition, design integration using jacket-specific controls and innovative fabrication and installation processes shall complete the overall cost saving potentials.

The following fields of interest, illustrated by Figure 2-1, are found in the sections of this report:

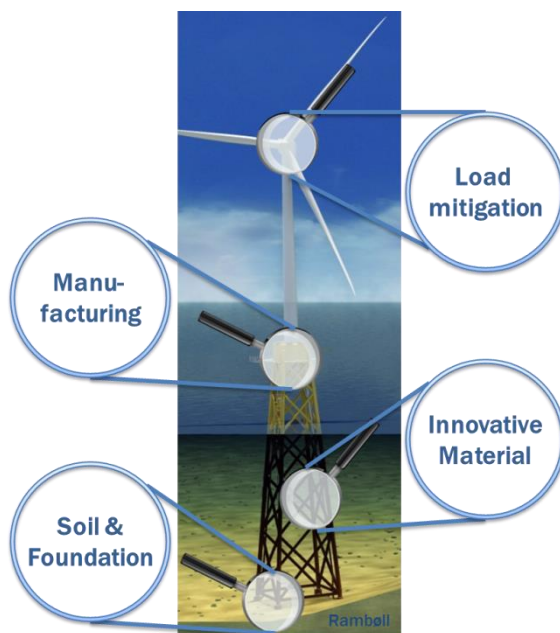


Figure 1 Subfields in Task 4.1.

### **Innovative materials:**

Hybrid materials, such as sandwich structures are introduced in section 3 by the partners Leibniz University of Hannover (LUH) and Knowledge Centre Wind turbine Materials and Constructions (WMC).

### **Soil & foundation:**

Improvements in the modelling and numerical simulation of the soil structure interaction as well as innovative support structure and foundation designs are treated in section 4 by the Fraunhofer Institute IWES Hannover (FhG-H), the Danish Technical University (DTU) and Aalborg University (AAU).

### **Load mitigation:**

Concepts for load mitigation, such as jacket-specific and structural control are investigated in section 5 by the Fraunhofer Institutes LBF Darmstadt (FhG-DA) and IWES Kassel (FhG-KS), as well as by the Danish Technical University (DTU) and ForWind Oldenburg (UOL).

### **Manufacturing:**

Rambøll (RAMBOLL) is focusing on innovations in manufacturing, mass-production and installation in section 6.

In INN WIND.EU’s task 4, innovations on component level are developed. In previous work in this task, these innovations were developed up to the 10 MW reference turbine scale. However, several absolutely new challenges will be faced when entering the 20MW class for which the current deliverable describes first solutions. The current report extends and applies the innovations on component level for the 10MW INN WIND.EU reference turbine for the new 20MW reference.

Following the innovations on component level, this report evaluates the necessary properties for application of sandwich tubular members and adhesive joining of these members, in chapter 3. Chapter 4 focuses on soil & foundations and covers the required developments in numerical and experimental methods. Introduction for piles and suction buckets, including their soil-structure interaction and innovative foundations. In Chapter 5, load mitigation methods will be described and the final chapter 6 will go into the manufacturing and installation of 20 MW turbines with these innovative solutions included.

## 2.1 References

- [2-01] The Crown Estate, "Offshore Wind Cost Reduction: Pathways Study", 2012.
- [2-02] InnWind.eu, "Annex I - "Description of Work"", Grant agreement no: 308974, 2012

### 3 INNOVATIVE MATERIALS (LUH, WMC)

#### 3.1 Sandwich material for tubes (LUH)

##### 3.1.1 Summary of main developments on component level for Task 4.1.3 and 4.1.4

To be suitable for use as structural components of supporting structures of OWT, sandwich tubes must have bearing capacity comparable to those of steel tubes. Considering that the present European and national codes are not fully covering this type of structural element, general methods for estimating the bearing capacity of different types of sandwich tubes developed in Keindorf [3-05] are presented in Deliverable 4.12 [3-02] and Deliverable 4.13 [3-03]. The outcomes of these methods applied to a 90 m high tower for wind turbines with an outer diameter of 5.5 m, constructed with different types of sandwich tube (Figure 2) was shown. Different types of core material (grout, elastomer, and concrete) and different steel grades (S235, S355, S460 and S690) of steel for the outer and inner face of sandwich tubes is used. The aim is to determine which combination of core material and steel grade would lead to the greatest benefits in terms of bearing capacity of the tower.

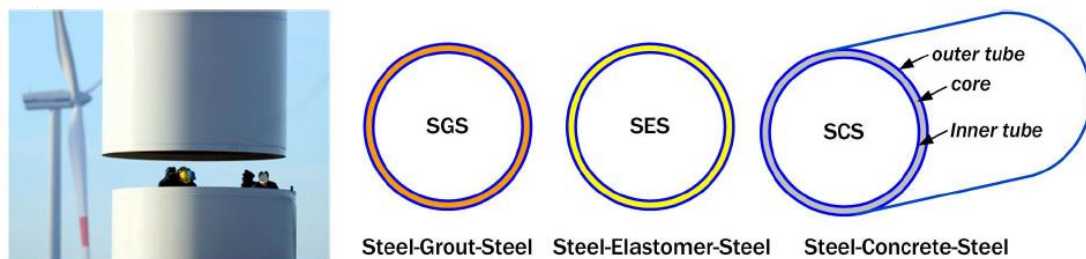


Figure 2 – Steel and different types of sandwich structures

The results of these investigations are summarised in Table 1, and Figure 3. A detailed description of the applied analytical methods and numerical models can be found in Deliverable 4.12 [3-02] and Deliverable 4.13 [3-03].

Table 1: Comparison of the axial load bearing capacity of steel and sandwich cylinders - [3-05]

Cross-section	Npl,Rk in [MN]			
	S235	S355	S460	S690
Steel type				
Steel thickness $t_{st}$ [mm]	50	32	24	16
ST	184 (100%)	190 (103%)	190 (104%)	190 (104%)
Layer thickness $t_{-1}/t_0/t_{+1}$ [mm]	24/80/2 4	16/80/1 6	12/80/1 2	8/80/8
SES ( $f_{ck,0} = 18$ MPa) - elastomer	207(112 %)	211 (107%)	211(115 %)	211 (115%)
SGS ( $f_{ck,0} = 100$ MPa) - grout	318 (173%)	322 (125%)	322 (175%)	322 (175%)
SCS ( $f_{ck,0} = 50$ MPa) - concrete	251 (136%)	255 (139%)	255 (139%)	255 (139%)

Table 2 Comparison of the plastic moment capacity of steel and sandwich cylinders -[3-05]

Cross-section	$M_{pl,Rk}$ [MNm]			
	S235	S355	S460	S690
Steel type	S235	S355	S460	S690
Steel thickness $t_{st}$ [mm]	50	32	24	16
ST	319 (100%)	330 (103%)	331 (104%)	332 (104%)
Layer thickness $t_{-1}/t_0/t_{+1}$ [mm]	24/80/2 4	16/80/1 6	12/80/1 2	8/80/8
SES ( $f_{ck,0} = 18$ MPa) - elastomer	331 (104%)	340 (107%)	341 (107%)	342 (107%)
SGS ( $f_{ck,0} = 100$ MPa) - grout	389 (122%)	399 (125%)	400 (125%)	402 (126%)
SCS ( $f_{ck,0} = 50$ MPa) - concrete	358 (112%)	368 (115%)	369 (116%)	370 (116%)

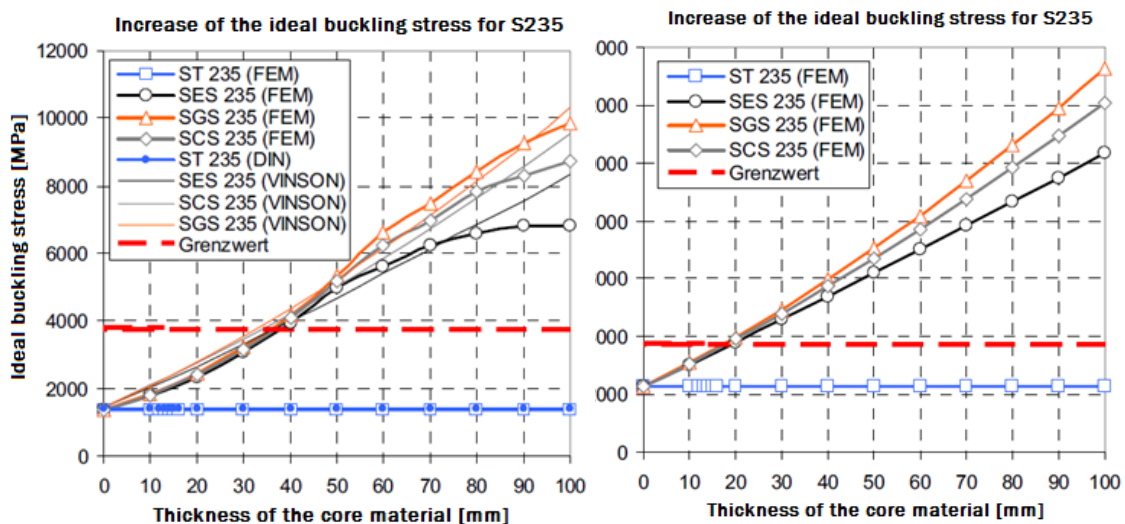


Figure 3 – Increase of the critical buckling stress under axial load (right) and bending moment (left) for S235 depending on the core thickness - [3-05]

The positive effect of the core material on the bearing capacity and stability of the tubes can be clearly observed. It should be noticed that the overall thickness of the compared steel and sandwich tubes was equal, with the difference that in case of sandwich tubes this thickness is divided between outer and inner tube. Thus all benefits of increased axial load and bending moment capacity, as well as the increase of critical buckling load, are attributable to the sandwich material. In Figure 3 the diagram of increase of the critical buckling stress is given for steel and sandwich tubes made with steel S235. Corresponding diagrams for higher steel grades can be found in [3-03] and [3-05].

Another important aspect of the sandwich material used for the chords and braces of a jacket sub-structure considers the bearing capacity of the tubes under a simultaneous action of axial force and bending moment. This kind of loading has not been studied before and for this reason experimental tests were performed. The results are presented in Deliverable 4.14. Sandwich tubes with grout as core material are tested statically under eccentric compressive load in order to determine their bearing capacity (Figure 4). Afterwards, a FE model of the tube is created and calibrated according to the experimental results and M-N interaction diagrams are obtained. Figure 4-right shows an interaction diagram for axial load and bending for the investigated sandwich component. Numerical results as well as the experimental results from Deliverable D4.14 are included in the diagram. The numerical results show a very good consistency with the experimental results. Further extension of the eccentricities result in expected behaviour, which is:

additional small compression load increases bending capacity whereas additional tension loading led to an approximately linear reduction in bending capacity. Furthermore, different capacities with respect to compressive and tensile loading are apparent from the diagram.

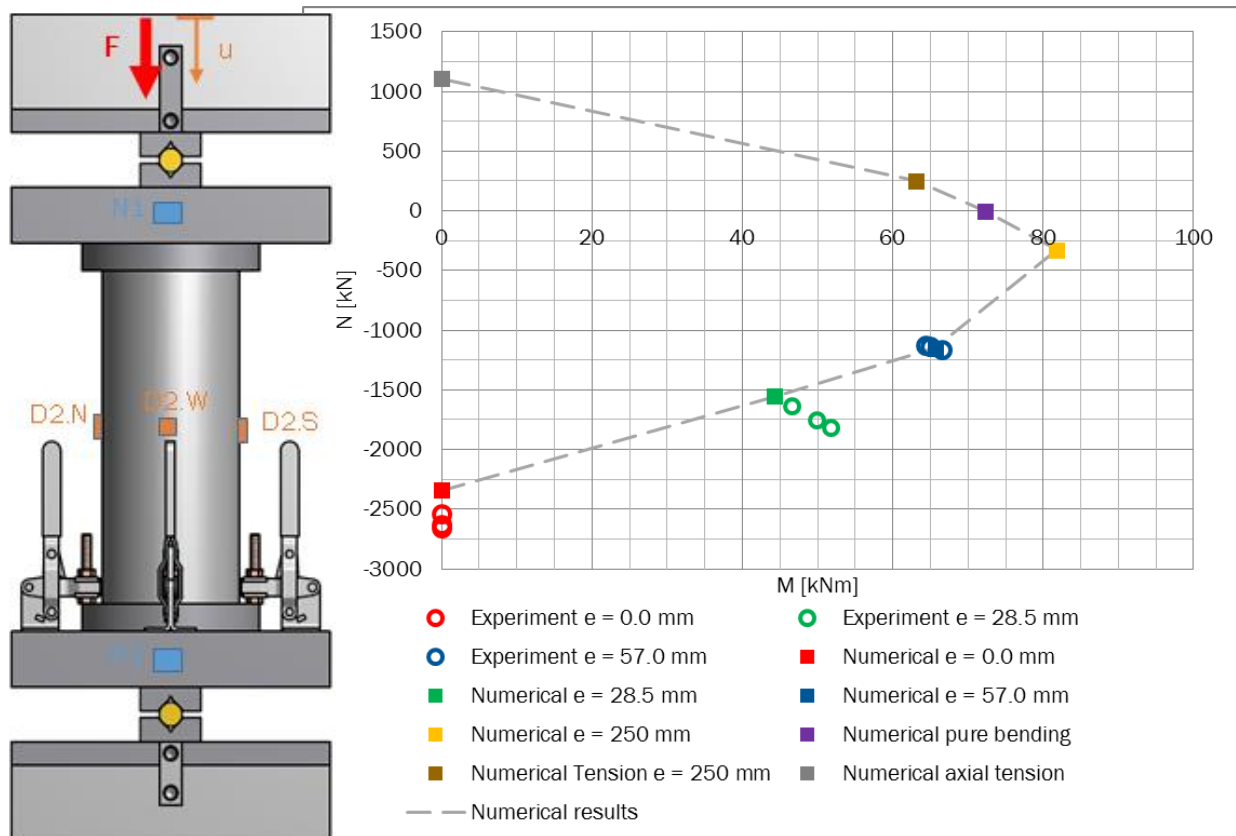


Figure 4 - Test setup (left; ) Validation of numerical model for Interaction of axial loading and bending (right)

### 3.1.2 Applicability of developments on 20MW turbines

Two main support structures currently used in the offshore wind industry are monopile and jacket. It is expected that these two structure types, with addition of floating solutions, remain the dominant support solutions for future generations of wind turbines with power of up to 20 MW. Nevertheless, the manufacturing and welding of steel components required for support structures able to support such large wind turbines will represent a big challenge. Furthermore, on the design side the fatigue may represent a limiting factor regarding the size and thickness of the single components. The solution for this issue may be use of sandwich section components instead of steel ones. As shown previously, such components can reach the bearing capacity of steel components allowing at the same time the use of slender steel tubes with higher steel grade. The advantages of the sandwich tubes come to light especially in components with large diameters and for structures with a small number of joints. This makes the monopile support structure a suitable solution for this innovative sandwich technology.

In this subsection the main features and possible bottle-necks for the monopile support structures made of sandwich components will be discussed.

### Monopile support structure – Hybrid tower

The monopile made of sandwich components can be seen as a hybrid tower (Figure 5). In the lower sections of the tower, where the maximal bending moments are expected, the use of sandwich components is advantageous. On the upper side, this part of the tower is connected with the slender sections made in steel. On the lower side the tower is connected to the foundation's pile or suction bucket. The connection between these different components may be performed in-situ via grouted connection.

Advantages of the sandwich components in terms of cost reduction are presented in [3-03]. It was shown that the quantity of steel necessary for the sandwich tubes varies significantly in relation to the strength of the used steel. The stability problems would have significantly reduced maximal capacity of the slender tubes, if the tubes were made in high strength steel. This is not the case for sandwich tubes, for which the early buckling and wrinkling are circumvented due to the presence of the core material. Thus, with the reduced quantity of steel the same load capacity of the steel section can be achieved. For steel S460 this reduction can be estimated to be up to 50 % [3-05].

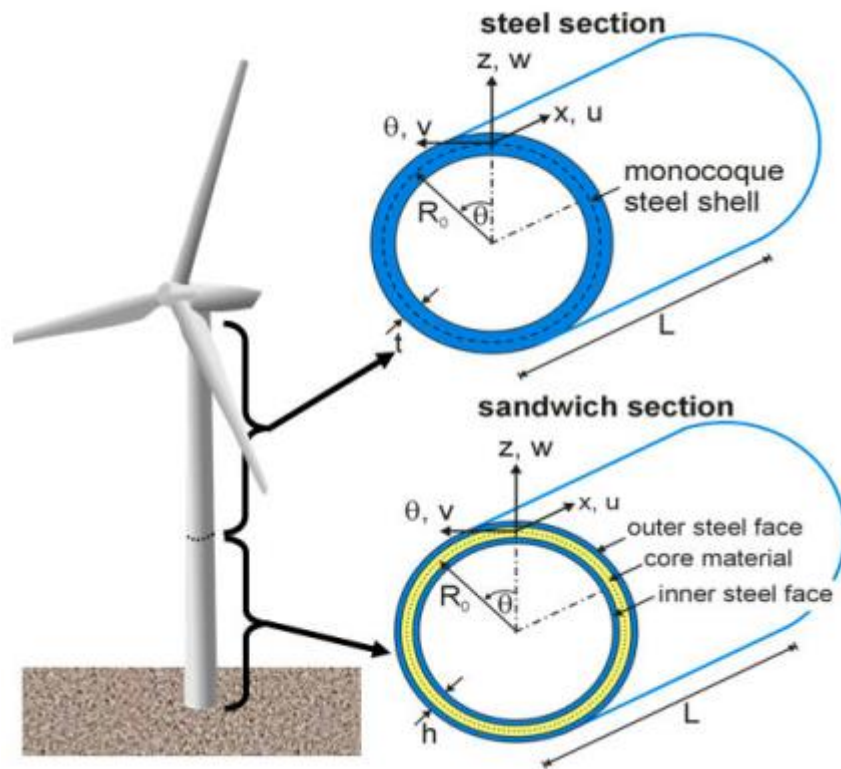


Figure 5 – Hybrid tower with lower sections in sandwich tubes and upper ones made in steel [3-06]

On the other hand it has to be taken into account that in the case of the hybrid jacket the number of the necessary steel tubes is double (inner and outer steel tubes) with respect to the steel jacket. Accordingly, the necessary time for steel sandblasting doubles. The standard speed for sandblasting is between 0.6 and 1.0 m/min and the steel thickness does not have any influence. Regarding the necessary manufacturing time, although the number of tubes is doubled, the cutting and forming process of steel plates, from which the tubes are made, requires an additional time of only 50 % (in case of S460) [3-02]. The cutting and forming time does not double because the plates have smaller thickness and consequently the cutting and forming process of a single plate is faster. Considering different steel grades, the maximal optimization according to [3-05] can be observed when using S460 where for the cutting process an additional time of 8% and for forming of about 45 % is estimated. The following phase in the manufacturing

of tubes is welding of the formed cylindrical section, which are created during the process of plate forming (Figure 6). In this phase a substantial time gain of up to 25 % is expected due to the smaller thickness of the tubes [3-05]. The welding is the most time consuming part of the manufacturing process and if the necessary manufacturing time is summed up, the steel tubes for hybrid jackets allow a saving of up to 50% in time in relation to the thicker tubes required for the reference steel jacket [3-02].

Finally, in case of the hybrid jacket, the core material and its injection represent additional costs which are not present in the standard steel jacket. An example of injection system is shown in Figure 7 [3-05]. The system is composed of a reservoir with core material which is pumped via pumps and injection tubes in the inter space between outer and inner steel tube. In Figure 7 are shown two systems working in parallel. The injection should be performed from the bottom upwards in order to avoid formation of air inclusions / voids.

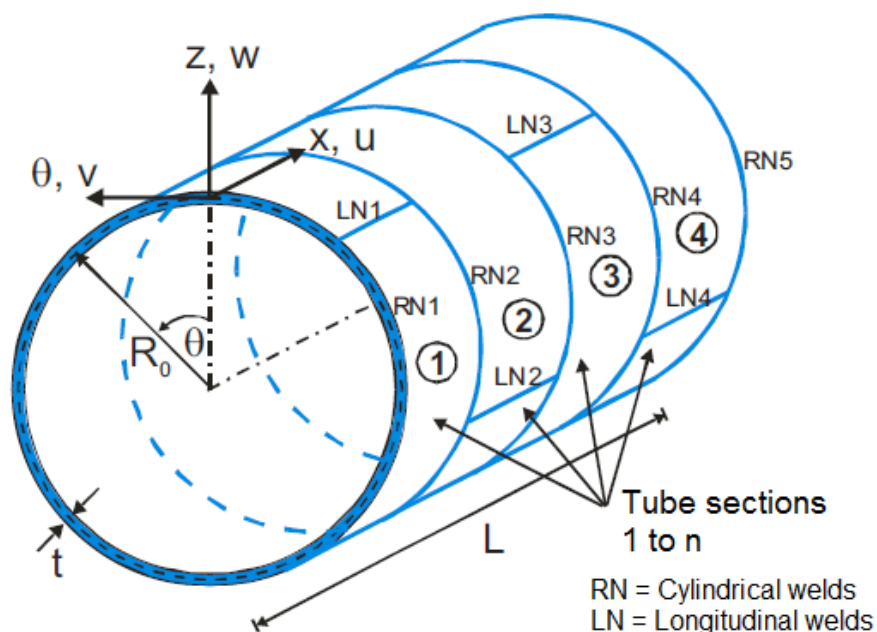


Figure 6 –Steel tube sections with positions of cylindrical and longitudinal welds [3-05]

The velocity of the pumps depends on the core material. In case of elastomer, according to the opinion of the producer, a velocity of ca.  $P_0 = 9$  to/min can be reached. On the other hand the velocity of grout is limited to ca.  $P_0 = 4-6$  t/h. Thus the height of the single section shall be chosen in the way that the section can be completed within a working day. As shown in Figure 7 the section can be also provided with the steel connectors which are used to connect two sections.

The connections solutions between two sandwich sections of the tower proposed in [3-05] are given in Figure 8. The proposed connection can be used to connect sandwich sections with steel sections or foundations as well as to connect two sandwich sections. It can be seen as a double grout joint in which the steel section or the upper sandwich section is already provided with the steel connector on its bottom is grouted between the outer and inner steel tube of the lower section. In case of joining two sandwich sections the steel connector is already embedded in the upper steel section during its manufacturing, see Figure 8. In order to make the grouting possible the upper part of the lower section should not be filled with core material for the length of overlapping with the steel connector. The mechanical characteristic of the joint may be improved by using shear keys (Figure 8).

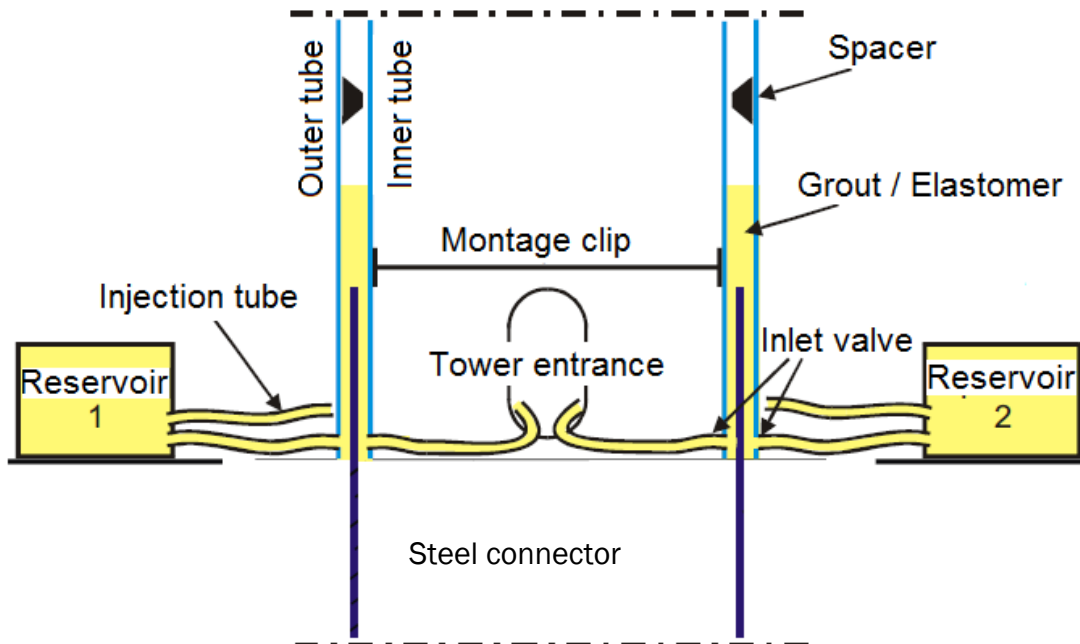


Figure 7 –Injection system for sandwich components

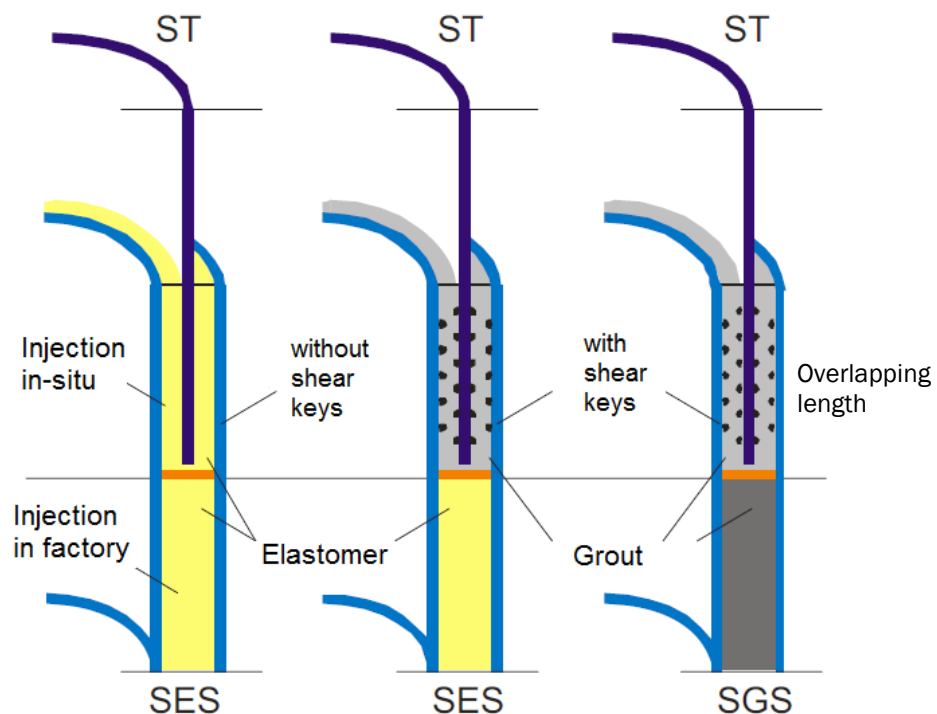


Figure 8 –Connections between different sections of the tower [3-05]

As in case of grouted joint, axial force and bending moment will be transfer between the upper steel section (or steel connector) and the sandwich section as shear forces with the building of compression struts in case of the connection with shear keys (Figure 9).

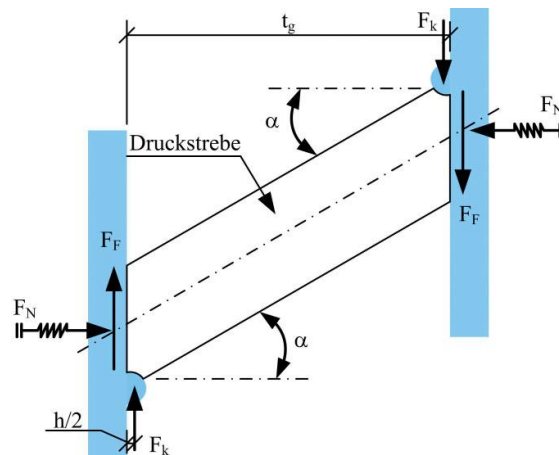


Figure 9 – Compression strut between shear keys with reaction forces [3-08]

This connection type has several advantages in comparison with standard bolted ring flange connections:

- Reduced use of steel due to lack of ring flange and bolts
- Eccentricities and imperfections can be tolerated with this connection type
- Maintenance cost is lower in comparison with prestressed bolts used for ring flange connections

### 3.1.3 Technology Readiness Level and Recommendations

The sandwich material for a monopile as well as chords and braces of a jacket sub-structure has never been used in the offshore wind industry. The analytical solutions and the test results in case of purely axial loading of the sandwich tubes are reported in [3-05] and [3-07]. Furthermore, in the previous deliverables D4.1.3 and D4.1.4 the bearing capacity of the sandwich tubes under axial force – bending moment interaction (M-N interaction) was investigated. The results are based on the experiments described in [3-04]. According to the technology readiness level (TRL) definitions given by the INNWIND.EU Project, the TRL of sandwich tubes for jacket sub-structures is 3.

In order to reach the next TRL, further investigations on the component level are necessary. These investigations regard the influence of the variation of the thickness of the outer and inner steel tubes on the bearing capacity of the sandwich material components. In addition, the behaviour of the sandwich tubes under consideration of the other core materials (elastomeric) shall be experimentally tested.

Another important aspect that should be studied is the fatigue behaviour of the sandwich tubes, as fatigue is often a design driving criterion for jacket sub-structures. The most critical point of the sandwich tube represents the joint region, where the sandwich tube is connected with the steel node.

## 3.2 Adhesives for tubular joints and sandwiches (WMC)

This chapter reports on the potential of the new joining methods investigated in deliverables 4.1.3 and 4.1.4 for 20 MW support structures. The applicability of the joining methods is evaluated based on the load and dimensional requirements for 20 MW support structures. Based on the evaluation recommendations for future research for 20MW will be given.

### 3.2.1 Summary of main developments on component level from task 4.1.3 and 4.1.4

In previous reports [3-03] and [3-05], the potential of adhesive joints was discussed as an alternative for welded connections. The main potential of adhesive joints can be summarised as:

- Adhesive joints foster structural continuity and avoids local reinforcements (no holes, e.g. platform legs can be continuous)
- Less fatigue sensitive than welds
- On-site assembly possible

On the other hand, typical issues with adhesively bonded joints are:

- Controlled application of bond lines
- Environmental influences on bond line integrity (temperature, humidity)
- Multi-axial stress states

Tests were performed at various scales in this project.

A set of quasi-static tests on single-overlap specimens consisting of a solid steel rod bonded into a steel tube was performed in tension, torsion, and a mix of tension and torsion. These tests show the relative influence of the stress concentration near the bond line edge, as the tension test results are effectively overlap tests in shear with a finite overlap length, whereas the torsion tests are overlap shear tests with an infinite bond length. A considerable amount of tests was performed at different load types and with variations in diameter, overlap lengths and adhesive thickness (Figure 10).



Figure 10: single overlap small-scale tension, torsion and mixed mode specimens [3-09]

Furthermore, tubular adhesive single-overlap joints were mechanically tested in compression, using different overlap lengths and fillet details, which demonstrated that the quasi-static strength is sensitive to these parameters. For the best performing adhesive fillet shape investigated (45° fillet angle), single-overlap tubular specimens failed in the steel part, not the bond line.

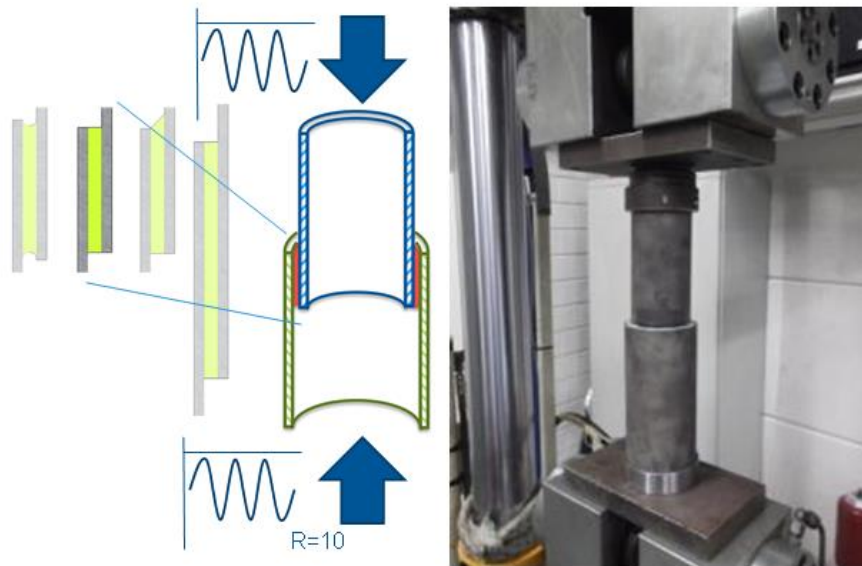


Figure 11: Single overlap tubular test set-up [3-03]

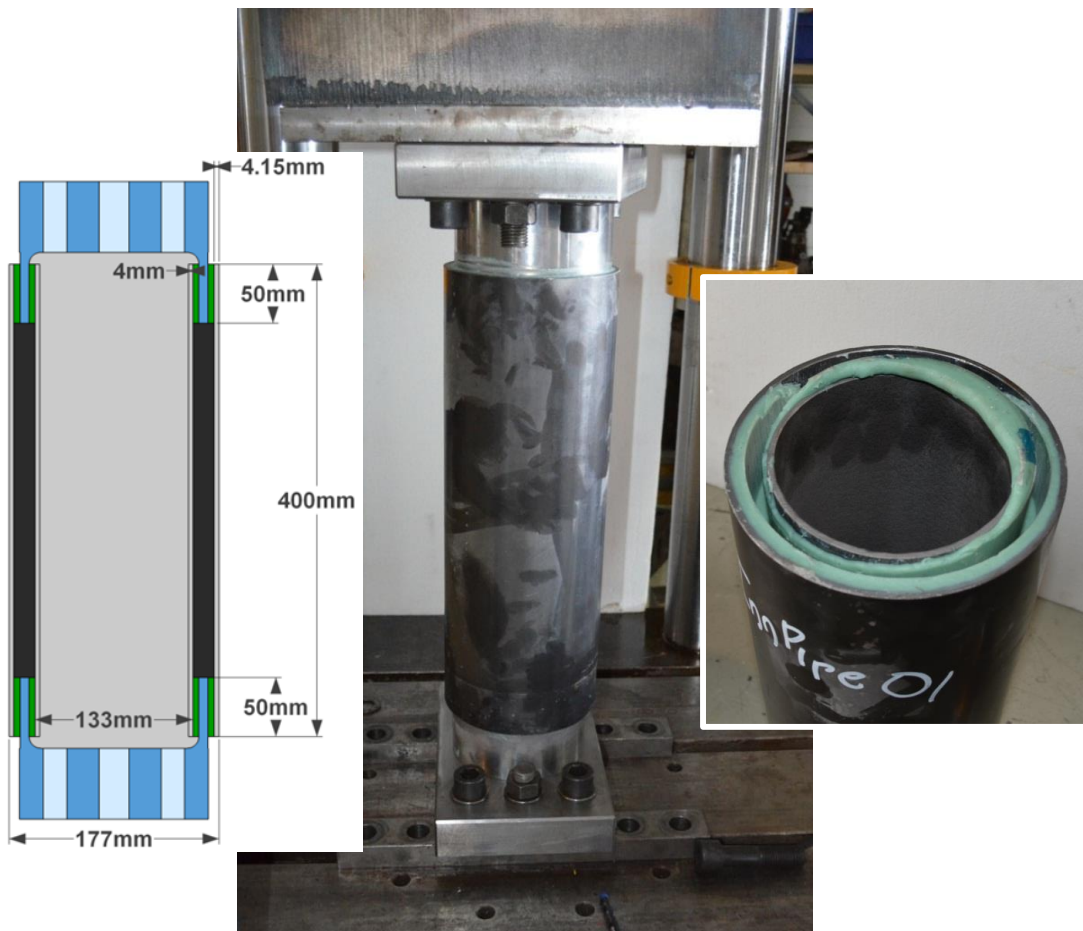


Figure 12: Hybrid joint specimen (left), tensile and fatigue test set-up, and post-mortem sandwich tube [D4.14]

A selection of bond line geometric parameters was used in fatigue tests at  $R=0.1$  shear fatigue, by applying an axial compression load to the tube assembly. For these specimens, the edges of the adhesive line were perpendicular to the load, and the overlap length was 50 mm, amounting to roughly half of the outer tube's diameter (Figure 11). The slope parameter for shear fatigue at  $R=0.1$  for adhesive bond lines in a single overlap tubular configuration was quite favourable at a value of ca. 16 in a double-logarithmic S-N curve. For 'standard' rotor blade composites, the slope is typically between 8 and 15 (glass-fibre reinforced epoxy).

The analysis of adhesive bonds was elaborated to obtain insight in the mechanical performance in hybrid joints. Hybrid joints are here defined as the adhesive joint between a solid-walled steel tube and a tubular, grout-filled, sandwich tube. The main expected source of problem in the hybrid joint was the interface between the solid-walled steel tube and the grout in the sandwich tube, which might be sensitive to fretting-type damage under compressive fatigue loads. This was prevented by applying a thin layer of adhesive between the steel and grouted parts.

A limited number of hybrid joint specimens (Figure 12) were subjected to tensile tests and  $R=-1$  fatigue tests. The test results were surprising in the sense that both the quasi-static and fatigue performance of the specimens was low. Quasi-static strength compared to the single-overlap tubes was a factor  $\sim 3.5$  lower. Fatigue strength was several orders of magnitude lower (on the life-axis) and the very limited data (three specimens) show a steep S-N curve, although no reliable conclusion can be drawn from such a small dataset.

**Table 3: Summary of bond line test results**

Test type (figure), diameter, overlap, adhesive thickness	Maximum shear stress in bond line [MPa]
Small scale tension (Figure 10), 50, 5, 50	18.3
Tubular compression (Figure 11), 85, 5, 50	16.9
Hybrid joint (Figure 12), 133, 5, 50	4.6

There are a few possible explanations for this poor performance of the hybrid joints compared to the tubular single overlap specimens.

#### Test load direction

Bonding tubular specimens in a single overlap configuration may give rise to test direction effects, as secondary deformation may occur, see the qualitative sketch below. In the hybrid joint, the mechanism is slightly different, resulting in unfavourable peel stresses between the inner tube and the central tube, albeit at smaller expected secondary deformations. Finite element analysis is required to quantify the severity of this effect.

#### Scale effects

Various studies have investigated the effect of bond line thickness on performance and some have revealed that larger thicknesses do not favour strength. In the current tests, however, the bond line thickness was quite similar (4-5 mm).

#### Bond line quality

For larger volumes of adhesive, a larger amount of voids may be expected, which have an adverse effect on bond line strength since they act as stress concentrators in the adhesive. This

may partly explain the difference in test results, since the adhesive volume in the hybrid joints was larger. Arguably more important was the lack of control over the inside bond line fillet in the hybrid joints (since the top tube was inserted into an adhesive-filled gap between the sandwich skins, the inside was not reachable for filleting). The single overlap tests have shown considerable effect of the fillet, but cannot fully quantitatively explain the difference.

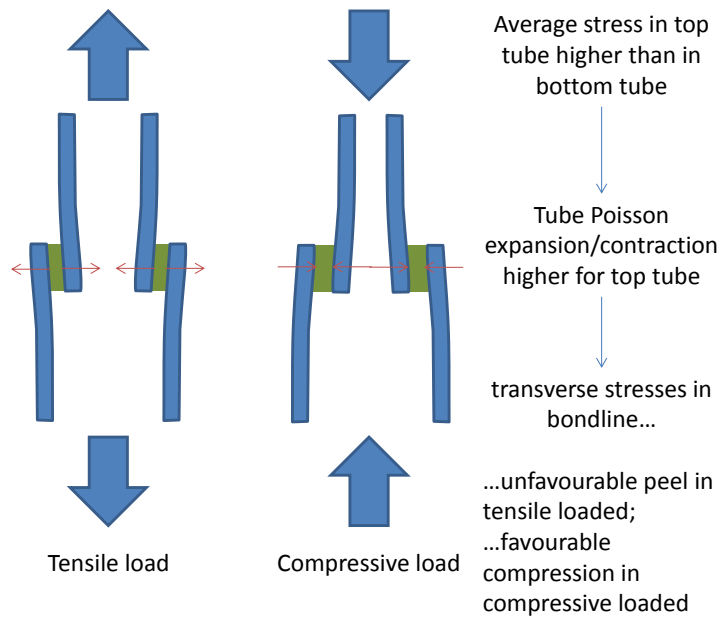


Figure 13: qualitative view of loading state in bond line (single overlap tubular joint)

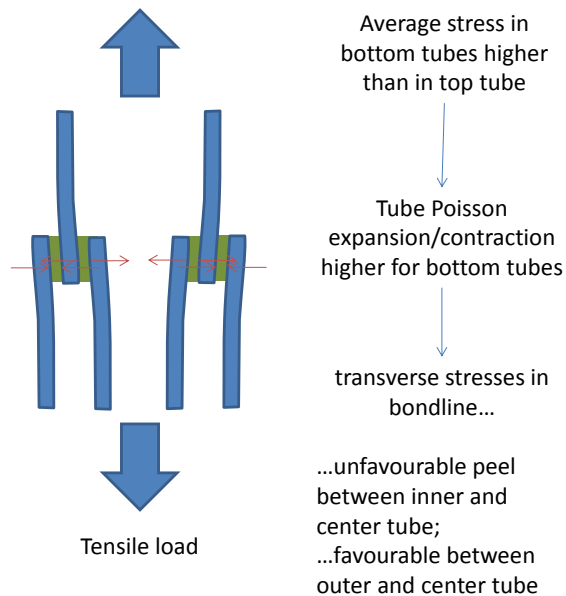


Figure 14: qualitative view of loading state in bond line (hybrid joint)

### Quality of pre-treatment

Before filling of the sandwich tubes with grout, the surfaces of the tubes were sandblasted (fixture, inner surface of outer tube and outer surface of inner tube). This pre-treatment was quite important; Results from tests with poorly pre-treated fixture tubes showed strengths that were roughly a quarter of the well-pre-treated specimens. Thus, a similar difference can be expected of the hybrid joint results compared to the single overlap tube results if the pre-treatment would be poor or e.g. rendered less effective through contamination while applying the grout.

### Test set-up effects

The single overlap tubular specimens were tested with a hinge at the load introduction, to avoid bending moments. The hybrid joints were bonded outside the test machine and subsequently bolted to the actuator. Although misalignment during manufacturing was reported to be below 0.2 degrees, it is possible that stresses were induced by fixing the hybrid joint to the test machine, resulting in lower apparent strengths.

### 3.2.2 Applicability of developments on 20MW turbines

In the framework of feasibility of installation, one of the main questions is, whether the adhesive can be inserted from the outside and still reaches the inside of the overlap structure ('blind' infusion). The feasibility of this was verified through a series of injection experiments, where three Plexiglass panels were positioned with a gap of approximately the adhesive bond line thickness (5mm), and a hole in the middle panel. Adhesive bonding paste was then injected between panel 1 and 2, and the resulting infusion between all panels was monitored, to see if bonding paste adhesive would reach the cavity between panel 2 and 3. Experiments were carried out with 1 and three holes, and injection locations were varied (injection at hole location or between holes). Screenshots of the experiments are shown in (Figure 15), demonstrating that there is some sensitivity of the injection performance to the injection point location, but that it is feasible to do a 'blind infusion'.

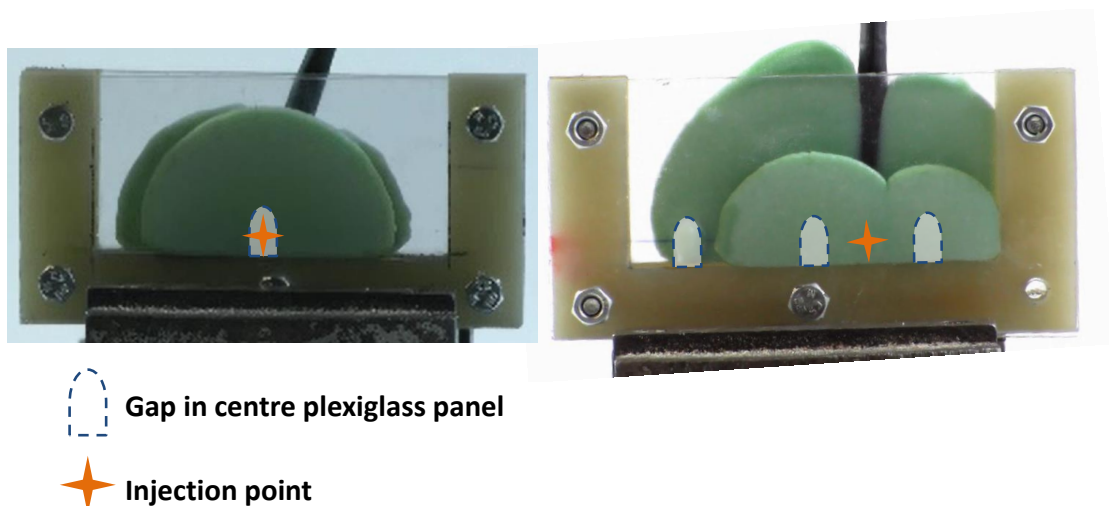


Figure 15: Adhesive injection experiments

### 3.2.3 Main challenges and bottlenecks for the upscaling to 20 MW

The below table gives the dimensions that are expected for a 10MW optimized 4-legged jacket, for the 20 MW jacket, and the relevant dimensions of the test specimens. This gives a basis for the challenges that are faced when extrapolating the current results to a 20 MW design.

For the 20 MW, a basic scaling approach was applied. For the 20MW, the thrust is ca. twice that of the 10 MW and the lever arm is slightly longer (142m vs 120). To achieve equal stresses in the legs, all dimensions scale with the  $1/4^{\text{th}}$  power. All dimensions were therefore multiplied by 1.24 ( $= (142/120 * 2)^{1/4}$ ) to arrive at the 20 MW sizes.

**Table 4: Typical dimensions in 10&20MW jacket designs versus bond line scaled test dimensions**

Dimensions (mm)	10 MW	20 MW (basic scaling rules)	Scaled tests
Leg diameter	594 (max.)	Ca. 735	
Leg wall thickness	74 (max.)	Ca. 100	
Brace diameter	Ca. 550	Ca. 680	40-102-177
Brace wall thickness	Ca. 60	Ca. 75	4-24

### 3.2.4 Conclusion and impact of innovations for 20MW turbines

#### Conclusions

- Quasi-static and fatigue strength of steel-epoxy paste adhesive bond lines are promising.
- Sensitivity to adhesive curing state is low
- Sensitivity to pre-treatment is high
- Quasi-static and fatigue performance of a sandwich hybrid joint (a grout-filled tubular sandwich adhesively connected to a steel tube) shows poor performance compared to single overlap tubular joints, which cannot be explained by scale effects.
- Syringe-type injection of adhesive paste in a double-lap tubular gap is feasible if adhesive transfer orifices are present.
- Thicker adhesive thicknesses may be required for 20MW, this will not lead to severe performance degradation.

### 3.2.5 Recommendations and further development needs

#### Detailed finite element modelling of the hybrid joint tests

The hybrid joints' poor performance compared to the single overlap tubular tests may be explained by large effects of small misalignment, adhesive edge geometry, and secondary deformations resulting in transverse adhesive stresses. These effects should be quantified in a detailed FEM analysis.

### **More accurate and extensive fatigue data required**

The uncertainty of the adhesive fatigue slope parameter in the tubular tests was high due to limited amount of tests. For the joint tests, the amount of fatigue tested specimens was not sufficient to draw conclusions from. The large difference in performance between single overlap tubular joint and sandwich hybrid joint may partly be due to test design. Further development of the hybrid joint test is necessary and additional testing is required for both tubular and hybrid joint test to obtain an improved estimate of the slope parameter, also for other conditions than a dry laboratory environment.

### **Geometrical details**

The current study has focussed on axially connecting prismatic elements with circular bond lines. In a realistic jacket structure, the trusses are typically welded to the legs at an angle, resulting in e.g. a K-joint connection. Adhesive bonding of trusses to the legs of a jacket was not explicitly investigated since it is quite geometry-sensitive, and is more likely to induce local peel stresses in the connection. On the other hand, the potential of such connections may include a reduction of local reinforcement and resulting weight saving.

### **Large thicknesses**

Adhesive thicknesses were not varied in this study and experiments were carried out at adhesive thicknesses of 5 mm, close to the thickness of the steel tubes used in the experiments (4 mm wall thickness). When typical truss wall-thicknesses of a 10 MW turbine are considered (60 mm, see Table 4), the experiments were scaled at a ratio of 15. For both the 10 MW and the 20 MW turbine, with expected truss wall thicknesses of 75mm, the question remains whether bond line thicknesses limited to 5 mm are feasible, especially in terms of installation tolerances, notably in the tubular components' diameters. Larger adhesive thicknesses may be required. Several sources have investigated large adhesive thicknesses >5 mm, and the overall impression is that there may be some deterioration in performance but this is limited to 10% in the strength [3-10], [3-11] and [3-12].

### **Development of monitoring techniques**

Contrary to steel welding, the use of adhesive joints enables the implementation in the bond line of monitoring sensors. For example, acoustic actuators and sensors may be integrated to do an (automated) periodic check of the bond line integrity. Methods to accurately and reliably monitor steel-adhesive bond lines from within the bond line may be derived from the state-of-the-art in monitoring techniques applied on composite rotor blades. Nevertheless, in that application, the low transmissivity / high damping of the materials calls for a high-density sensor network, and the systems for rotor blades are not one-on-one transferable to support structures, thus additional study is required in this field.

### **Mixed mode loading, fracture energy, including humidity**

In the experiments carried out thus far, the multi-axial stress state was taken into account implicitly by modifying fillet parameters, and investigating the influence of 'infinite' vs finite bond lines. In a realistic structure, a mixed-mode loading may be expected, especially near the bond line edges, where a peel stress is likely to effectively degrade the shear load capacity of the bond line. A local peel stress is expected to interact unfavourably with any humidity load. Thus, local adhesive performance is affected by water uptake, ingress may be accelerated as reduced

bonding to the substrate results in capillarity in the bond line. In the presence of cracks, the fracture energy (a measure for the sensitivity to propagation of a crack) might also be affected by humidity and is surely a function of the (mixed mode) local stress state. An investigation into more complex structural connections such as a truss-leg connection will require more detailed insight in the mixed mode behaviour as well as fracture energy of the bond lines.

### Effect of voids

The currently explored syringe-type injection method in combination with the highly viscous adhesive paste is prone to creating voids, which are known to have an adverse effect on the cohesive strength of the bonding paste.

### Potential of different adhesive types, and preparation- and application methods

In the current project, a bonding paste typical for rotor blade assembly was used. This was a short glass-fibre filled epoxy resin. The filler material adds viscosity to the resin, enabling the adhesive to be applied as a paste, while still being injectable (e.g. in gaps between components) to a certain degree. In operation, the glass filler adds stiffness. Epoxy is known to have good adhesive properties in combination with steel, relatively good resistance to water damage, and has a favourable curing cycle resulting in limited internal stresses, compared to e.g. polyester. The contact surfaces of the steel substrate were sandblasted to clean and degrease the surface and to improve the mechanical bonding at the surface. In a feasibility study regarding the application method, the epoxy was injected between panels using a syringe.

It is recommendable to evaluate additional ways of pre-treatment of the substrate and application methods, in combination with different types of adhesive and filler.

The filler has an influence of water ingress; viz. the filler material can provide a path (e.g. capillarity) through the resin, accelerating water ingress. Using short fibres, or e.g. glass microspheres can significantly influence the water uptake.

Syringe-type injection is one possible means of adhesive application, with the advantage that it can be applied on-site, and, by introducing adhesive distribution orifices in the overlaps, it is feasible to create a double-overlap adhesive joint. Other application methods have not been investigated, but one straightforward method may be to pre-apply the adhesive before assembly of the parts. Another method may be to use a self-expanding adhesive (taking into account the effect of voids), or built-in injection ports.

The key to successful application of the adhesive is to find a method that is robust, i.e. insensitive to weather conditions and can thus be implemented in the field.

### 3.3 References

- [3-01] INN WIND.EU Design report - Reference Jacket, "InnWind\_DesignReport\_ReferenceJacket\_Rev00.docx", Internal teamsite, uploaded 2014-01-16, accessed 2014-08-12.
- [3-02] INN WIND.EU: Innovations on component level (Interim report - Revision). Deliverable 4.1.2, 2015.
- [3-03] INN WIND.EU: Innovations on component level (Final report - Revision). Deliverable 4.1.3 2016.
- [3-04] INN WIND.EU: Validation of innovations by tests on component level (Revision). Deliverable 4.1.2, 2016.
- [3-05] Keindorf, C., "Tragverhalten und Ermüdungsfestigkeit von Sandwichtürmen für Windenergieanlagen", Dissertation, Institute for Steel Construction, Leibniz University Hannover, 2010, (in German)
- [3-06] Schaumann, P. Keindorf, C. (2008) "Sandwich-Towers for Wind Energy Converters". DEWI Magazine no. 33, August 2008.
- [3-07] Lindschulte, N., "Drucktragverhalten von Rohren aus Ultrahochfestem Beton mit Stahlblechummantelung", Dissertation, Institute of Building Materials Science, Leibniz University Hannover, 2013, (in German).
- [3-08] Vinson, J.R. (1993): The behavior of shells composed of isotropic and composite materials, University of Delaware, USA, Kluwer Academic Publishers. Schaumann, P et al. (2010) Durchdrtschende Grout-Verbindungen in OWEA-Tragverhalten, Instandsetzung und Optimierung. Stahlbau 79 (2010), Heft 9
- [3-09] Ruigewaard, S "Testen van "E+E" lijm voor toepassing als dikwandige lijmverbinding voor sandwich constructies van de mast van een windturbine" (2016) Master thesis. Hogeschool Inholland Alkmaar.
- [3-10] Tankut, N. (2007). The effect of adhesive type and bond line thickness on the strength of mortise and tenon joints. International Journal of Adhesion and Adhesives, 27(6), 493–498. doi.org/10.1016/j.ijadhadh.2006.07.003
- [3-11] Kawashita, L. F., Kinloch, A. J., Moore, D. R., & Williams, J. G. (2008). The influence of bond line thickness and peel arm thickness on adhesive fracture toughness of rubber toughened epoxy-aluminium alloy laminates. International Journal of Adhesion and Adhesives, 28(4–5), 199–210. doi.org/10.1016/j.ijadhadh.2007.05.005
- [3-12] Davies, P., Sohier, L., Cognard, J. Y., Bourmaud, A., Choqueuse, D., Rinnert, E., & Créac, R. (2009). Influence of adhesive bond line thickness on joint strength. International Journal of Adhesion and Adhesives, 29(7), 724–736. doi.org/10.1016/j.ijadhadh.2009.03.002

## 4 SOIL & FOUNDATION (AAU, FHG-H)

### 4.1 Soil pile interaction / axial pile loading (FHG-H)

The vibratory-driven (VD) technology, as an alternative to the impact-driven (ID) technology, has the potential to significantly reduce the costs associated with installing piled foundation for offshore wind turbines. The economic advantages of this technology include: the absence of noise mitigation systems, the reduction of the time of the installation and the reduction of the fatigue load in the pile steel otherwise induced by impact hammers.

Previous studies on vibratory-driven piles investigated both installation mechanisms [4-01] and the behavior of the foundation under axial and horizontal loading (see [4-02], [4-03] and [4-04]). From the mentioned previous studies it appears that vibro-driven piles show reduced mechanical characteristics when compared to the more traditional pile driven with impact hammer. This conclusion was also corroborated by the experimental data presented and preliminarily interpreted in the previous two deliverables of this project (see [4-07] and [4-08]).

As a result of these recommendations and previous studies, there is still scepticism in using this technology in a wind farm project. Indeed, in industry practice, vibro-driven piles are usually impact-driven at the end of the installation in order to enable dynamic pile tests to be carried out and assess thereby the capacity of the foundation. German recommendations on pile design [4-01] state for instance that a reduction of the resistance for driven piles is to be expected unless a pile is impact-driven for the last 8 equivalent diameters. Although this enables a check on the pile activated resistance, it also neutralizes most cost savings of vibratory-driven technology.

Given that piles installed with vibro-driven technology, to achieve the same design capacity, must be larger than those installed with impact hammer, it is not clear whether the economic advantages mentioned above would be able to outweigh an increase in fabrication costs. Therefore, the general aim of this study is to estimate the size difference between VD and ID piles for a 10 MW turbine sub-structure. On the base of this size difference estimation, a conceivable cost difference will be evaluated. In addition an object-oriented numerical model which enables the behaviour assessment also of piles for a 20 MW turbine will be presented.

While deliverables [4-07] and [4-08] focused on presenting and preliminary interpreting large-scale test results of VP, this contribution has the following objectives:

- Extending and finalizing the interpretation of the experimental results by presenting and evaluating a second and more realistic large-scale tensile test of a vibro-driven pile (Section 4.1.1).
- Providing information on the possible cost saving potential of fabrication and installation of VD pile on the base of large-scale test results and standard CPT methods (Section 4.1.1).
- Presenting a flexible numerical model which, if properly calibrated, will be able to predict the behaviour of piles for jacket substructures of any dimension (Section 4.1.3).

#### 4.1.1 Combining experiments and CPT methods to assess required geometry of vibro-driven piles

##### Description of the experimental works

In this section, all the steps overtaken before and during the tensile tests are described. As already mentioned in [4-07] and [4-08], two test piles named Pile 1 and Pile 2 are considered in this study. Figure 16 and Figure 17 depict installation and test phase of Pile 2. Pile 1 was installed

first and was subjected to pre-loading before being tested under tensile loading. Pile 2 was installed thereafter subjected to tensile loading until failure. No pre-loading was induced to Pile 2. In a previous deliverables of this project, [4-08], the test regarding Pile 1 is documented in detailed. During the tensile loading tests the piles were monitored with the load cell of the actuator, displacement transducer of the actuator and external displacement transducer. The actuator used for the test has a capacity of 500 kN. The external displacement transducer was installed in order to enable a system-independent measurement of the pile uplift during tensile loading. The external transducer and the internal transducers of the actuator are connected to an analyser unit which in turn broadcasts the signal to the computer unit where the data are stored with a sampling rate of 100 Hz. The installation of the piles was carried through by an external firm specialized in deep foundations. Pile 1 was installed on February 5<sup>th</sup>, 2015 and tested on October 15<sup>th</sup>, 2015. Pile 2 was installed on August 6<sup>th</sup>, 2015 and tested on August 28<sup>th</sup>, 2015. The installation was performed by an excavator. The vibratory hammer was connected to the arm of the excavator which in turn grabbed a properly designed adaptor placed at the pile head. The pile penetrated the sand with a velocity of approximately 0.1 m/s. Pile 2 was installed with a vibrator type ICE 8RFB, which has a maximum frequency of 38 Hz. Pile 1 was installed with a vibrator type Müller MS-5 HFBV, which has a maximum frequency of 45 Hz. The layout of the testing field is illustrated in Figure 18. Further technical information on pile geometry and preparation of the sample can be found in [4-08].



**Figure 16: Installation of Pile 2 with vibratory technology. Test campaign set-up by Fraunhofer IWES at the test centre for support structure in Hannover (Testzentrum Tragstrukturen Hannover, TTH), 2015.**



**Figure 17: Tensile testing of Pile 2. Test campaign of Fraunhofer IWES at the test centre for support structure in Hannover (Testzentrum Tragstrukturen Hannover, TTH), 2015.**

As already indicated above, Pile 1 was subjected to relevant pre-loading before being axially tested in tension. The pre-load applied in this phase consisted of cyclic horizontal quasi-static load with different amplitudes. Additionally, a 0.8 m deep scour was artificially created. In this manner the influence of set-up effect (roughly 240 days after the installation), scour, and pre-loading were to be explored. Given the scale of the system it was not possible to apply the different effects to more than one foundation. As a result of that the implications of these affecting variables could not be possibly decoupled. However, it is well known that the set-up effect is generally beneficial to the bearing behaviour of piles as also recently reported by [4-09]. Further, scouring phenomena

are doubtlessly negative for the bearing behavior. The question arises as whether pre-loading produces beneficial or detrimental effects on the pile shaft capacity.

A steel gantry properly set up over the test piles was used to enable the tensile loading application. A 500 kN actuator was connected to the horizontal part of the gantry and by means of a steel adapter plate, to the flange of the pile. The test was performed in a displacement-controlled manner. To make sure that no pore pressure building up could possibly occur during the tensile loading test, a very low displacement rate (0.01 mm/s) was designated. This displacement rate applied by the actuator was confirmed by the external displacement transducer. Before the tensile loading test a difference of 82 cm between soil on the inside and on the outside of the pile was measured (Plug length Ratio of 86%). After the test the difference between soil level in and soil level out the pile was measured again with the same result. As expected the behavior of the pile was fully plugged during the tensile loading test proving the internal shaft capacity to be larger than the soil weight inside the pile.

#### 4.1.2 Presentation of the experimental results

A magnified view of the curves for the first 10 mm vertical displacement is depicted in Figure 19. The entire load-displacement curve for both tests is shown in Figure 20 together with the CPT methods predictions. In the initial 0.4 mm of vertical displacement the curves appear to be identical. After this similar initial stiffness branch, it is evident that the two piles show essentially different behaviours. Pile 2 tends to flatten for the whole load path, showing no peak capacity. Pile 1 shows a distinct peak resistance in correspondence to a displacement of approximately 6 mm ( $\approx 1/100 D$ ). The ultimate capacity of Pile 1 is 177 kN and was taken as the peak load reached at circa 6 mm of displacement. The ultimate capacity of Pile 2 is 115 kN and was taken according to the well-established  $1/10 D$  criterion. Even disregarding the negative presence of the scour and the higher installation frequency, set-up and pre-loading effects seem to benefit the tensile ultimate resistance by at least 53%.

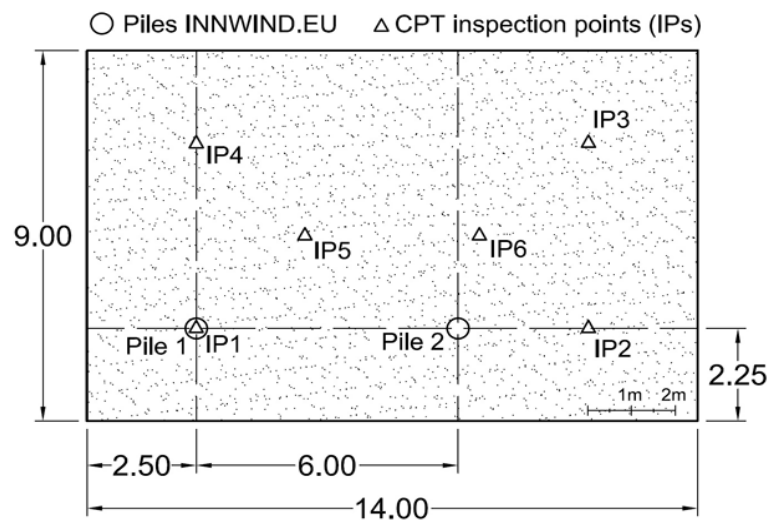
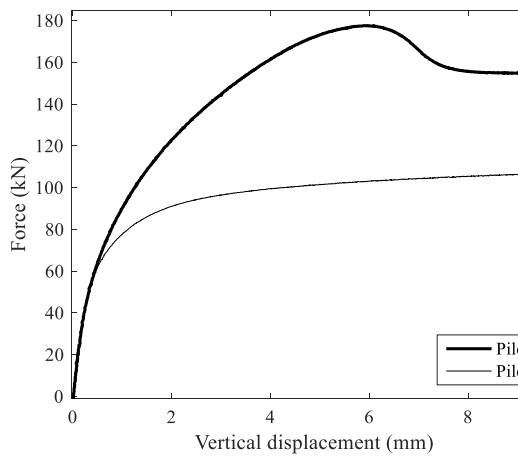
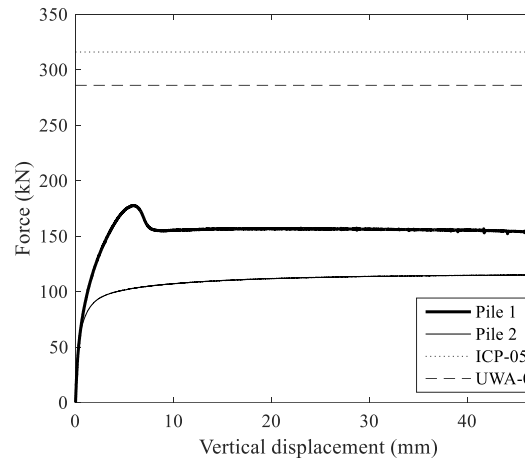


Figure 18: Layout of the field tests with pile and CPT positions



**Figure 19: Magnified view of the initial stiffness for Pile 1 and Pile 2**



**Figure 20: Extended view of the experimental curves of Pile 1 and Pile 2 with CPT-Methods prediction**

### Interpretation of the ultimate resistance by means of the CPT methods

The CPT methods for axially loaded piles are empirical formulas developed by four different research groups: Imperial College (ICP), University of Western Australia (UWA), Norwegian Geotechnical Institute (NGI) and the company Fugro. They relate CPT measurements to the axial capacity in tension and in compression of purely axially loaded piles. A comprehensive and comparative review of the methods is given in [4-09]. The methods are also included in the offshore foundation standard [4-10] with the names ICP-05, UWA-05, Fugro-05 and NGI-05. This nomenclature will be retained in this paper as well. Other studies conducted by Fraunhofer IWES [4-12] and international excellence literature such as [4-11] and [4-13] reported that the most suitable approaches for open-ended piles in tension are the ICP-05 and the UWA-05. This seems to be confirmed also by the test data of this study, which show the smaller deviation for the ICP-05 and UWA-05 methods. Accordingly, in this contribution, only ICP-05 and UWA-05 are taken into consideration in the analysis. The calculations concerning CPT-methods presented in this report were performed with the IGtH Pile software developed by the Institute of Geotechnical Engineering (IGtH), Leibniz Universität Hannover, Germany.

Usually, the input data for CPT methods are an average of raw CPT data calculated over a specified distance step. The distance step chosen was 0.5 m. Table 5 gives an overview of the CPT based method predictions in comparison with the tensile capacity tests. It is immediately apparent that the experimental tensile capacity is over predicted by the CPT methods. The experimental result of Pile 2 is in proportion between 38% of the ICP-05 prediction and 42% of the UWA-05 prediction. The experimental result of Pile 1 is in proportion between 68% of the ICP-05 prediction and 74% of the UWA-05 prediction. The experimental curve against the CPT-method predictions is visually presented in Figure 19.

The quite relevant discrepancy between CPT-based estimation and experimental result is not surprising and can be attributed to the installation method used. As already mentioned in [4-07], CPT-based approaches were calibrated with impact-driven and pressed piles data. CPT-based methods can therefore not be adopted to estimate the bearing capacity of vibro-driven piles. If these methods are to be used to assess vibro-driven piles they should be properly adjusted. In the next paragraph, the results of Pile 1 (prediction and actual experimental test) are used to estimate the minimum design length of a real-scale vibratory-driven pile.

**Table 5: Experimental against predicted ultimate capacity**

Test name	Ultimate Capacity (kN)			Experimental Capacity / Predicted Capacity (-)	
	ICP-05	UWA-05	Test	ICP-05	UWA-05
Pile 1	300	272	177	0.68	0.74
Pile 2	261	239	115	0.38	0.42

**Dimensions of the pile, vibro-driven vs. impact-driven**

In this paragraph a CPT-method-based procedure to estimate the minimum size of a real-scale pile is presented. Besides, on the base of the above reported large-scale test, the minimum length required by a vibro-driven pile with comparable ultimate capacity of an impact-driven pile is evaluated. The loads for which the piles are pre-designed are those also acting on the reference jacket for a 10 MW turbine and can be found in [4-14].

In the analysis the following assumptions have been taken into account:

- The soil deposit consists of uniform well-graded sand; see the CPT tip resistance profile in Figure 20.
- The constant volume friction angle between sand and steel is  $\delta_{cv} = 26^\circ$ .
- The effective unit weight of the soil is  $\gamma' = 10 \text{ kN/m}^3$ .
- The pile thickness is  $t = 40 \text{ mm}$  and remains constant throughout the pile length.
- CPT-Methods provide reliable design indication for impact-driven piles. This assumption was corroborated by previous experiences in industry practices and experimental campaigns conducted by Fraunhofer IWES ([4-12], [4-13]).
- The cost of the steel for the piles is taken equal to 1200 €/t according to [4-18].

The last assumption allows the direct use of the deviation between prediction and experimental value of Pile 2 (Table 5, column 3) as a reduction factor to apply to CPT-methods prediction (Table 6 and Table 7, column 2) to obtain the expected vibro-driven pile capacity (Table 6 and Table 7, column 3). The results of this simple assessment are shown in Table 6 and Table 7.

**Table 6: Length and price difference according to UWA-05**

Pile length (m)	Capacity Impact-Driven (MN)	Capacity Vibro-driven (MN)	Volume (m <sup>3</sup> )	Weight (t)	Price (k€)
46	15.84	11.73	14.45	112.72	135.26
59	21.28	15.76	18.54	144.58	173.49

**Table 7: Length and price difference according to ICP-05**

Pile length (m)	Capacity Impact-Driven (kN)	Capacity Vibro-driven (MN)	Volume (m <sup>3</sup> )	Weight (t)	Price (k€)
46	15.57	10.56	14.45	112.72	135.26
62	22.87	15.51	19.48	151.93	182.31

It is first of all reassuring that the pile length calculated with two different CPT-methods comes to the same value (46 m). According to UWA-05 and the test results, a vibro-driven pile should be 28% longer than an impact-driven pile to reach comparable ultimate capacity. When considering ICP-05 the pile length should be 34% longer. Figure 21 shows the axial capacity of the vibro-driven piles with depth. The price difference is around 38 k€ for UWA-05 and around 47 k€ for ICP-05.

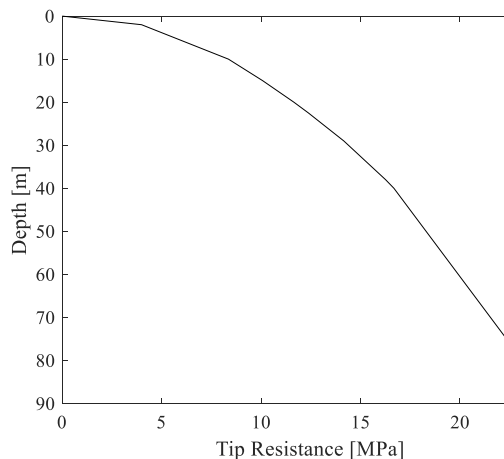


Figure 21: CPT profile used for the pre-design of the pile

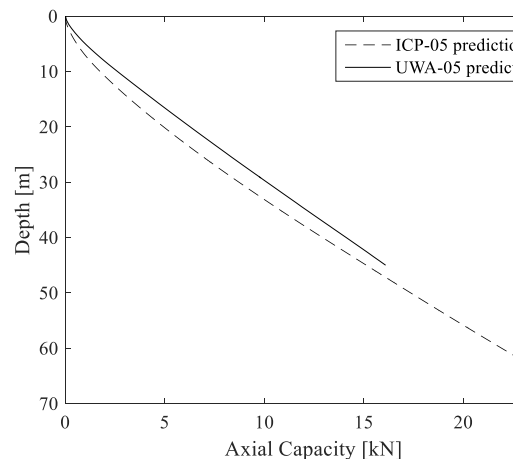


Figure 22: Axial capacity with depth of vibro-driven piles according to Table 6 and Table 7.

#### 4.1.3 Numerical model for axially loaded piles in tension

Object-oriented programming enables numerical models to generalize problems and offer thereby a useful tool for engineering assessments. In [4-07] it was demonstrated that the initial stiffness of an axially loaded pile could be simulated by means of a simplified axisymmetric numerical model. In this chapter it is presented how the same model can be generalized to any given pile geometry by implementing it with object-oriented programming. Such an extended model can be seen as a supporting tool for the design of piled foundations for jackets of any size. In the following sections the model is described and a number of insightful analyses are proposed.

#### 4.1.4 Description of the model

The computational analysis was carried through with the finite element program ABAQUS [4-16]. As mentioned in [4-07], the physics of the engineering problem (foundation and type of loading) allows for a two dimensional axisymmetric implementation of the computational model. The pile section is simplified with a solid section with mechanical and physical parameters equivalent to a hollow steel section with soil inside (see [4-07] and [4-15] for further details on this simplification). As a result of that, the pile resistance relies solely on the self-weight of the equivalent pile and on the contact friction between outer pile shaft and soil adjacent to the pile. 4-noded elements of the type CAX4 were used in the simulation. The tangential contact between pile and soil was simplistically defined as elasto - perfectly plastic by setting the built-in contact model "Penalty" with a default value Elastic-Slip calculated on an element length of 35mm. Thus, the frictional resistance acting on the pile outer surface depends on the horizontal stresses (which in turn depend on vertical stress and lateral earth pressure coefficient  $K$ ) and the friction angle between steel and sand,  $\delta$ . The boundary conditions were set by restraining the horizontal displacement of the external vertical border to nil, and by impeding vertical and horizontal

displacements on the bottom border. Although the model design aims at simulating the tensile capacity of piles, computations of piles undergoing compression are also possible and will be showed further in this paper. Each numerical computation consists of three steps:

- Geostatic Step; where only the soil with its own weight determines the initial stress field.
- Self-weight Step; where a defined part of the soil mass is replaced with the pile and the total weight of it is transferred to the soil elements.
- Load Step; where the pile is loaded in tension or compression by designating a displacement to the pile head.

The vertical stresses of at the end of the Geostatic Step and of the Load Step are shown in Figure 23 and Figure 24.

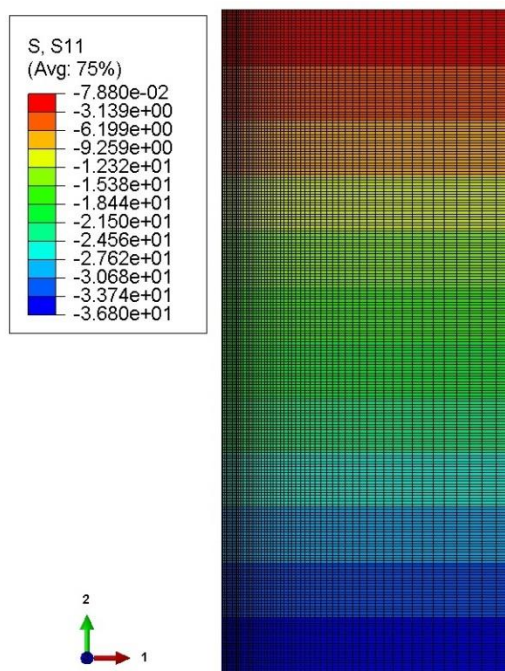


Figure 23: Image of the model after the geostatic step with representation of the vertical stress distribution. Pile part not yet active in the model.

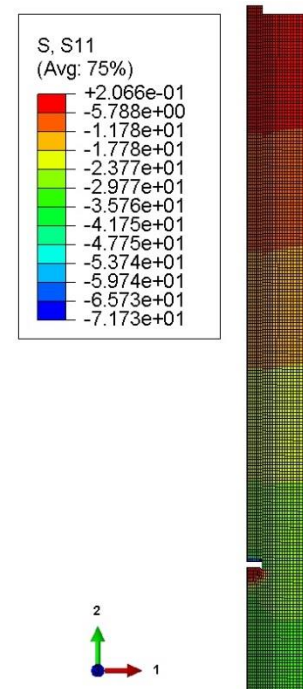


Figure 24: Zoom image of the pile model at the end of the Load Step with representation of the vertical stress distribution. Pile was 5 mm uplifted. Displacements are magnified in the image.

The numerical model of a pile subjected to tensile loading described above was generalized by means of object-oriented programming. The aim of the object-oriented programming was to be able to model piles of various geometry, representing any possible turbine upscaling, and different kinds of soil profiles. Object oriented programming enabled the following elements of the model to be flexibly implemented:

- Pile geometry: piles with different diameter,  $D$ , length,  $L$ , and wall thickness,  $t$  can be created and tested. As a result of the geometry chosen the dimensions of the model changes accordingly. The length of the model,  $h$  was after appropriate numerical study set to  $1.6 L$ . The width of the model,  $h$  was after appropriate numerical study set to  $10 D$ .
- Soil layers: different soil layers with different parameters can be implemented. The parameter of each soil layer can be independently assigned.

#### 4.1.5 Numerical analyses to assess the plausibility of the model

A critical issue when creating numerical models is to evaluate how representative the simulation is with respect to the engineering problem they aim to solve. To assess this property the model underwent three tests that proved its fundamental reliability and its resemblance to the reality of the engineering problem.

The parameters and the pile dimensions used in these simulations are listed in Table 8 and Table 9.

**Table 8: Parameters of sand and steel material used in the tests**

Property	Symbol	Unit	Value		
			Test 1	Test 2	Test 3
Length	L	m	6.30	6.30	5.30
Wall thickness	t	mm	6.30	6.30	6.30
Diameter	D	m	0.37	0.37	0.37

**Table 9: Parameters of sand and steel material**

Parameter	Symbol	Unit	Value
Sand material			
Friction angle	$\phi'$	°	33
Dilation angle	$\psi''$	°	10
Poisson ratio	$\nu$	-	0,27
Effective unit weight	$\gamma''$	kN/m <sup>3</sup>	10,7
Lateral earth pressure coefficient	$K$	-	0.45
Young's modulus	$E$	MPa	30
Steel material			
Soil-pile friction angle	$\delta$	°	17
Poisson ratio	$\nu_{steel}$	-	0,3
Effective unit weight	$\gamma'_{steel}$	kN/m <sup>3</sup>	6800
Young's modulus	$E_{steel}$	GPa	210

A first test was attempted at the end of the Self-weight Step and consisted in proving whether the sum of the normal stresses of the soil at pile toe,  $\Sigma\sigma_{vt}$ , added to the sum of the tangential stresses of the soil at pile shaft,  $\Sigma\tau_s$ , resulted in the total equivalent weight of the pile,  $W_{eq}$ :

$$\sum \sigma_{vt} + \sum \tau_s = W_{eq} \quad \text{Eq. 1}$$

This should reflect the property of the model to transfer each load applied to the piled foundation to the soil mass. The equivalent weight of the pile was 9.04 kN, while  $\Sigma\sigma_{vt}$  and  $\Sigma\tau_s$  were 6.49 and 2.55 respectively.

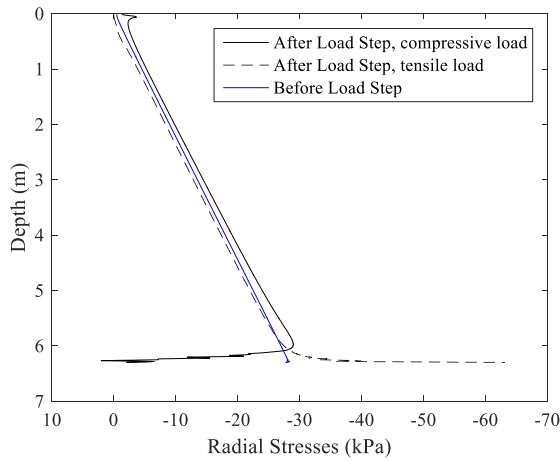


Figure 25: Radial stresses of the sand element adjacent to the pile shaft in three different steps. Before the Load Step in blue and after the Load Step in tension and compression.

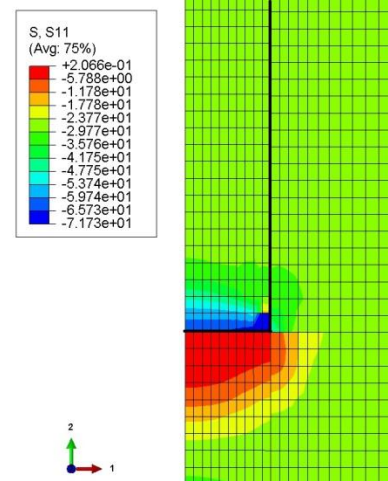


Figure 26: Radial stresses of the sand and steel elements at the pile toe.

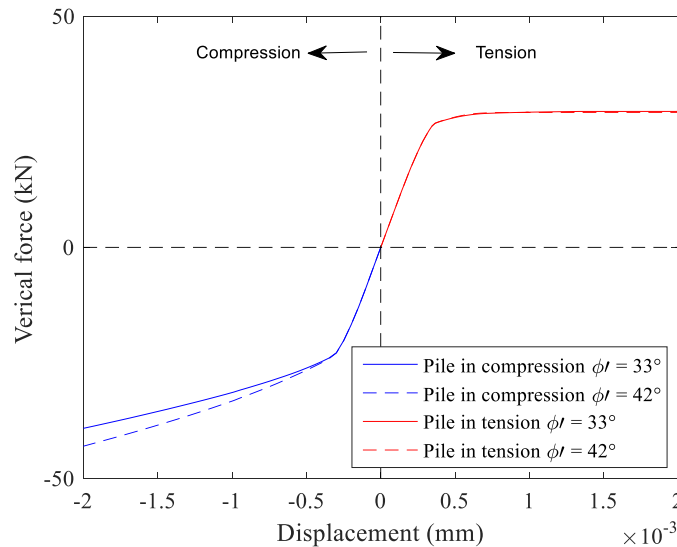


Figure 27: Simulations of force-displacement curves for tensile and compressive case and two different friction angles. In this simulation  $\delta$  was set to 22.

A second analysis involved the stress field of the soil elements adjacent to the pile in three different phases of the simulation: at the end of the Self-weight Step, at the end of the Load Step after compressive load and at the end of the Load Step after tensile load. The stress distribution with depth is illustrated in Figure 25. It is immediately apparent that after the compressive load the radial stresses increases whereas after the tensile load the radial stresses decreases. This phenomenon was expected and is in line with the theoretical expectations outlined in [4-17]. To physically explain such phenomenon two mechanisms can be evoked:

- The contraction/expansion of the pile shaft as a result of compressive/tensile loading, so called Poisson's effect.
- The tendency for the total field stress surrounding the pile to decrease when the pile is subjected to tension and to increase when the pile is subjected to compression

Another observation that can be made by examining Figure 25 is that close to the pile tip the tendency tends to reverse. This was also reported in [4-17], and can be ascribed to the particular stress distribution at pile tip and to the overlapping between the contact interfaces of pile shaft and pile toe. In Figure 26, a magnified view of the peculiar stress field around the pile tip after pile uplift is illustrated.

The third test dealt with the examination of the different failure mechanisms occurring in piles subjected to axial tension and compression. In Figure 27 computational simulations of force-displacement curves for tensile and compressive cases and for two different friction angles are shown. It must be noted that in this simulations  $\delta$  was set equal to 22 and thus independent of the friction angle  $\phi'$ . The initial stiffness of the curves in tension and compression appear to be very similar. This feature of the model can also be physically explained by recognizing that the mobilization of shaft resistance needs less displacement than that needed for the tip resistance (available only for piles under compression). In addition, not surprisingly, the friction angle does not influence the initial stiffness.

Further in the load-displacement curves, after the initial stiffness branch the behavior of the pile in tension differs considerably from that of the pile in compression. It is seen that friction angle affects only the pile in compression. This is a reflection of the fact that the soil underneath the pile undergoes plastic deformations when the pile is subjected to compressive load. Conversely,  $\phi'$  seems not to affect the post-initial stiffness curve of the pile in tension. This observation is also in line with theoretical and physical expectation and corroborates another peculiarity regarding piles undergoing axial loading which is the prominent role of the interface friction angle,  $\delta$ , in uplifted piles. Indeed for piles under tensile loading, the tip resistance does not offer any contribution and the failure occurs as soon as the contact friction between external pile shaft and adjacent soil reaches failure.

#### 4.1.6 Conclusions

The results of an experimental campaign including two large-scale impact-driven piles have been presented and interpreted by using CPT methods. Soil profile and steel price were assumed and are regarded to be rather realistic values. The analysis carried out with loads referring to a 10 MW wind turbine reveals that, on the base of the tests carried out, the price difference between impact-driven and vibro-drive piles is around 38 k€ when adopting UWA-05, and around 47 k€ when adopting ICP-05.

A numerical model with augmented flexibility provided by object-oriented programming was developed and is presented in this section. The plausibility of the model was tested by carrying out three tests which included stress analysis of the soil adjacent to the pile and load-displacement curve of piles in tension as well as of piles in compression. These model-corroboration tests were successful, and show that the model is able to reflect the physics of the engineering problem. Piles for jackets can be defined with variations in size, placed in different soils and can be assessed with the presented tool.

The experimental data collected are necessary but not sufficient to fully calibrate and validate the model. A natural subsequent step towards the optimization of the model would be the conduction of a second, comprehensive test campaign. Further experiments should be carried out to clarify the following crucial points:

- Stress field around the pile as a result vibro- or impact-driven installation.
- Better modelling of the contact interface. From an elastic-perfectly plastic model to a more appropriate formulation.
- Effect of preloading on ultimate capacity and initial stiffness and by means of that set-up effects.

The model should then be complemented with the latter points to obtain a fully validated tool to be used with confidence in piled foundations design.

## 4.2 References

- [4-01] Viking K.: Vibro-driveability – A field study of vibratory driven sheet piles in non-cohesive soils. PhD thesis, Royal Institute of Technology Stockholm, 2002.
- [4-02] Lammertz P.: Ermittlung der Tragfähigkeit vibrierter Stahlrohrpfähle in nicht bindigem Boden. PhD thesis, Universität Duisburg-Essen.
- [4-03] Borel S., Bustamante M., Rocher-Lacoste F.: The comparative bearing capacity of vibratory and impact driven piles. International symposium on vibratory pile driving and deep soil vibratory compaction, 2006.
- [4-04] Matlock B.G.W.M.: Comparison of the lateral bearing capacities of hammered and vibrated piles. 5<sup>th</sup> International Conference Offshore Foundations, 2015.
- [4-05] Deutsche Gesellschaft für Geotechnik e.V., Empfehlungen des Arbeitskreises "Pfähle" - EA-Pfähle (5.4.4.2), Berlin: Ernst & Sohn Verlag, 2012.
- [4-06] Matlock B.G.W.M.: Comparison of the lateral bearing capacities of hammered and vibrated piles. 5<sup>th</sup> International Conference Offshore Foundations, 2015.
- [4-07] INNWIND.EU: Innovations on component level (final report). Deliverable 4.1.3, 2015.
- [4-08] INNWIND.EU: Validation of innovations by tests on component level. Deliverable 4.1.4, 2015.
- [4-09] Lehane, B. A., Schneider, J. A. & Xu, X.: The UWA- 05 method for prediction of axial capacity of driven piles in sand. Proc. International Symposium 'Frontiers in Offshore Geotechnics'. Perth, Australia, Taylor & Francis Group, 2005.
- [4-10] API 2011: ISO 19901-4:2003 (Modified), Petroleum and natural gas industries-Specific requirements for offshore structures, Part 4-Geotechnical and Foundation Design Considerations.
- [4-11] Achmus M., Müller M.: Evaluation of pile capacity approaches with respect to piles for wind energy foundations in the North Sea. 2nd International Symposium on Frontiers in Offshore Geotechnics, 8-10 November 2010, University of Western Australia, Perth.
- [4-12] IRPWind: Deliverable 7.2.2 Report on geotechnical tests with model structures. (To be published in Feb. 2017)
- [4-13] Yang T., Jardine R., Guo, W., Chow F.: A comprehensive database of tests on axially loaded piles driven in sand. Elsevier, 2015.
- [4-14] INNWIND.EU: Innovative design of a 10MW steel-type jacket structure. Deliverable 4.3.4, 2015.
- [4-15] Achmus M., Lemke K., Abdel-Rahman K., Kuo Y.-S.: Numerical approach for the derivation of interaction diagrams for piles under cyclic axial loading. Proceedings of the Twenty-fifth International Ocean and Polar Engineering Conference, 2015.
- [4-16] ABAQUS 6.14 User's Manual. Simulia, Providence, USA, 2014.
- [4-17] De Nicola, A. und Randolph, M. 1993. *Tensile and compressive shaft capacity of piles in sand*. Journal of Geotechnical Engineering 119(12).
- [4-18] INNWIND.EU: PI-based Assessment of Innovative Concepts. Deliverable 1.2.3, 2014.

## 5 LOAD MITIGATION (UOL, DTU)

### 5.1 LOAD MITIGATION (Forwind-UOL)

#### 5.1.1 Semi-active damping devices

For large offshore wind turbines with taller towers, stronger winds hit the blades and consequently more power can be extracted from the air. Because the structure is subjected to severe wind and wave excitations, the fatigue loads are increased which is the main challenge in the design of the wind turbine support structure.

In recent years, the application of supplemental damping strategies for response reduction of the tower structure has received significant attention. In principle, load mitigation can be achieved through passive or active techniques. The majority of the research activity focuses on passive devices whereas the operation does not require an external power source. Active control systems, on the other hand, are extensively studied and tested for civil structures to protect the building against wind excitation and earthquakes. The operation of these systems requires continuous external power. On the other hand, semi-active devices combine the best features of both strategies, offering the reliability of passive devices while maintaining the versatility and adaptability of active devices [5-01].

For semi-active systems, the mechanical properties of the damper are adjusted according to the feedback from the structure to which it is attached. In addition, these devices require very small amount of external power compared to active dampers. The control force from the semi-active damper opposes the structural motion to alleviate external forces.

A detailed summary on the main research activities performed in the last years for the control of the wind turbine structures using damping devices is available in [5-02]. The numerical simulations performed by passive control devices include tuned mass dampers (TMD) [5-03][5-04], tuned liquid column damper (TLCD) [5-05][5-06] and viscous dampers [5-07][5-08]. The experimental investigations are mainly limited to down-scaled models in the laboratory with passive control strategies [5-09] or the recently published investigation with magnetorheological dampers by Caterino [5-02]. He has developed a control strategy to reduce the wind induced vibrations of a 1/20 scaled wind turbine tower using an adjustable restraint at the tower base. He has highlighted the performance of the proposed strategy in reducing the bending stress imposed by the wind actions.

Passive tuned mass dampers have been studied in Deliverable D4.13 [5-11] to mitigate the tower top displacements. It was shown that depending on the mass ratio of the TMDs, the DELs can be reduced up to 30% in sideways direction while the effectiveness of these devices is marginal in fore-aft direction. Semi-active dampers operate in a broad frequency bandwidth and are more effective in both directions. This section investigates the numerical modelling of a magnetorheological (MR) damper to semi-actively mitigate wind induced vibrations of large wind turbines. The numerical model of a MR damper is developed in Simulink. The aero elastic simulation of the 20 MW reference wind turbine is created in DNV.GL's Bladed software. Firstly, an eigenvalue analysis is performed and Eigen frequencies of the tower and blades are compared with those for the 20MW RWT in Deliverable D1.25 (a) [5-12]. Secondly, time domain simulations are performed at different wind speeds and the bending force and moments are extracted at the tower base. Finally, the simulations with an integrated MR damping system are carried out and damage equivalent loads (DEL) are calculated versus wind speed. The results show the effectiveness of the developed semi-active damping system within the whole operational range of the wind turbine.

### Magnetorheological damper

A magnetorheological damper is a damper which consists of a hydraulic cylinder, electromagnetic coils and magnetorheological fluid as shown in Figure 28. The MR damper is controlled by a magnetic field and its damping characteristics can be continuously controlled by varying the power of the magnetic field. In the presence of a magnetic field, the particles in the MR fluid are formed into chain-like fibrous structures.

The MR damper is operating as a passive damper without the presence of the magnetic field. Applying a magnetic field to the damper, it behaves as a semi-active damper. The main characteristics of MR dampers are listed below:

- It requires low power sources, i.e. only several Watts are needed to generate damper forces as large as 3 kN.
- Response time is very small, i.e. less than a few milliseconds, and it can be easily controlled.
- The MR performance is quite stable within a broad temperature range between -40 to 150°C

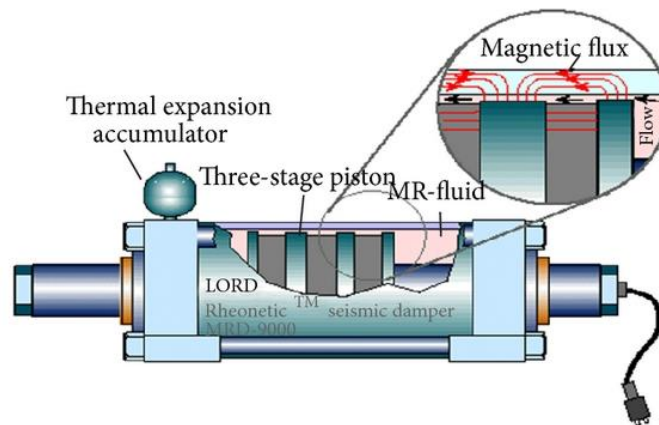


Figure 28: Schematic of a large-scale MR fluid damper which is 1-meter long and weighs 250 kg. This damper can exert 20 tons (200 kN) of force [5-02]

### Dynamic modelling of a MR damper

In order to characterize the behavior of MR dampers several models are proposed by different researchers [5-02][5-10]. The most well know model is proposed by Spencer et al. [5-01] which describes the MR behavior using the modified Bouc-Wen model represented in Figure 29. He showed that this model accurately captures both the force–displacement and the force–velocity hysteresis loops.

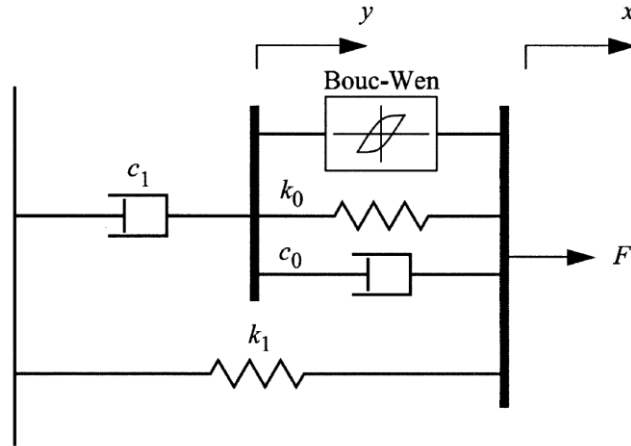


Figure 29: Modified Bouc-Wen model for the MR damper

According to the modified Bouc-Wen model, the damper force can be predicted from the following differential equations:

$$F = c_1 \dot{y} + k(\dot{x} - x_0). \quad \text{Eq. 2}$$

$$\dot{z} = -\gamma |\dot{x} - \dot{y}| |z| |z|^{n-1} - \beta (\dot{x} - \dot{y}) |z|^n + A (\dot{x} - \dot{y}). \quad \text{Eq. 3}$$

$$\dot{y} = \frac{1}{(c_0 + c_1)} [\alpha z + c_0 \dot{x} + k_0 (x - y)] \quad \text{Eq. 4}$$

with

$z$  and  $\alpha$ : revolutionary variables which describe the hysteretic behavior of the damper,

$c_0$ : viscous damping at high velocities,

$c_1$ : viscous damping at high velocities,

$k_0$ : stiffness at large velocities,

$k_1$ : accumulator stiffness,

$x_0$ : initial displacement of spring with stiffness  $k_1$ ,

$\gamma, \beta, \alpha$  and  $A$ : parameters to adjust the shape of the hysteresis loop,

$c_0, c_1$  and  $\alpha$  are defined as below:

$$\alpha = \alpha_a + \alpha_b u \quad \text{Eq. 5}$$

$$c_1 = c_{1a} + c_{1b} u \quad \text{Eq. 6}$$

$$c_0 = c_{0a} + c_{0b} u \quad \text{Eq. 7}$$

$$\dot{u} = -\eta(u - v) \quad \text{Eq. 8}$$

where  $\alpha_a, \alpha_b, c_{0a}, c_{0b}, c_{1a}$  and  $c_{1b}$  are parameters which account the dependency of the MR damper on the applied voltage. A first-order filter with time constant of  $\eta$  is applied to the input voltage,  $v$  to get the output voltages,  $u$ . The constructive equations Eq. 2 to Eq. 4 are modelled in Simulink software whereas the inputs are voltage and displacement and the damper force is the only output. This model is tested and verified by a step voltage and triangular displacement as described by Spencer in [5-01]. The generated damper force satisfactory agrees with his results. However, both displacement and velocity signals are required in calculation of the MR damper force. As the next step, the time domain simulations performed in DNV.GL Bladed should be

coupled with the MR damper model in Simulink to transfer these signals and calculate the applied damper force. In what follows, the procedure to couple the MR damper model with the time domain simulations will be discussed.

### 5.1.2 Description of the performed studies of the innovation

#### Boundary conditions

The performed studies on the mass damper at the tower top are based on the INN WIND.EU reference design [5-11]. The aero elastic simulation tool DNV GL Bladed has been used to perform the simulations in the time domain. The site parameters are chosen according to the wind turbine class IA. The wave characteristics, i.e. wave period and height, are taken from the UpWind.eu design basis for the deep water site [5-13]. The values are shown in Table 10.

**Table 10 - Environment conditions for wind turbulence and sea state parameters**

V [m/s]	2	4	6	8	10	12	14	16	18	20	22	24
TI [%]	29.2	20.4	17.5	16	15.2	14.6	14.2	13.9	13.6	13.4	13.3	13.1
Hs [m]	1.07	1.1	1.18	1.31	1.48	1.7	1.91	2.19	2.47	2.76	3.09	3.42
Tp [m]	6.03	5.88	5.76	5.67	5.74	5.88	6.07	6.37	6.71	6.99	7.4	7.8

#### Mechanism to calculate the MR damper forces

Figure 30 demonstrates the mechanism to calculate the MR force using the tower top simulated accelerations. A Simulink model of a MR damper is developed and connected to Bladed via an external Dynamic-Link Library (DLL). The simulated time series of accelerations at the points where it is attached to the tower are recorded. Velocity and displacement signals can be attained by integrating the simulated accelerations. The damper force,  $F_D$ , is then obtained in Simulink according to Bouc-Wen model represented by Equations Eq. 2 to Eq. 4. This force is returned to the Bladed and is applied as a reaction force at the damper location (see Figure 30).

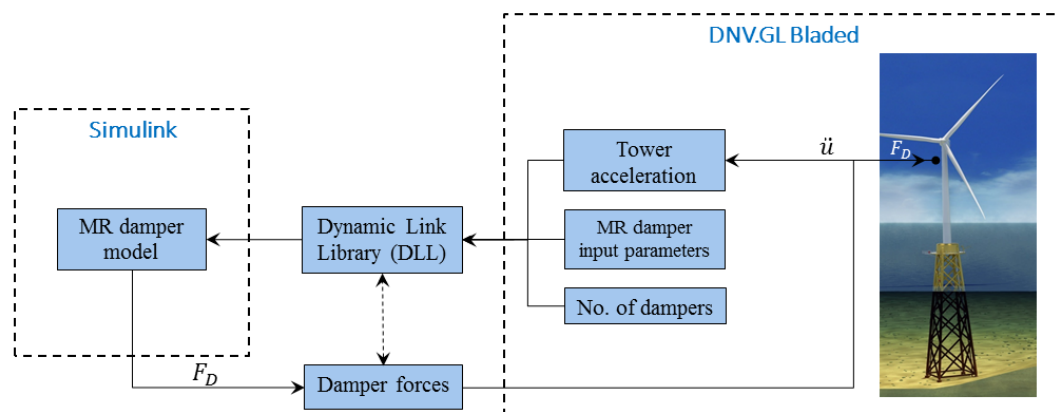


**Figure 30: Numerical modelling of the MR damper shows the mechanism to calculate the damper forces using the tower accelerations.**

Results of the performed studies of the innovation

In this section, results of the load verification with integrating the semi-active MR damper are discussed. A typical time interval of the nacelle displacements in the fore-aft and side-to-side directions are demonstrated in Figure 31. It is obvious that the tower top vibration, particularly in the sideways direction, is considerably dissipated compared to the reference configuration. The MR damper is mainly effective in the sideways direction. This is due to the low aerodynamic damping in this direction. The aerodynamic damping is the dominant phenomenon in the fore-aft direction and therefore the performance of the MR damper is marginal in this direction.

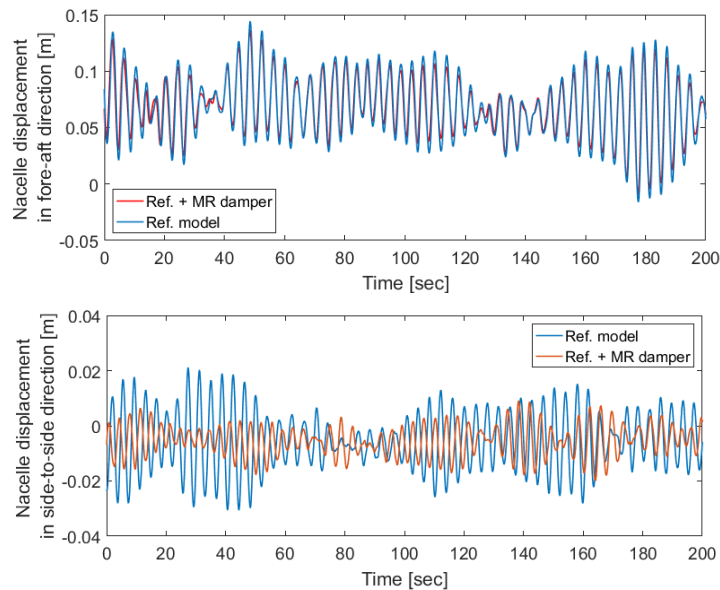


**Figure 31: Nacelle displacement with and without MR damper in the fore-aft (top) and side-to-side (bottom) at 4 m/s mean wind speed**

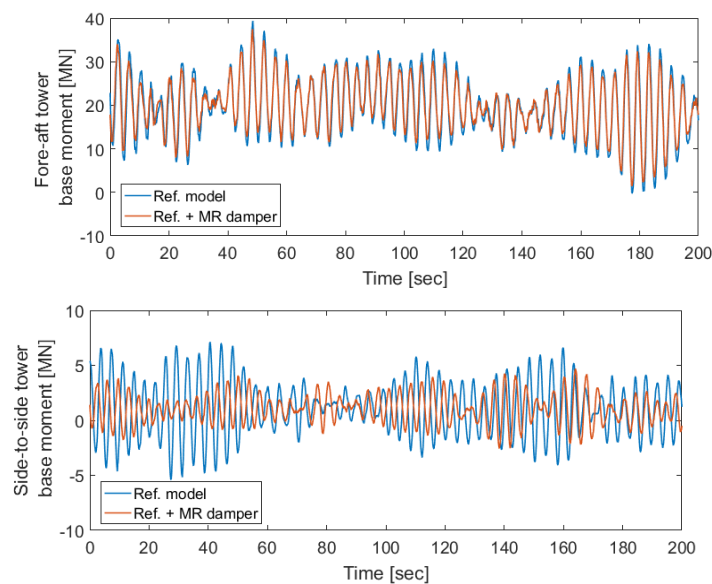


**Figure 32: Tower base moment with and without MR damper in the fore-aft (top) and side-to-side (bottom) at 4 m/s mean wind speed**

Figure 6 demonstrates the tower base moments in the fore-aft ( $M_y$ ) and side-to-side directions ( $M_x$ ), respectively. Although the MR damper is mounted in the fore-aft direction, the reduction of the tower base moments is obvious only in the side-to-side direction.

### 5.1.3 Conclusion

In this section, the results of innovative concepts on the component level for the 20 MW reference wind turbine are shown. The numerical model of a semi-active MR damper is developed to mitigate the structural vibrations at the tower top location. The preliminary results show that the semi-active damper can effectively alleviate the external loads within the whole operational range. The improved tower base loads are obtained and compared with the reference design. The integration of the semi-active dampers in the early stage phase of the jacket design could significantly alleviate the interface loads which would result in an optimized and economic jacket structure.

## 5.2 Development of magneto-rheological damper for jacket substructure for 20 MW wind turbines at 50 m water depths (DTU)

### 5.2.1 Summary of main developments on component level from task 4.1.3: applicability of developments, main challenges, and bottlenecks for the upscaling to 20 MW

Passive tuned vibration absorbers (TVAs) and passive tuned mass dampers (TMDs) have been studied as load mitigation techniques for the DTU 10 MW reference wind turbine in Deliverable D4.1.3 [5-14]. It has been shown that the TVAs are able to reduce the tower top displacement by nearly 36%. The TMDs succeed to reduce the sideways bending moment at the tower base by up to 25%. However, it has been noted that these load mitigation techniques, which operate on the support structure as a whole, affect only a narrow frequency range, which is non-optimal for a system with multiple excitation frequencies. Moreover, as the wind turbine becomes larger, disturbances and changes in natural frequencies can lead to the de-tuning of the damper system: whence passive device becomes non-operational.

Semi-active magneto-rheological (MR) dampers have been proposed as an alternative to the passive systems. MR dampers can have a local effect and can be used in multiple units to accommodate various exciting frequencies. They are moderate in size and may not require extra space. They can be put in place at the substructure level, eliminating the necessity of integrated design of the couple made of the support structure and the rotor-and-nacelle assembly. If these devices can relatively easily be up scaled, they can work under various operational conditions: passive, semi-active, and active. The objective of this study is to mitigate fatigue loads on jacket substructure using MR dampers.

### 5.2.2 Reference 20MW wind turbine, jacket substructure, and environmental conditions

#### Environmental conditions and aero-hydro-servo-elastic simulations

The environmental conditions corresponding to the IEC class 1C [5-15] along with the site specific ocean conditions [5-16] as shown in Table 11. The fatigue load assessment is carried out based on the IEC 61400-3 [5-17] design load case DLC 1.2 using the hydro-servo-aero-elastic software package HAWC2 [5-18].

Table 11: Metocean conditions used for load assessment on the structure [5-16]

Wind speed [m/s]	Normal turbulence Intensity [%]	Expected significant wave height, Hs [m]	Peak period, Tp [s]	Expected annual frequency [%]
5	22.44	1.140	5.820	10.65
7	18.60	1.245	5.715	12.40
9	16.47	1.395	5.705	12.88
11	15.11	1.590	5.810	12.63
13	14.17	1.805	5.975	11.48
15	13.48	2.050	6.220	9.36
17	12.95	2.330	6.540	7.22
19	12.54	2.615	6.850	4.78
21	12.20	2.925	7.195	3.57
23	11.92	3.255	7.600	2.39
25	11.69	3.600	7.950	1.70

The operational wind range is divided into 11 mean wind speed bins, which are each linked to a particular sea state characterized by an expected significant wave height and a peak spectral

period. A total of 16 primary wind directions equally spaced around the jacket are used in the computation of the fatigue damage equivalent loads. This set of conditions provides  $11 \times 1 \times 3 \times 16 = 528$  10-minute load time series. The wave height is modelled based on JONSWAP spectrum at the expected value of the sea state characteristics conditional on the mean wind speed.

### 20 MW reference wind turbine

The wind turbine considered here is the INN WIND.EU 20 MW reference wind turbine (INN WIND.EU 20 MW RWT) whose characteristics are presented in Table 12 [5-19]. It is a variable-speed, pitch-controlled, direct drive machine.

**Table 12: Key design parameters of the INN WIND 20 MW RWT**

Parameters	Values
Wind regime	(see table 1)
Rotor type, orientation	3 bladed - Clockwise rotation - Upwind
Control	Variable speed - Collective pitch
Cut-in, rated, cut-out wind speed	4 m/s, 11.4 m/s, 25 m/s
Rated power	20 MW
Rotor, hub diameter	252.2 m, 7.9 m
Hub height	167.9 m
Drivetrain	Medium speed, Multiple-stage Gearbox
Minimum, maximum rotor speed	4.45 rpm, 7.13 rpm
Maximum generator speed	339.4 rpm
Gearbox ratio	47.6
Maximum tip speed	90.0 m/s
Hub overhang	10.0 m
Shaft tilt, coning angle	5.0°, -2.5°
Blade prebend	4.7 m
Rotor mass including hub	632,016 kg
Nacelle mass	1,098,270 kg

### Jacket substructure

The substructure is a jacket obtained by upscaling the 4-legged jacket designed at the 10 MW scale to 20 MW. The 10 MW version has been proposed in [5-20]. The mean sea level is identical in 10 MW and in 20 MW cases, which means that the jacket is not to be up scaled vertically but only horizontally. To obtain an adequate scale factor, a hypothesis is made: the optimal scale factor is between 1.0 (no scaling) and 1.414 (scaling with the same proportion as that of the turbine). Some iterations result in a scale factor of about 1.3, which is not optimal but appropriate to satisfy ultimate limit state (ULS) and fatigue limit state (FLS).

The new jacket is described as per Table 13. It has been checked against ULS by applying a design load of 9000 kN as thrust force at its rotor hub centre. At the selected hotspots, the maximal utilisation factor after considering partial safety factor is 0.96 when a steel of 235 MPa yield strength is used. The fatigue damage accumulated over 25 years is 0.71.

**Table 13: Jacket substructure properties**

Jacket general	Dimensions	Value
Base Width	[m]	22.39
Top Width	[m]	13.53
Interface elevation	[mMSL]	26
Transition Piece height	[m]	10
Number of horizontal braces		4 (mudbraces)
<b>Number of legs</b>		4
Jacket legs outer diameter (upper / lower leg)	[mm]	979.6/905.8
Jacket legs maximum wall thickness	[mm]	97.6
Jacket legs minimum wall thickness	[mm]	60.7
<b>Number of x-braces levels</b>		4
Max. Upper x-braces diameters (outer)	[mm]	712.4
Max. Upper x-braces wall thicknesses	[mm]	26.4
Max. Middle upper x-braces diameters (outer)	[mm]	923.1
Max. Middle upper x-braces wall thicknesses	[mm]	131.7
Max. Middle lower x-braces diameters (outer)	[mm]	714.0
Max. Middle lower x-braces wall thicknesses	[mm]	27.2
Max. Lower x-braces diameters (outer)	[mm]	712.4
Max. Lower x-braces wall thicknesses	[mm]	26.4
<b>Natural frequency overall structure</b>		
1 <sup>st</sup> Eigen frequency (1 <sup>st</sup> bending mode)	[Hz]	0.1841

### 5.2.3 Magneto-rheological damper device

#### Physical description and mathematical modelling

. Magneto-rheological dampers are schematically made of a piston which translates in a magneto-rheological fluid. External actions that tend to move the piston exert strain on the fluid and the generated stresses develop a force that resists the external displacement. Other contributions to the force include the fluid inertial effect and the elastic contribution of the accumulator. Kim Y et al. [5-21] have offered the schematic representation of a typical magneto-rheological damper device as depicted in Figure 33.

The relationship between the exciting external actions on the piston (displacement, velocity, and acceleration) and the reaction force developed by the damper system is extremely nonlinear and presents a hysteretic loop. In order to accurately represent the physics of MR dampers, various phenomena, e.g. fluid inertia and shear thinning effects should be considered [5-22]. Yang G et al. [5-22] proposed a phenomenological model based on Bouc-Wen hysteresis model [5-23] as shown in Figure 34. The specificity of this model rests on the variable damping coefficient. In addition to its superior ability to estimate the MR damper behaviour, this model has the advantage to use few parameters and state variables compared to the other state-of-the-art models [5-22].

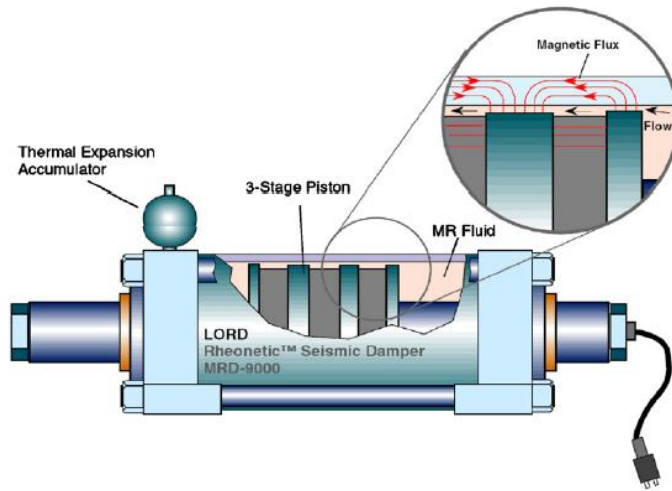


Figure 33: Schematic representation of a typical MR damper [5-21]

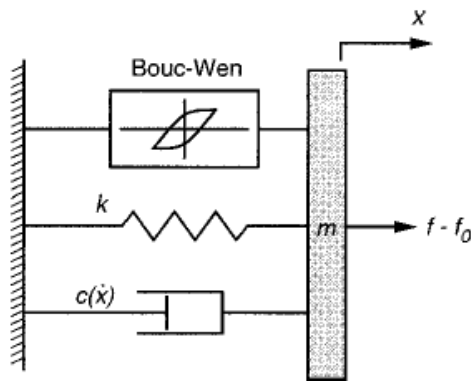


Figure 34: Phenomenological model of MR damper proposed by Yang G et al. [5-22]

The force equilibrium along the x-axis gives the damper force:

$$f = m\ddot{x} + c(\dot{x})\dot{x} + kx + az + f_0 \quad \text{Eq. 9}$$

with the evolutionary variable  $z$  from the Bouc-Wen model [5-23] is obtained by:

$$\dot{z} = -\gamma|\dot{x}|z|z|^{n-1} - \beta\dot{x}|z|^n + A\dot{x} \quad \text{Eq. 10}$$

and the variable damping coefficient:

$$c(\dot{x}) = a_1 e^{-(a_2|\dot{x}|)^p} \quad \text{Eq. 11}$$

where the variables are described in Table 14 for a constant current  $I_{max} = 2.0 \text{ A}$ . The dynamics when the MR fluid reaches the rheological equilibrium needs to be accommodated by a first order filter:

$$H(s) = \frac{31.4}{s + 31.4} \quad \text{Eq. 12}$$

**Table 14: Variable describing the MR damper model**

Symbols	Unit	Description	Values
$\gamma$	$m^{-1}$	Bouc-Wen constant	25 179.04
$\beta$	$m^{-1}$	Bouc-Wen constant	27.1603
$A$	$m^{-1}$	Bouc-Wen constant	1 377.9788
$k$	$\frac{N}{m}$	Accumulator stiffness and MR fluid compressibility	20.1595
$p$	-	Positive constant	0.2442
$\alpha$	N	Positive constant	2.3000 E 5
$a_1$	$\frac{N}{s/m}$	Positive constant	35.000 E 6
$a_2$	$\frac{s}{m}$	Positive constant	4 335.00
$m$	kg	Equivalent mass which represents the MR fluid stiction phenomenon and inertia effect	22 000
$n$	-	Bouc-Wen constant	6.7300
$f_0$	N	Damper friction force due to seals and measurement bias	5 126.00

In contrast to the automobile industry, large scale MR dampers have been developed for the civil engineering structures. For instance, Yang G *et al.* [5-22] have studied the dynamic behaviour of a 200 kN damper whose variable values are given in Table 32-4. For the wind energy industry where structures and their components are larger, parallel assemblages of such MR dampers may be required, i.e. a pair of MR dampers is used to obtain a total capacity of 400 kN per equipped brace.

The selected 200 kN device is 1.00 m and about 300 mm wide with 203 mm inside diameter. It is composed of 5.0 litres of MR fluid and 1.5 km of coil wire for a mass of 250 kg. The total coil has an induction of 6.6 H and a resistance of 21.9  $\Omega$ . With a stroke of  $\pm 80$  mm, about 90 cm<sup>3</sup> of fluid is energized by the magnetic field at any given instant.

#### Operational conditions and control strategy

The observation of the selected MR damper mathematical model indicates that even with zero current, MR dampers will still react to external actions. This property allows a minimum service even if a failure occurs or the input energy is null. In the other extreme, the current at which the saturation of the MR effect starts can be applied. The input energy is then maximal but not necessarily needed by the damper if the excitation requirements are not considerable for example. Between the two extreme cases, a control strategy can help to efficiently use the input energy. The idea is to input a current proportional to exciting actions. Several studies have shown the appropriateness of fuzzy logic as a control methodology for this type of problems ([5-24], [5-25]). These three operational strategies respectively correspond to passive, active, and semi-active case. As the total energy needed by the damper devices are relatively small (see below), the active strategy is opted in the present study.

#### Application on jacket and installation process

The vibrations of the jacket braces engender the motions of the brace ends and inversely. Exerting an action that counteracts the relative motions of brace ends will reduce brace vibrations. If a force was set to inhibit brace node motions, braces would vibrate less, and less fatigue would be engendered. MR damper devices are suitable for this purpose as the piston basically resists to the exterior actions. Inserted inside a brace with its base attached to one brace end and its piston

to the second brace end, the relative motion of the brace nodes is hindered by the damper force, which should translate into reduction of the global fatigue damage.

The system MR damper and brace described above can be built up during the jacket manufacturing in four main steps (Figure 35):

1. **Step (a):** a can with flattened side(s) that firmly fits the leg interior is inserted into the leg; if necessary, an extra fixative point like bolt can be added. The MR damper base is hooked to the can.
2. **Step (b):** The X-brace is put in place with the relevant brace set around the MR damper, which is possible due to the transversal size of the damper (less than 600 mm).
3. **Step (c):** The piston is pulled off and hooked to the second can, which is already set inside the other leg.
4. **Step (d):** The second leg is put in place as the piston is brought to its neutral position.

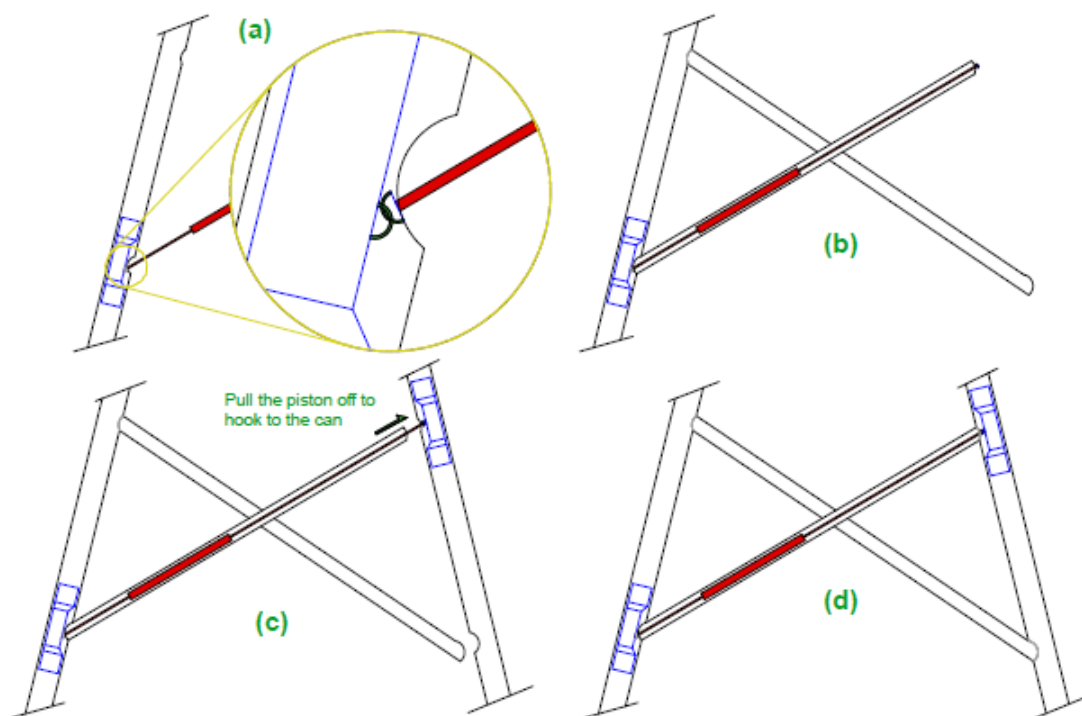


Figure 35: Installation steps of the MR damper into the jacket brace. (a) Hooking of the first MR damper end on the inserted can. (b) The X-brace is put in place. (c) Hooking of the second MR damper end. (d) Welding of the legs to the X-brace.

## 5.2.4 Simulations and results

### Fatigue calculations

The welds between the legs and the braces at the lower level are selected as the hotspots ([5-14], [5-20]). The stress concentration factors (SCFs) have been calculated according to DNV RP C203 [5-26]. For a given joint, the joint parameterization as given by Figure 36 is used for the SCF calculation. The characteristic stresses around the welds along with the SCFs for K-joints are given

by the relations from DNV RP C203 [5-26]. From the hotspot characteristic stresses,  $\sigma_i$ , the design stresses are obtained by:

$$\sigma_{di} = \gamma_f \cdot \gamma_m \cdot \gamma_n \cdot \gamma_x \sigma_{ni} \quad \text{Eq. 13}$$

where the safety factors are taken from Ref [5-27]:  
 $\gamma_f = 1.20$  is the partial safety factor associated to fatigue stress range counting;  
 $\gamma_m = 1.25$  is the partial safety factor associated to the material properties;  
 $\gamma_n = 1.10$  is the partial safety factor associated to the component's consequence of failure.  
 $\gamma_x = 1.50$  is an additional partial safety factor due to increased uncertainty in stress concentration resulting from weld distortion or corrosion etc.

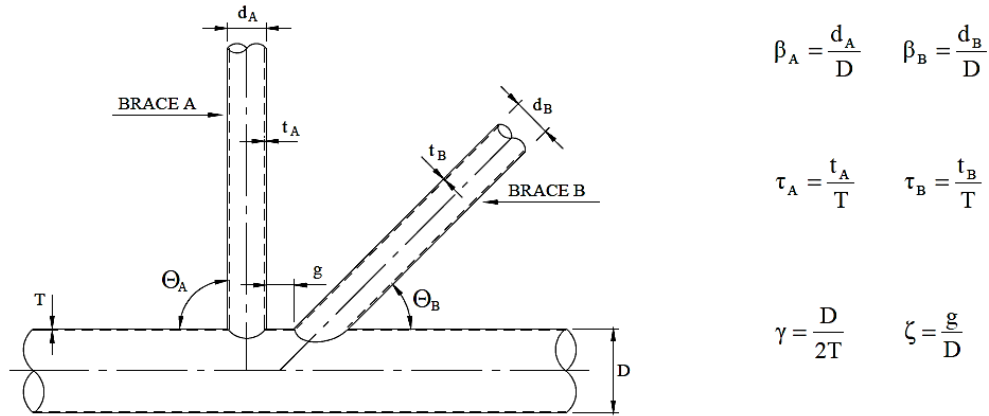


Figure 36: K-joint parameterization [5-26].

The stress ranges are obtained from the Rainflow counting method applied on the design stress time series. The number of cycles,  $N$ , corresponding to full damage induced by a given stress range,  $\Delta\sigma$ , is obtained by the design S-N curve, i.e. the T-curve in sea water with cathodic protection as per DNV RP C203 [5-26], which is described as:

$$\log(N) = \log(\bar{a}) - m \cdot \log\left(\Delta\sigma \cdot \left(\frac{t}{t_{ref}}\right)^k\right) \quad \text{Eq. 14}$$

Where,

- $m$  and  $\log a$  = the negative inverse slope of the S-N curve and the intercept of  $\log N$  axis, respectively. For S-N curves in seawater with cathodic protection, ( $m = 3$ ,  $\log a = 11.764$ ) for  $N < 10^6$ , and ( $m = 5$ ,  $\log a = 15.606$ ) for  $N > 10^6$ ;
- $t$  = the thickness through which the crack will most likely grow;  $t = t_{ref}$  if  $t < t_{ref}$ ;
- $t_{ref}$  = the reference thickness equal to 32 mm;
- $k$  = the exponent of fatigue strength.  $k = 0.25$  for  $SCF < 10.0$  and  $k = 0.30$  for  $SCF > 10.0$ .

Palmgren Miner's rule is applied to accumulate the induced damage. During one year, the accumulated damage is expressed as:

$$D_1 = \gamma_{DF} \frac{T_1}{T} \int_{V_{in}}^{V_{out}} \int_{\Delta\sigma_A}^{\Delta\sigma_B} \frac{n(\Delta\sigma|V, T)}{N(\Delta\sigma)} p(V) d\Delta\sigma dV \quad \text{Eq. 15}$$

where  $\gamma_{DF} = 3.0$  is the fatigue reserve factor associated with lack of possibility for inspections,  $T_1$  is the number of seconds in one year,  $T = 600\text{ s}$  is the simulation duration,  $N(\Delta\sigma)$  is the number of cycles that can cause full damage under the stress range  $\Delta\sigma$ ,  $n(\Delta\sigma|V, T)$  is the actual yearly number of cycles corresponding to the stress range  $\Delta\sigma$ , given a wind speed  $V$  and the simulation duration  $T$ , and  $p(V)$  is the probability of occurrence of the wind speed  $V$ . The change in fatigue damage from the reference setup to a new one is computed as,

$$\Delta(D_1) = D_1^{new} (D_1^{ref})^{-1} - 1. \quad \text{Eq. 16}$$

### Reference case and brace selection

Design load case (DLC) 1.2 simulations are carried out for the reference case, which is the structure with no damper. The fatigue analysis at the 16 hotspots reveals that the maximum fatigue damage (0.71) occurs at node 2 of side Q (see Figure 37), whose X-brace is used for the MR damper installation. Figure 37 shows the nomenclature used for sides and nodes.

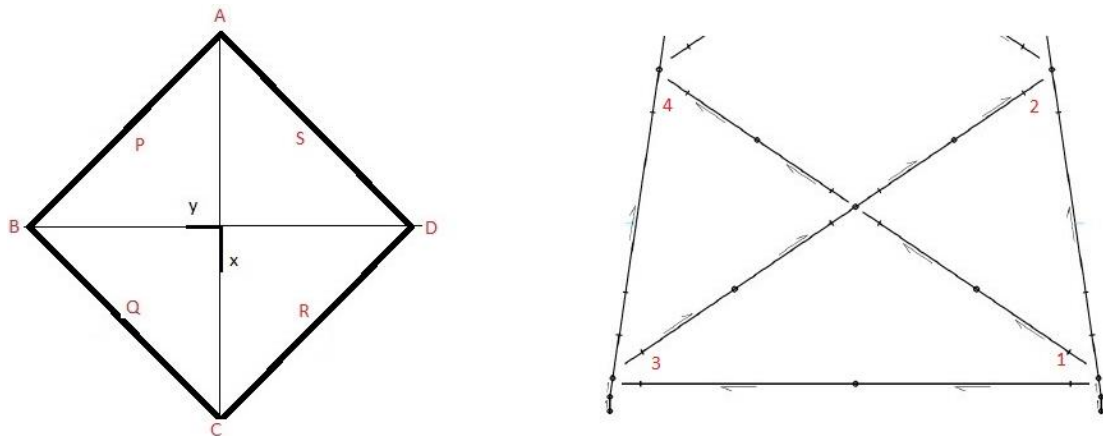


Figure 37: Geometry of the jacket. (Left) plan view with side label. (Right) position of the selected hotspots on a typical jacket side. A joint name is made of the side label name (P, Q, R, or S) and the joint position (1, 2, 3, or 4). For example, joint names can be P1, P2 etc. Sides are looked at from the inside of the jacket.

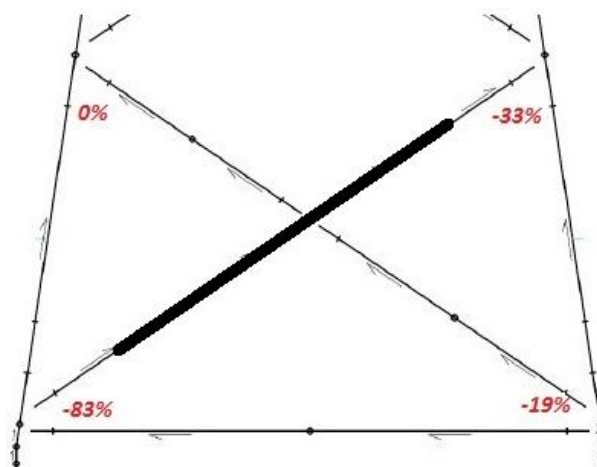


Figure 38: Damage reduction on side Q after setting-up a pair of damper.

### Efficiency of a double MR damper inserted in one brace

In order to alleviate the fatigue damage that occurs at the critical hotspot as detected in the reference structure, a pair of MR damper is inserted into the brace Q2-Q3. The simulations have shown a damage reduction of 33% at node Q2 and 83% at node Q3. At nodes Q1 and Q4, the reductions are 19% and 0%, respectively, as depicted in Figure 38.

The reductions are mainly due to the reduction of the axial load amplitude. Indeed, the damper systems counteract the axial deformation of the equipped brace, which reduces the axial strain amplitude and ultimately the axial force amplitude as shown in Figure 39.

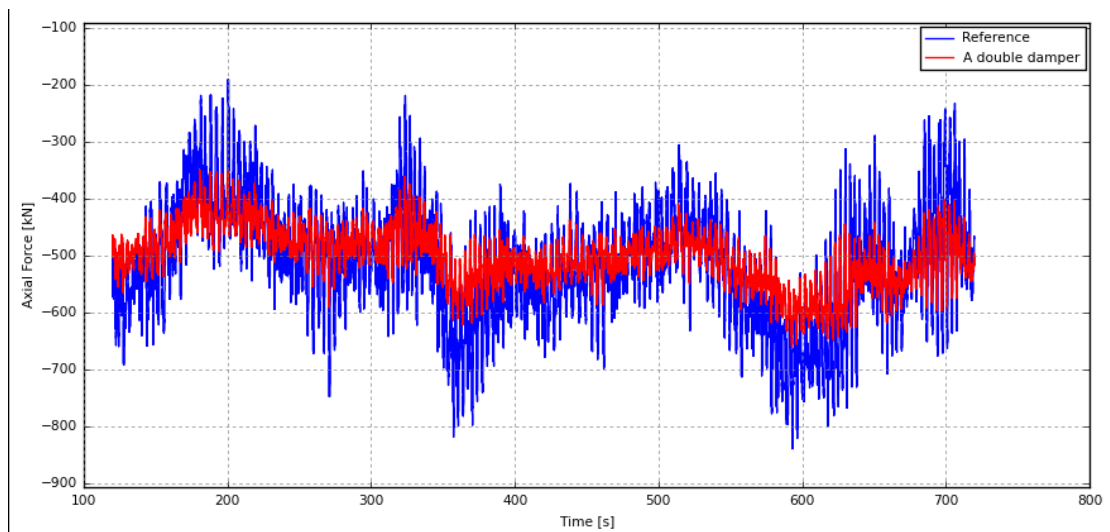


Figure 39: Time series of the axial forces at node Q2. The reference axial force (in blue) shows higher amplitude than the axial force with a double damper (in red).

The reduction in amplitude of the axial force translates in reduction of fatigue loads as can be seen in Figure 40, showing the spectra of the time series presented in Figure 39. It can be seen that the energy is significantly reduced with the damper.

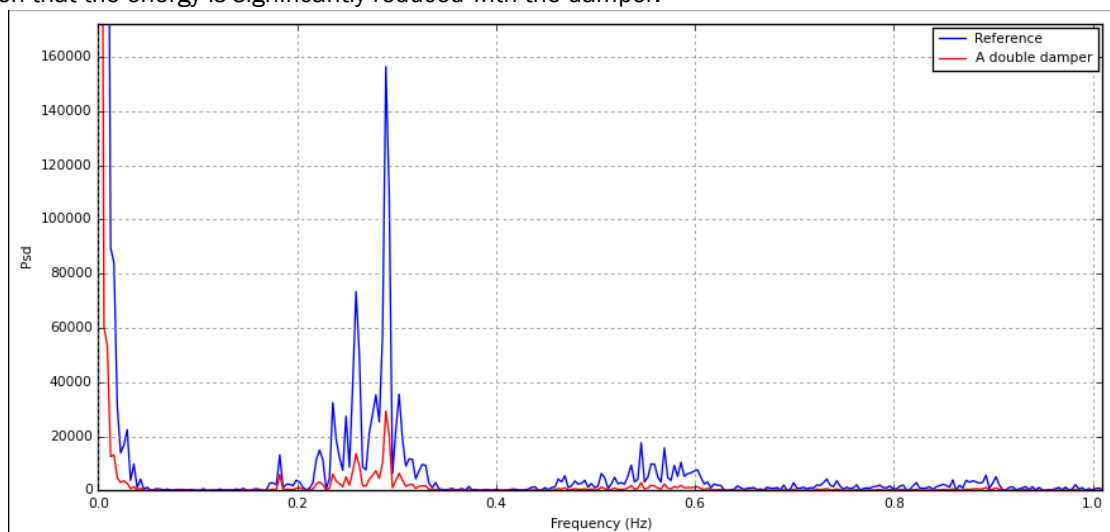


Figure 40: Spectra of the axial forces at node Q2. The reference axial force (in blue) shows higher amplitude than the axial force with a double damper (in red).

However, the fatigue damage due to bending moments at the equipped brace nodes is not decreased. Figure 41 shows the time series and the spectra for the out-of-plane bending moments at node Q2. A relatively small increase of the fatigue damage can be noted from the spectra. This is due to the fact that the connection between the K-joint and the brace gets a limited displacement and behaves more like a rigid joint, thus attracts more loads.

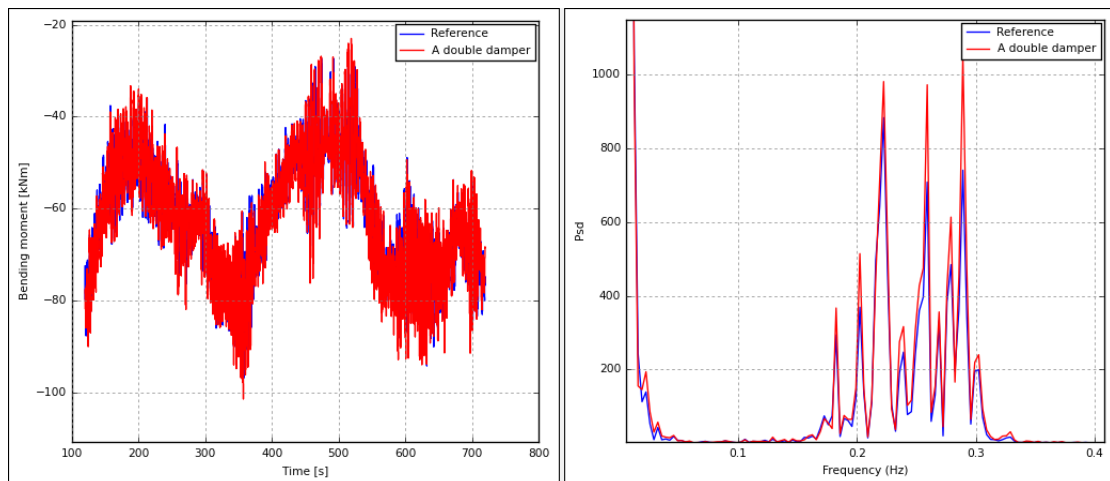


Figure 41: Time series and spectra of the out-of-plane bending moment at node Q2. The reference load (in blue) shows relatively smaller amplitude than the load with a double damper (in red).

At node Q1, the fatigue reduction is caused by the vibration reduction of leg Q1-Q2. However, there is no noticeable change at node Q4 as the damper system does not significantly affect leg Q3-Q4. In addition, the impact of the MR damper in brace Q2-Q3 has shown a negative effect on the other nodes, where the fatigue damages increase by 2% to 102%. This can be due to the increased share of vibrations by the other sides as side Q has been rigidified. In particular, joints S4 and Q2 are adjacent to side P at legs A and B, respectively. The vibration reduction at joint Q2, which leads to a damage reduction of 33%, contributes to an increase of vibratory motion at joint S4, which leads to an increase of fatigue damage of 102%. This negative effect requires a design strategy of multiple MR damper setups which conjointly impact at different joints.

#### Efficiency of four pairs MR dampers

With the purpose of reducing the negative effect caused by one double damper set in brace Q2-Q3, one pair of MR damper is inserted in one brace in each side. Two configurations are investigated.

1. **Configuration 'Boat':** pairs of MR dampers are ascending in one side and descending in the adjacent side. In other words, damper assemblages are alternatively put in place in a left-down-and right-up manner (ascending) in one side and in a left-up-and-right-down manner (descending) in the next side.
2. **Configuration 'Rain':** the pairs of MR dampers are consistently set either ascending or descending in all sides.

Figure 42 depicts the fatigue damage change for each node between the reference case and each MR damper setup case. In addition to the three aforementioned cases, the results for the case with a unique 200 kN MR damper mounted in brace Q2-Q3 are shown. Insignificant improvement is partially obtained in side Q but nowhere else. The double damper positively affects the whole side Q, but shows some negative effects on the other sides as said above. Configuration 'Boat' shows a consistent reduction of fatigue damage varying from 4% to 79% except at node Q4

and at node S4 where slight increases are observed. With Configuration 'Rain', a similar behaviour is observed: fatigue damage reduction is general except for the nodes P1 and S4. This shows that an appropriate distribution of the MR damper around the jacket can contribute to the mitigation of fatigue damage at every point of interest depending on the design objectives.

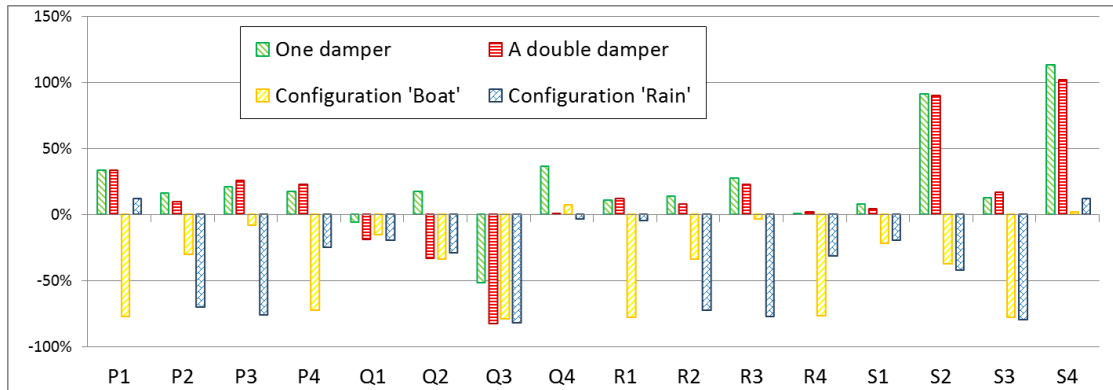


Figure 42: fatigue damage change for different MR damper setups and at different hotspots at the lower level of the jacket. Positive changes correspond to fatigue damage increases and negative changes to reductions

### Energy balance

The input energy as required for one year is computed in order to evaluate how beneficial the semi-active condition is. The electrical energy used in one year is obtained by:

$$W_{elec} = \frac{T_1}{T} \int_{V_{in}}^{V_{out}} \int_0^T U(t|V) I(t|V) p(V) dt dV \quad \text{Eq. 17}$$

where the voltage  $U(t|V) = L \dot{I}(t|V) + R I(t|V)$ ;  $L$  and  $R$  are the damper coil inductance and resistance, respectively [5-22]. As the current  $I(t|V)$  is set to the constant value  $I_{max} = 2.0 A$  the electrical power expression reduces to  $W_{elec} = \vartheta T_1 R I_{max}^2$ , where  $\vartheta$  is the proportion of operational duration in one year.  $T_1$  is the number of seconds in one year,  $T = 600 s$  is the simulation duration, and  $p(V)$  the probability of occurrence of the wind speed  $V$ . This gives a total electrical power of 2.46 GJ per active damper per year, i.e. about 77.95 W.

Similarly, the mechanical work of the damper force in one year can be computed as

$$W_{mech} = \frac{T_1}{T} \int_{V_{in}}^{V_{out}} \int_0^T |F(t|V)| |\dot{x}(t|V)| p(V) dt dV \quad \text{Eq. 18}$$

where  $F(t|V)$  is the damper force at each instant for the wind speed  $V$  and  $\dot{x}(t|V)$  is the piston tip velocity for the wind speed  $V$ .

Table 15 presents various energies for the cases of unique pair MR dampers and four pairs of dampers in each configuration. The proportion of dissipated energy calculated as the relative difference between the electrical energy (input) and the mechanical work can serve as a measure of the efficiency of MR damper setups.

Table 15: Energy balance for the different cases for one year

	A double damper	Configuration 'Boat'	Configuration 'Rain'
Electrical energy [GJ]	4.92	19.68	19.68
Mechanical energy [GJ]	1.05	4.13	4.10
Dissipated energy [GJ]	3.87	15.55	15.58
Dissipated energy [%]	78.66	79.01	79.17

### 5.2.5 Conclusion and impact of innovations for 20 MW turbines

The present study proposes magneto-rheological dampers as a means of fatigue load mitigation on a jacket for a 20 MW wind turbine. The proposed solution addresses some of the problems encountered with passive tuned vibration absorbers (TVAs) and passive tuned mass dampers (TMDs) for the DTU 10 MW reference wind turbine namely (i) the width of the operational frequency range; (ii) the size of the device especially for larger structures; and (iii) the interaction between multiple devices.

The study reveals the potential of MR dampers to alleviate fatigue damage. Indeed, up to 77% of fatigue damage reduction at a critical joint can be obtained. The energy balance shows that about 78 W is needed for one damper, which opens the possibility to have multiple devices on the same jacket. By considering various configurations, results show the necessity of selecting appropriate configurations in order to maximize the benefits of the fatigue reduction strategy at specific links, without causing any increased damage at other sections.

Further studies may be required to propose a procedure of smart distribution of the devices around the jacket. The robustness of the system with respect to external actions and manufacturing tolerances may also be investigated, as well as the effect of the additional mass on the equipped brace. The MR damper used in this study is developed for civil engineering applications; it is encouraged to design dedicated MR devices for jacket. The latter may be of smaller diameter, longer, and of large nominal capacity. As the excitation actions in jacket are of small ranges (in the order of 1 - 2 mm for the displacement for example) the dedicated MR dampers for jacket application may be more sensitive.

### 5.3 References

- [5-01] Spencer, B. F., S. J. Dyke, M. K. Sain, and J.D. Carlson. "Phenomenological model for magnetorheological dampers." *Journal of engineering mechanics* 123, no. 3 (1997): 230-238
- [5-02] Caterino, Nicola. "Semi-active control of a wind turbine via magnetorheological dampers." *Journal of Sound and Vibration* 345 (2015): 1-17.
- [5-03] Murtagh, P. J., Ghosh, A., Basu, B. and Broderick, B. M. (2008), Passive control of wind turbine vibrations including blade/tower interaction and rotationally sampled turbulence. *Wind Energ.*, 11: 305–317. doi:10.1002/we.249
- [5-04] Lackner, Matthew A., and Mario A. Rotea. "Passive structural control of offshore wind turbines." *Wind energy* 14, no. 3 (2011): 373-388.
- [5-05] Colwell, Shane, and Biswajit Basu. "Tuned liquid column dampers in offshore wind turbines for structural control." *Engineering Structures* 31, no. 2 (2009): 358-368.
- [5-06] H.R. Karimi, M. Zapateiro, N. Luo, Semiactive vibration control of offshore wind turbine towers with tuned liquid column dampers using H1 output feedback control, Proceedings of the IEEE International Conference on Control Applications, Yokohama, Japan, 2010.
- [5-07] Rodriguez, A., C. Carcangiu, I. Pineda, T. Fischer, B. Kuhnle, M. Scheu, and M. Martin. "Wind turbine structural damping control for tower load reduction." In *International Modal Analysis Conference (IMAC)*. Jacksonville, FL: Society for Experimental Mechanics. 2011.
- [5-08] Shirzadeh R., Kühn M., Application of two passive strategies on the load mitigation of large offshore wind turbines, Wind Europe Summit 2016, September 27-29, Hamburg, Germany
- [5-09] J. Chen, C. T. Georgakis, Tuned rolling-ball dampers for vibration control in wind turbines, *Journal of Sound and Vibration* 332 (2013) 5271–5282.
- [5-10] Li WH, Yao GZ, Chen G, Yeo SH, Yap FF. Testing and steady state modelling of a linear MR damper under sinusoidal loading. *J Smart Mater Struct* 2000;9(1):95–102.
- [5-11] INN WIND Deliverable D4.1.3 – Innovations on component level (final report), 2016.
- [5-12] INN WIND Deliverable D.1.25 (a) - 20 MW Reference Wind Turbine Aeroelastic data of the onshore version
- [5-13] UpWind.EU, Design basis – Upwind K13 deep water site, 2010
- [5-14] INN WIND Deliverable D4.1.3 – Innovations on component level (final report), 2016.
- [5-15] IEC 61400-1, Wind turbines Part 1: Design requirements, Edition 3, 2005
- [5-16] Von Borstel T. INN WIND.EU Deliverable 4.3.1 – Design report – Reference jacket, 2013
- [5-17] IEC 61400-3, Wind turbines Part 3: Design requirements for offshore wind turbines, 2009
- [5-18] Larsen, T.J., Hansen A.M.: How 2 HAWC2, the user's manual. DTU Risoe, 2014.
- [5-19] Chaviaropoulos P. and Milidis A. INN WIND.EU Deliverable 1.2.5(a) - 20 MW Reference Wind Turbine - Aeroelastic data of the onshore version, 2016. [https://share.dtu.dk/sites/INN WIND\\_28450/The%20reference%20turbine/Forms/AllItems.aspx?RootFolder=%2Fsites%2FINN WIND%5F28450%2FThe%20reference%20turbine%2F20%20MW%20Reference%20Turbine&FolderCTID=0x0120008CB2037CE4C874448D27A4C972D11DAA&View=%7B1B96D924%2D6C31%2D414A%2D916F%2DB8C940E4274F%7D](https://share.dtu.dk/sites/INN WIND_28450/The%20reference%20turbine/Forms/AllItems.aspx?RootFolder=%2Fsites%2FINN WIND%5F28450%2FThe%20reference%20turbine%2F20%20MW%20Reference%20Turbine&FolderCTID=0x0120008CB2037CE4C874448D27A4C972D11DAA&View=%7B1B96D924%2D6C31%2D414A%2D916F%2DB8C940E4274F%7D).
- [5-20] Stolpe M, Njomo Wandji W, Natarajan A. "Modularized Jacket Design" in INN WIND.EU Deliverable 4.3.4 – Innovative design of a 10MW steel-type jacket, 2016. [https://share.dtu.dk/sites/INN WIND\\_28450/Work%20package%204/Task%204.3/D4.34%20-%20Innovative%20design%20of%20a%2010MW%20steel%20type%20jacket/DeliverableD434\\_Innovative%20Design%20of%20a%2010MW\\_steel%20jacket\\_Rev00.pdf?Web=1](https://share.dtu.dk/sites/INN WIND_28450/Work%20package%204/Task%204.3/D4.34%20-%20Innovative%20design%20of%20a%2010MW%20steel%20type%20jacket/DeliverableD434_Innovative%20Design%20of%20a%2010MW_steel%20jacket_Rev00.pdf?Web=1)
- [5-21] Kim Y, Langari R, Hurlebaus S. Semi active nonlinear control of a building with a magnetorheological damper system, *Mechanical Systems and Signal Processing* 23 (2009) 300–315.
- [5-22] Yang G, Spencer Jr. B F, Jung H-J, Carlson J D. Dynamic Modeling of Large-Scale Magnetorheological Damper Systems for Civil Engineering Applications, *Journal of Engineering Mechanics* 130:9 (2004) 1107–1114.

- [5-23] Wen Y K (1976). Method for random vibration of hysteretic systems, Journal of Engineering Mechanics. 102:2 (1976) 249–263
- [5-24] Liu Y, Gordaninejad F, Evrensel C A, Hitchcock G. An Experimental Study on Fuzzy Logic Vibration Control of a Bridge Using Fail-Safe Magneto-Rheological Fluid Dampers, Smart Structures and Materials 2001: Smart Systems for Bridges, Structures, and Highways 4330 (2001) 281-288.
- [5-25] Kang H-S, Kim M-H, Aramanadka S S B, Kang H-Y. Semi-Active Magneto-Rheological Damper to Reduce the Dynamic Response of Top-Tension Risers. International Society of Offshore and Polar Engineers (ISOPE) (2013) 837-844, Anchorage, Alaska, USA.
- [5-26] DNV-RP-C203, Fatigue Design of Offshore Steel Structures, 2011
- [5-27] Sorensen J D, Toft H S. Safety Factors. (Risoe: DTU Wind Energy – E – Report 0066(EN)), 2014

## 6 MANUFACTURING (RAW)

### 6.1 Introduction

The challenges regarding manufacturing and installation of a substructure supporting a 20MW offshore wind turbine (OWT) are studied in the following chapter. The transition from 10MW to 20MW turbines and their support structures is based on extrapolation of the primary dimensions and masses. A final design solution is not available in the current project phase, but for the purpose of concept evaluation and the identification of the bottlenecks it is assumed to be sufficiently accurate. In general it is believed that the manufacturing itself is technically feasible with technologies currently applied in the offshore and marine market, for instance when comparing jacket components (legs and braces) with large monopiles or structures designed in the oil and gas business. However, the overall size of the structure becomes challenging for transport and installation and the current vessel fleet for installing large structure is small and expensive. It contributes significantly to the overall costs of an offshore wind park and therefore special focus is given to the installation procedures.

### 6.2 Manufacturing

#### 6.2.1 Jacket assembly strategies and manufacturing costs

Optimization of the jacket with respect to manufacturing needs to consider the share of the four main manufacturing cost contributors – namely material, welding, coating and assembly costs as outlined in Figure 43. This methodology is believed independent of the size of the structure and the general layout. It only assumes that the fabrication facilities are able to process larger individual components and assemblies. Therefore it is assumed valid for the assessment of support structures for 20MW wind turbines. A jacket concept design for this turbine class is not available in the current project phase. A potential bottleneck can be the overall dimensions (i.e. width, height and mass) of the jacket structure, which is discussed in the next sections.

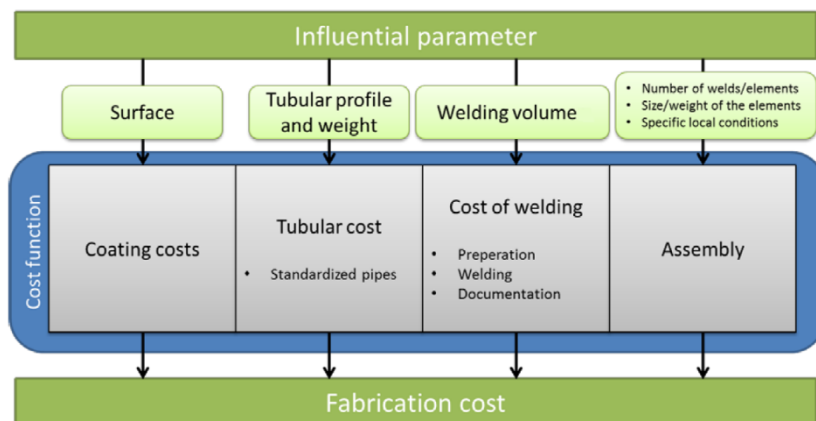


Figure 43: Manufacturing cost contributions

#### 6.2.2 Current jacket design

The current jacket design philosophy for wind turbines up to 10MW rated power in water depths up to 50m is based on pre-installed pile foundation using an installation template. The

jacket typically has three or four main legs with diameters between 1-2m. The transition piece connects the jacket legs with the tower and carries the external access platform. Braces are connecting the legs in order to stiffen the structure. A challenge for the fabrication process and the logistics at the harbour base is the overall height and width of the structure. Table 16 shows main parameters of the innovative INN WIND.EU jacket for the 10MW reference wind turbine [6-01] and the estimated dimensions of a 20MW jacket for the same site. The total height of the assembled jacket exceeds 80m for this reference site and can lead to additional costs for transport, installation and storage. The lifting mass is strongly increased, but still manageable when comparing with the mass of current substation structures, which have a topside mass above 2000t, or platforms in the oil and gas business.

The tubular members for legs and braces are available even for large jackets with diameters up to 2500mm (approximately 100 inch) and pipe lengths up to approximately 12m, e.g. the pipe production from EEW [6-03]. Considering the diameters of monopiles this might not be the technical limit, moreover it can become an economic limit for subsequent costs of transport and installation.

**Table 16: Estimated jacket dimensions for 20MW offshore wind turbines**

Parameter	Unit	Reference jacket for 10MW	Estimated jacket for 20MW
RNA mass <sup>1</sup>	[t]	676	1730
Interface level	[mLAT]		26
Water depth	[mLAT]		50
Width <sup>2</sup> at mudline	[m]	33	35-38
Width <sup>2</sup> at top	[m]	16	18-22
Total height <sup>3</sup> of assembled jacket	[m]	~82	~84-88
Lifting mass	[t]	900-1100	1500-2000

<sup>1</sup> according to INN WIND.EU reference wind turbine [6-02]

<sup>2</sup> with respect to centre of leg, neglecting appurtenances

<sup>3</sup> including leg extension below mudline

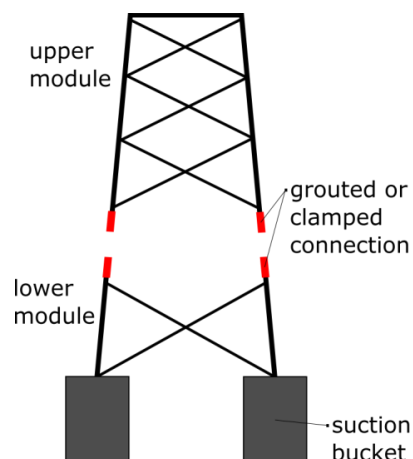


**Figure 44: Modular jacket design**

### 6.2.3 Modular jacket design

An alternative design concept is the combination of a modular jacket with a suction-bucket foundation. This concept includes two jacket modules: a lower module, which contains the suction-

buckets and the lowest x-brace level and an upper jacket module, which contains the upper brace sections and the transition piece. The modules will be connected offshore, for instance by a grouted or clamped connection. A graphical representation is given in Figure 44.

It is desirable to keep the number of offshore lifting operations as low as possible, which influences the installation costs significantly. The modular jacket with buckets requires two lifting operations and at the same time the height and mass of each module is lower compared to one single jacket structure. The requirement on vertical alignment has to be checked for both modules. Another drawback of this concept is the huge footprint of the lower module, which is determined by the width of the jacket and additionally the diameter of the suction buckets. The bucket size depends significantly on the soil conditions. It can be assumed that the bucket diameter is larger than 15m for a 20MW wind turbine, considering the current concept design for 10MW [6-04]. Hence, the overall width of the lower module easily exceeds 45x45m, which will become a logistical issue for fabrication and the transportation. Furthermore the connection of the modules requires a large unbraced length which is a very critical point for the design and results in high uncertainty of its feasibility. Due to these facts, the modular jacket concept is not considered any further currently.

### 6.3 Assumptions for Transportation and Installation

In this chapter, several assumptions regarding the environmental conditions and the jacket main dimensions are presented as well as an installation cost model.

#### 6.3.1 Dimensions of the Jacket

As indicated in the past chapter, a conventional jacket design has been chosen to support the 20MW offshore wind turbine.

The dimensions of the jacket mainly depend on the water depth and the turbine size. Taking WTGs from 4MW to 10MW in water depths between 34m and 49.5m into account, an extrapolation leads to an estimated mass of about 2300t for the 20MW WTG at a water depth of 50m. This mass includes the contribution from the transition piece and the piles. The weight of the piles can be deducted for the offshore lifting operation as they are assumed pre-installed. A more realistic value for the relevant mass amounts to 1500 – 2000t.

The total height of jacket is considered to be between 84-88m and is built up as following: 8m of transition piece, 18m free space above the waterline, 50m between LAT and mudline and about 6m of pile sleeves as shown in Figure 45. The footprint of the jacket is about 38 x 38m whereas the top area is about 24 x 24m. These figures are conservatively estimated and can be subjected to change.

#### 6.3.2 Environmental Conditions

The construction site for the 20MW OWT is located at a water depth of 50m. Therefore it is possible to make similar assumptions regarding the environmental aspects as for the deep water site of the UpWind project [6-06]. For this project the values of the K13-platform from the UpWind Design Basis form WP4 have been adopted for the further investigation. The data was collected between January 1979 and December 2000.

To transport and install jacket foundations specific types of vessels are required which can travel to the wind park location under certain maximum conditions. The limiting factors are wave height, wind speed and currents. Not only their magnitude and direction is decisive, also their interaction requires consideration.

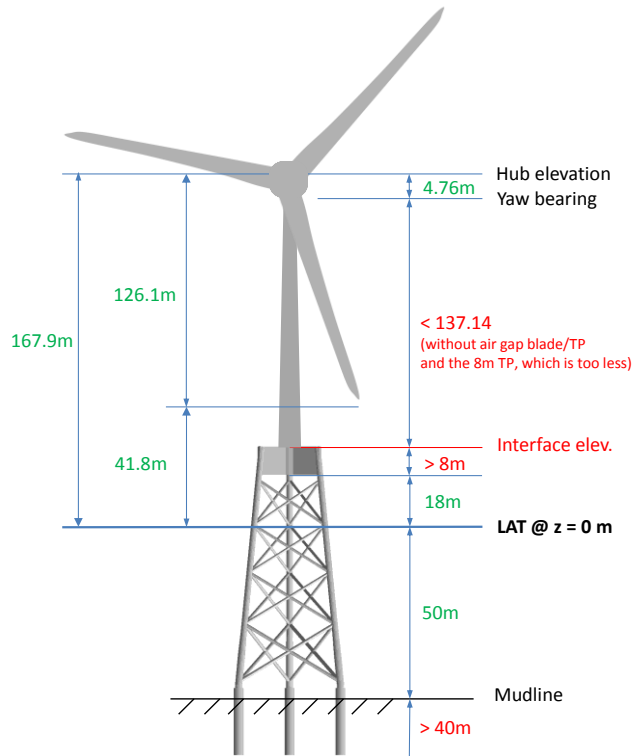


Figure 45: Estimated dimensions of the 20 MW jacket

all windspeeds		Tp [s]																	
		< 0,5	1	2	3	4	5	6	7	8	9	10	11	>11,5					
Hs [m]	9,5														0,00000				
	9														0,00000				
	8,5														0,00000				
	8														0,00000				
	7,5														0,00000				
	7												0,00003		0,00003				
	6,5											0,00002	0,00009	0,00005	0,00016				
	6											0,00019	0,00014	0,00005	0,00037				
	5,5										0,00008	0,00061	0,00033	0,00005	0,00106				
	5										0,00084	0,00138	0,00031	0,00006	0,00260				
	4,5										0,00011	0,00342	0,00132	0,00014	0,00002	0,00501			
	4										0,00003	0,00240	0,00663	0,00087	0,00019	0,00002	0,01013		
	3,5										0,00058	0,01269	0,00709	0,00078	0,00008	0,00002	0,02123		
3										0,00002	0,01058	0,02576	0,00478	0,00045	0,00003	0,00006	0,04167		
2,5										0,00098	0,05074	0,02189	0,00263	0,00050	0,00011	0,00002	0,07696		
2										0,00006	0,03047	0,07924	0,01285	0,00255	0,00028	0,00002	0,00000	0,12547	
1,5										0,00649	0,11598	0,06449	0,01419	0,00252	0,00014	0,00002	0,00003	0,20385	
1										0,00313	0,08888	0,12814	0,04869	0,00978	0,00143	0,00011	0,00003	0,00003	0,28022
0,5										0,00008	0,04740	0,10613	0,05166	0,01355	0,00241	0,00082	0,00017	0,00003	0,22225
<0,25										0,00224	0,00560	0,00120	0,00006					0,00910	0,00910
		0,00000	0,00000	0,00000	0,00008	0,05276	0,20716	0,32844	0,26795	0,10207	0,03279	0,00681	0,00151	0,00042	1,00000				

Figure 46: scatter diagram for all wave directions and all wind speeds [6-06]

Figure 46 shows the 2-D dimensional scatter diagram for all wind speeds and gives the average occurrence probability (in %) of different sea states. The peak spectral period ( $T_p$ ) and the significant wave height ( $H_s$ ) define the sea state and are derived from spectral analysis. Summation of the probabilities below a certain significant wave height allows an estimate of the possible working period for the transportation and installation process. Additionally the probability of a weather window with sufficient length (with a maximum sea state) to carry out the

transportation and installation process needs to be considered [6-09]. For this project the percentage of a suitable weather window is assumed to be 70%. Future cost models may be expanded with a more detailed calculation.

The total transport probability can be found by multiplication of the individual probabilities. The influence of wave direction, wind speed/direction and current speed/direction can be neglected for the transportation duration but needs to be considered during installation. The calculated delay time due to unsuitable weather conditions affects the costs of transportation and installation as the day-rate still applies.

### 6.3.3 Port and harbour requirements

According to [6-07], the following requirements to the wind farm base harbour apply:

The distance between the harbour and the wind farm should be limited as the substructures, the towers and RNAs, the equipment, etc. need to be transferred to the wind farm and in general it can be concluded that the shorter the way the smaller is the transportation cost.

The berth at quayside needs to have a sufficient water depth for the (in some cases) deep drafted installation vessels at any time of tide. Additionally, also the berth needs to be of sufficient length to reach the complete deck area by the harbour cranes.

Those cranes need to have sufficient loading capacity (mass and hook height) to shift the jackets on the vessel.

The storage and handling area is another critical factor of the harbour infrastructure.

The above list does not claim to be complete but shall indicate that the choice of the wind farm base harbour requires a thorough investigation and assessment of the infrastructure.

### 6.3.4 Installation cost model

The aim of the model is to reduce costs of the installation and transportation process. The main cost contributors for offshore 20MW jacket installation are vessel charter rate, transportation, installation and downtime costs. To minimize each of these cost items a variation of influencing parameter is needed to find the least expensive transportation and installation strategy. Figure 47 shows an overview of the cost model set-up. The following section will describe each of the cost items which are then used to estimate the installation costs per foundation.

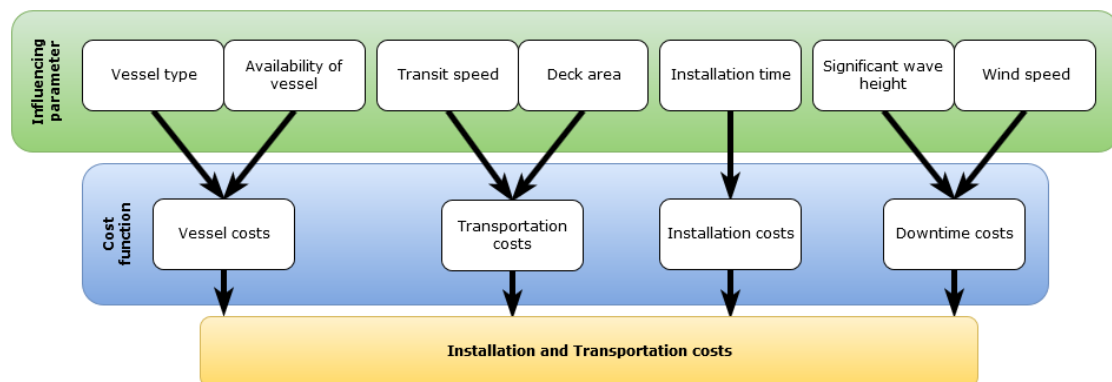


Figure 47: Structure of installation and transportation cost model

### 6.3.5 Vessel costs

The costs for vessel charters greatly depend on the type of vessel that is used for the transportation and installation process. Daily charter rates for vessels are determined using a complex function which includes many parameters. In general availability, dimensions of the vessel, crane capacity and hook height have the strongest influence. Estimates of charter rates for short time scenarios (charter periods of less than 1 year) on the spot market are very difficult to predict. However it is possible to define a price range that depends on seasonality. As harsh weather conditions restrict the installation and transportation process of jacket installation, it is expected that the demand is the lowest in winter months and hence the price at a minimum [6-08]. Possible vessel types are further discussed in Section 6.4.

#### Transportation costs

Transportation includes loading and sea fastening of the jacket as well as the transfer to the wind park and return back to the base harbour. Transfer costs depend primarily on transit speed of the vessel, distance to the wind park and the amount of jackets that can be transported simultaneously. Vessels that are not self-propelled must be accompanied by tugs and thus have a lower transit speed. Offshore and anchor handling tug costs are included in the transportation costs. Additionally some self-propelled vessel types might require tug assistance in the harbour area. The distance to the wind park can be minimized by selecting the nearest harbour as the base. However especially for 20MW jacket foundations the appropriate infrastructure and harbour equipment needs to be available, see also the section above. If the deck area of a vessel is able to accommodate more than one jacket structure, the transportation costs are greatly decreased as fewer transfers are required. Especially heavy lift vessels and jack-up vessels can be able to transport multiple jackets.

It is assumed that the wind park is located in the European North Sea and has a total of 50 wind turbines (1000MW total). The distance from the base harbour to the wind park location is defined to be 75 NM.

#### Installation costs

Installation includes the precise positioning of the vessel and the unfastening and positioning of jackets on pre-installed piles. For this cost model it is assumed that the piles are already installed and are not considered in the calculation. The costs for the installation of pre-installed piles are the same for every installation concept since it is usually carried out by a smaller and cheaper vessel. The total installation time that is needed for each jacket determines the costs for installation. Positioning of the vessel can be realized using a dynamic positioning system (DP) by using its own propellers and thrusters or a mooring system that is tug assisted. The unfastening and positioning of jackets on the seabed is barely dependent on the type of vessel.

#### Downtime costs

Downtime costs occur if the weather conditions do not allow safe operations at sea. The two influencing parameter are significant wave height and wind speed. In specific locations for example close to estuaries or in areas with large tidal influence, the current speed can also have a strong impact on downtime. Estimates of downtime can be made using wave-scatter diagrams

that show probabilities of wave occurrence depending on significant wave height, peak period and wind speed. A detailed explanation can be found in Section 6.3.2. Downtime costs are related to the vessel costs as the daily charter rate still applies during downtime.

## 6.4 Assessment of installation concepts

The installation concept describes the detailed procedure of jacket installations and is shown graphically in Figure 48. In general the installation procedure follows a similar path independent of the vessel type.

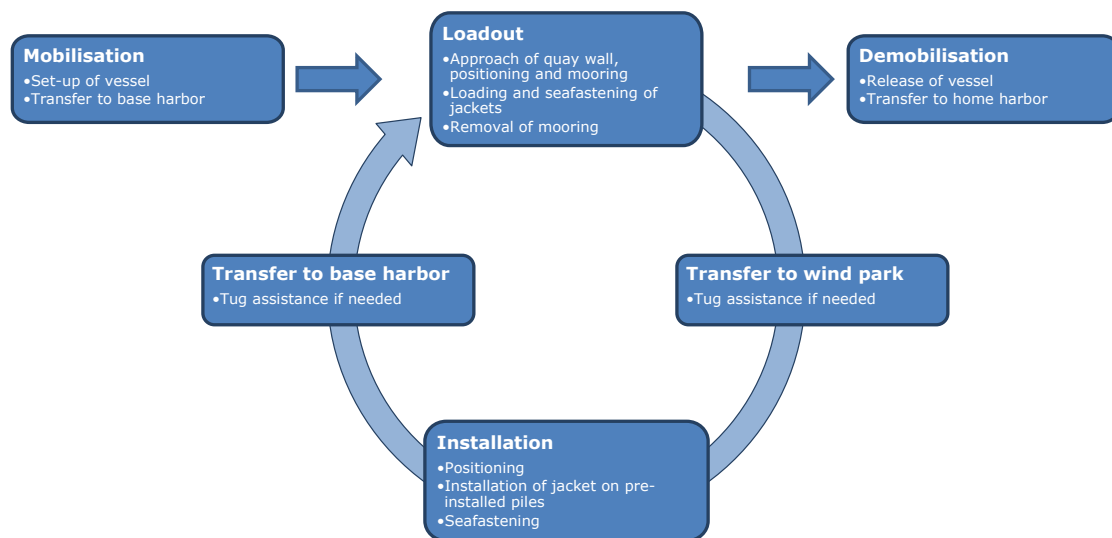


Figure 48: Overall concept of offshore installation

In a first step the vessel is being mobilized which includes the set-up, loading of consumables, installation of special grillages and sea fastening and loading of site specific equipment. Afterwards the vessel is transferred from its home harbour to the base harbour where the jacket foundations are stored during the installation period. The base harbour represents the starting point for the feeder and installation cycle.

The loadout process starts with the positioning of the vessel relative to the quay wall in order to take over the jacket structure. A stable position is achieved by mooring systems to ensure safe crane operations in the harbour area. The mooring system is released once the jacket has been securely loaded and sea fastened so that the vessel is ready to leave for the wind park location. Sailing out of the base harbour and transfer to the wind park might require tug assistance as some vessel types are not self-propelled or need harbour guidance.

The installation process is initiated by precise positioning at the installation location. Depending on the type of vessel a DP or mooring system is used. The jacket structure and installation equipment is unseafastened so that the crane can lower the jacket onto the pre-installed foundation piles. Tools and equipment are sea fastened and a change to a different installation location is performed depending on the amount of jackets left on the vessel. Once every loaded jacket is successfully installed the vessel heads for the base harbour to restart the loadout process.

The loadout and installation cycle is repeated until the desired amount of jackets in the wind park is installed. Finally the jacket is transferred back to its home harbour and a reverse mobilization process is carried out.

Below, four vessel types for possible installation of 20MW jacket foundations are introduced. Furthermore, the detailed installation procedure is listed and an estimation of the installation time is given. To conclude installation costs are estimated and a share of each cost contributor is shown.

### 6.4.1 Sheerleg crane

A floating sheerleg is a vessel equipped with a crane. The crane is not capable of rotating independently of its hull and needs to be maneuvered precisely to place loads. Positioning is usually done by a spread mooring system. Several anchor handling tugs are needed for positioning and movement of the sheerleg as they are usually not self-propelled.

The installation concept using a sheerleg is applied in several offshore wind parks, which have low significant wave heights, e.g. Wikingen OWF (40m water depth, 625t Jacket, ~60km offshore). A feeder system is used where onshore cranes lift jackets from the quay wall onto a barge. At the location the sheerleg (Taklift 4, Boskalis) hooks on the jacket from the barge and lowers it onto the pre-installed piles [6-010]. The maximum crane capacity at a height of 40m is 2200t and decreases to 1400t at the maximum height of about 75m [6-011]. This capacity is insufficient for 20 MW jackets as shown in Section 6.3.1. A list of possible floating sheerlegs with a crane capacity of 2000t at 75 m lifting height can be found in Appendix (Table 22).

Vessels like the Asian Hercules III shown in Figure 49 are used for heavy offshore lifting operations but are limited in maximum sea state.



Figure 49: Asian Hercules II + III - floating sheerlegs [6-012]

#### Transportation and installation procedure

The majority of suitable sheerlegs are situated in the Asian area where they are usually used as assistance in shipbuilding, loading and unloading large cargo and bridge building. The transfer

from Asia to northern Europe can take up to 3 month depending on the route. The sheerleg can be pulled by tugs but extreme weather conditions can prevent advancement. Another solution is to dismantle big parts of the sheerleg and move them by heavy-cargo vessel. Both solutions are associated with additional costs. Additionally the return transfer and demobilization also needs to be taken into account.

As sheerlegs are designed to operate in harbour areas with low wave impact, the sea fastening of jackets needs special consideration. To prevent swinging during transportation, cables are attached to the lower part of the jacket and tightened with tugger winches located on the hull.

The repeated feeder and installation cycle already addressed at the beginning of Section 6.4 is listed below in detail:

#### **Loading and sea fastening of jacket**

1. Sheerleg crane approaches quay wall with tug assistance
2. Positioning with mooring system in order to achieve stable position for loadout
3. Since the crane is not able to rotate the sheerleg needs to be positioned precisely
4. The crane boom is moved over the jacket and the hook is carefully attached to the transition piece of the jacket
5. Jacket is slowly lifted in upwards direction
6. Crane boom is pulled in the direction of the sheerleg
7. To prevent swinging of jacket, a wire is connected from the hull to the lower part of the jacket and is slightly tightened. The pull in force is applied by tugger winches or similar machines.
8. As a result the jacket is in a slightly tilted position with one degree of freedom (in the direction to the hull, extreme swinging could be a problem at significant wave heights close to 1.5m)

#### **Transfer from base harbour to wind park**

1. Mooring lines are collected
2. Tugs guide sheerleg out of base harbour
3. Transfer to the wind park with tug assistance (2-3 tugs) as sheerlegs are usually not self-propelled (transit speed on average 6-7 knots [6-014])

#### **Installation**

1. Positioning with X-point spread mooring system: first tug keeps sheerleg at a constant position, the remaining tugs load up anchor lines and position the anchors
2. Unseafastening of horizontal cable that kept the jacket tilted
3. Crane boom is brought into position and the jacket is lowered onto pre-installed piles
4. Crane hook is released with a hydraulic system
5. Sea fastening of additional equipment

#### **Transfer from wind park to base harbour**

1. Tugs collect anchor lines and anchors
2. Tugs guide sheerleg back into base harbour
3. Overall cycle is repeated

#### **Assumed maximum sea state**

- **Sheerleg:  $H_{s,max} = 1.0 - 1.5m$**
- **Percentage  $H_s < 1.0 m$ : 50.2%**
- **Percentage  $H_s < 1.5 m$ : 70.6%**

Sheerleg vessels do not possess an own propulsion system. The underwater hull shape in general is similar to the hull shape of pontoons with a shallow draft and a large water plane area.

Hence, a seaway excitation of sheerleg vessels usually leads to larger hull motions and accelerations than in case a heavy lift vessel is selected for installation. The values of the maximum survival significant wave height are best estimates based on experience and public data.

### Time consumption

Table 17 shows the activity times for two floating sheerlegs with a crane capacity of more than 2000t which are suitable to perform the offshore installation. The mobilization/demobilization time of both sheerlegs is similar as they are of the same vessel type. The Asian Hercules III is based in Singapore and hence the transfer to base harbour takes a great amount of time compared to the RAMBIZ 3000 which is based in Bruges (Belgium). The same principle applies to the return transfer. The Asian Hercules III performs a faster feeder cycle as the transit speed is slightly higher. The time for the installation cycle only differs in the type of mooring. Both feeder and installation cycle have to be repeated for every jacket as floating sheerlegs can only transport one jacket at a time.

**Table 17: Activity times for Asian Hercules III and RAMBIZ 3000**

Activity	Total time [hours]	
	Asian Hercules III	RAMBIZ 3000
Mobilization	280	280
Transfer to base harbour	1250	90
Feeder cycle	39	42
Installation cycle	28	26
Transfer to home harbour	1250	90
Demobilization	180	180

### 6.4.2 Heavy lift vessel

A crane ship is equipped with a crane for lifting heavy loads. Most vessels are conventional monohulls, but semi-submersibles have also been designed for high capacity cranes. The main advantage of semi-submersibles is the increased stability in severe sea states. The crane is able to rotate about its vertical axis and its capacity is usually dependent on the radius of operation. Via dynamic positioning (DP) the vessels are able to hold the position for the installation. Heavy lift vessels are often manufactured for the installation of pre-assembled modules for the offshore oil and gas industry. A typical operation is the installation of topside structures as seen in Figure 50.



**Figure 50: Oleg Strashnov - heavy lift vessel [6-013]**

## Transportation and installation procedure

Heavy lift vessels are in general not built for a fixed operation site. They are chartered for a project or rather a period of time that is expected for the certain project. In this case the heavy lift vessel might be outfitted with special grillages and sea fastening equipment at the base harbour. The demobilization is also executed at the base harbour.

The repeated feeder and installation cycle already addressed at the beginning of Section 6.4 is listed below in detail:

### Loading and sea fastening of two jackets

1. Heavy lift vessel approaches quay wall with tug assistance
2. Parallel positioning to quay wall with mooring lines
3. Crane on vessel rotates so that crane hook is above transition piece of jacket
4. Hook is attached and the jacket is slowly lifted upwards onto the deck area in upright position.
5. Sea fastening of jacket on deck. Due to the large height of the jacket, special applications for sea fastening might be required.
6. Crane hook is released and the second jacket is loaded

### Transfer from base harbour to wind park

1. Tug assistance needed for sailing out of harbour
2. Heavy lift vessels are self-propelled (transit speed on average 14 knots [6-014])

### Installation

1. DP at installation site
2. Unseafastening of jacket and equipment
3. Hook on jacket and lower onto pre-installed piles with rotational crane
4. Sea fastening of additional equipment
5. Move to next location and repeat installation cycle for additional jacket/s

### Transfer from wind park to base harbour

1. Tug assistance needed for sailing into harbour
2. Overall cycle is repeated

## Assumed maximum sea state

- **Heavy lift vessel:  $H_{s,max} = 1.5 - 2.0m$**
- **Percentage  $H_s < 1.5 m$ : 70.6%**
- **Percentage  $H_s < 2.0 m$ : 83.2%**

Heavy lift vessels usually can do the transfer to the installation site in more severe sea states than sheerlegs. A ship like underwater hull shape or even a semi-submersible type of vessel allow for a much better seaway performance of the vessel. The response motion and accelerations are significantly lower. Lower ship motion will lead to lower motion of the crane. Nevertheless, at the site, the installation process will also be dependent on the wind speed. The values of the maximum survival significant wave height are best estimates based on experience and public data.

### Time consumption

Heavy crane vessels feature fast transit speeds in combination with a deck area that in general allows two jackets to be transported simultaneously. Since the feeder cycle includes the load out of both jackets, the time period is longer compared to other installation concepts. However the cycle is only repeated half as often as the installation cycle. Table 18 shows typical activity times for the Oleg Strashnov (as shown in Figure 50).

**Table 18: Activity times for Oleg Strashnov**

Activity	Total time [hours]
Mobilization	280
Transfer to base harbour	290
Feeder cycle	39
Installation cycle	28
Transfer to home harbour	290
Demobilization	180

### 6.4.3 Jack-up vessel

A jack-up vessel is able to raise its hull by placing several legs on the seafloor. Usually they are self-propelled units using DP for positioning. The hull is lifted over the sea surface and provides a stable crane operation. Today, jack-ups are therefore commonly used in the offshore wind industry for the installation of wind turbine. The 2015 built jack-up vessel shown in Figure 51 is equipped with a crane capacity of 1500 tons at a height of approximately 105m. This is state of the art but not sufficient for lifting 20 MW jackets.[6-015]



**Figure 51: Seajacks Scylla – jack-up vessel [6-015]**

## Transportation and installation procedure

Jack-up vessels are already used for offshore foundation and WTG installation. They are chartered for a project or rather a period of time that is expected for the certain project. In this case the jack-up vessel might be outfitted with special grillages and sea fastening equipment at the base harbour. The demobilization is also executed at the base harbour.

The repeated feeder and installation cycle already addressed at the beginning of Section 6.4 is listed below in detail:

### Loading and sea fastening of two jackets

1. Jack-up approaches quay wall with tug assistance
2. Preloading to ensure stable position while crane operation takes place
3. Jack-up in order to operate the crane on vessel
4. Crane rotates so that crane hook is above transition piece of jacket
5. Hook is attached and the jacket is slowly lifted upwards onto the deck area in upright position
6. Sea fastening of jacket on deck
7. Crane hook is released and the second jacket is loaded (assuming that the deck area increases for jack-up vessels of the next generation)
8. Jack-down and recording of footprints from jack-up legs so that the preloading time for future loadouts can be reduced

### Transfer from base harbour to wind park

1. Tug assistance for sailing out of harbour if required
2. Jack-up vessels can be self-propelled (transit speed on average knots 9 [6-014]) or need tug assistance (jack-up barge, transit speed on average 5 knots [6-014])

### Installation

1. DP2 positioning at precise location
2. Preloading to prevent punch-through while operating the crane
3. Jack-up to about 20 m deck height above still water level to ensure that waves cannot hit the platform
4. Unseafastening of jacket and equipment
5. Hook on jacket and lower onto pre-installed piles with rotational crane
6. Sea fastening of additional equipment
7. Jack-down
8. Move to next location and repeat installation cycle for second jacket

### Transfer from wind park to base harbour

1. Tug assistance for sailing into harbour if required
2. Overall cycle is repeated

## Assumed maximum sea state

- **Jack-up:  $H_{s,max} = 1.5 - 2.0m$**
- **Percentage  $H_s < 1.5 m$ : 70.6%**
- **Percentage  $H_s < 2.0 m$ : 83.2%**

Former jack-up vessels were usually characterized by a barge ship hull which resulted in a large downtime. The shallow draught and the small molded depth lead to the fact that the jack-ups took green water on deck even in calm sea states. Vessels that have been built in the recent past and that will be built in the coming years are characterized by a ship like hull shape and a larger

draught. Hence, their response to seaway excitation is reduced. The values of the maximum survival significant wave height are best estimates based on experience and public data.

### Time consumption

The activity times for Jack-up vessels are similar to those of heavy lift vessels due to the fact that they will probably be able to load two jackets simultaneously. Feeder and installation cycles are both slightly longer because of the time-consuming jack-up process in the harbour and at installation locations. Table 19 shows estimated activity times for future jack-up vessels (3<sup>rd</sup>/4<sup>th</sup> generation).

**Table 19: Activity times for jack-up vessel 3<sup>rd</sup>/4<sup>th</sup> generation**

Activity	Total time [hours]
Mobilization	280
Transfer to base harbour	150
Feeder cycle	50
Installation cycle	33
Transfer to home harbour	150
Demobilization	180

### 6.4.4 U-barge

The U-barge is a preliminary design vessel especially developed for the purpose of transportation and installation of a specific jacket structure. It can be imagined as a simple barge fitted with an open moonpool. There is no special lifting equipment other than winches needed which lower the jacket onto the pre-installed piles. As the field of application is limited to installation of jacket structures the U-barge can only be used for this purpose. The u-barge is not self-propelled and needs tug assistance for transfer and positioning as the positioning at the location would be realized with a mooring system. Figure 52 shows the preliminary 3-D design whereas Figure 53 shows the front view with labelled components.

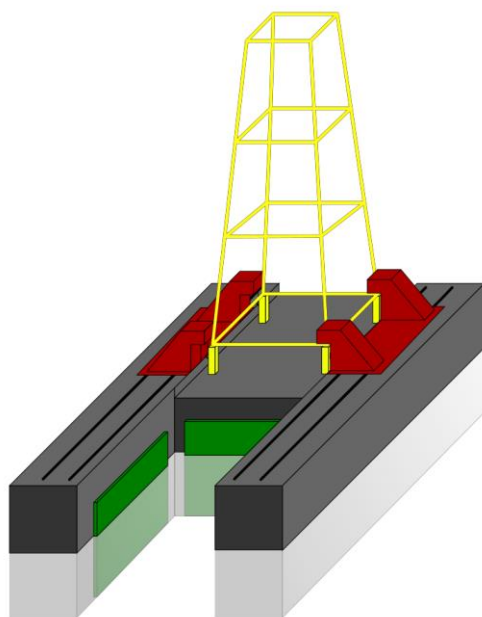


Figure 52: Conceptual design of a U-barge

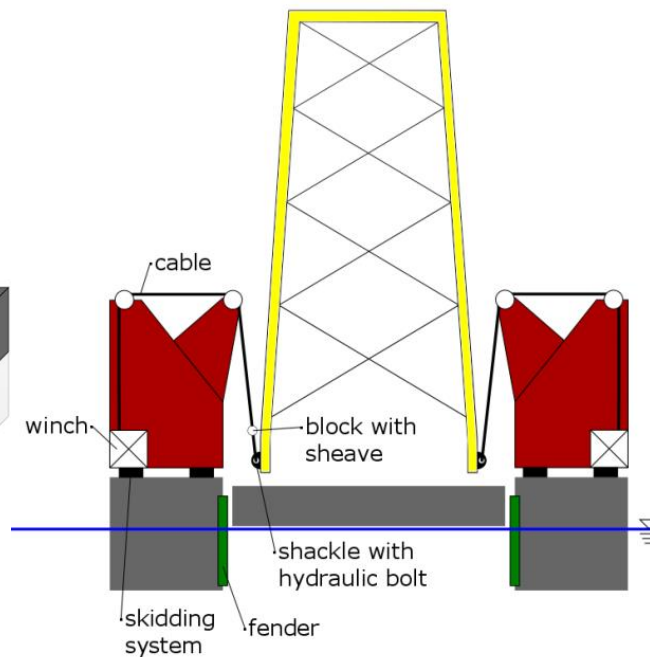


Figure 53: Labelled front view of a U-barge

### Transportation and installation procedure

The barge is preferably built at a construction site nearby the base harbour to reduce the transfer costs. After construction the barge needs to be equipped with a special purpose sea fastening system. An onsite crane with a capacity of at least 2000t at the base harbour is needed to lift the jackets onto the barge. It is possible that the barge will be decommissioned after the operation as there might not be a suitable future application.

The repeated feeder and installation cycle already addressed at the beginning of Section 6.4 is listed below in detail:

#### Loading and sea fastening of jacket

1. Mooring of the barge at the quay
2. Preparation of the deck
3. Lifting the jacket with an external crane onto the barge
4. Connecting the cable of the winch with the jacket
5. Sea fastening of jacket and all other equipment

#### Transfer from base harbour to wind park

1. Mooring is detached
2. Tugs guide barge out of base harbour to the wind park
3. Tug assistance (2-3 tugs) needed for entire duration as the barge will probably not be self-propelled (transit speed on average 6-7 knots [6-014])

#### Installation

1. Positioning with X-point mooring system: first tug keeps barge at a constant position, the remaining tugs load up anchor lines and position the anchors

2. Unseafastening of the jacket when barge is in the right position and the sea condition allows a safe operation
3. The jacket is slightly raised above the deck using the already connected winches
4. The winches are moving the jacket to the open part of the barge with the help of a hydraulic skidding system
5. While lowering the jacket fenders hold the jacket in position and prevent damage to the barge
6. When the jacket is located above the pre-installed piles the hooks of the winches are released with a hydraulic system
7. The cables are pulled upwards and all the additional equipment is sea fastened
8. Tugs collect the anchors and release the mooring system

During the complete installation process, it is essential that the floating position of the barge is monitored in real-time. The mass shift of the jacket needs to be absorbed by a ballasting plan to ensure that the jacket is lowered vertically.

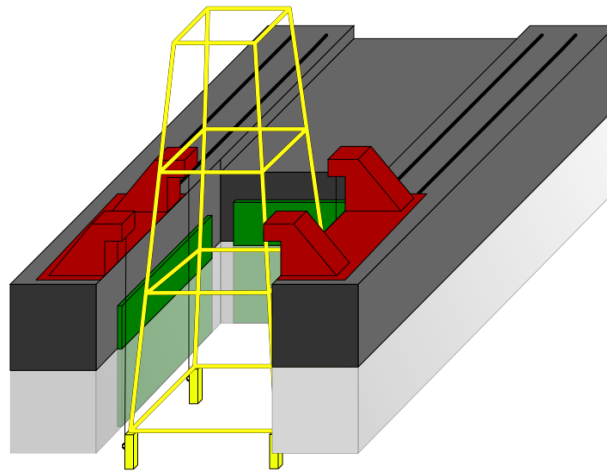


Figure 54: Installation process of the jacket by use of a U-barge

#### Transfer from wind park to base harbour

1. Tug assistance for sailing into harbour
2. The barge is fastened at the quay
3. Overall cycle is repeated

#### Assumed maximum sea state

- *U-barge:  $H_{s,max} = 1.0 - 1.5m$*
- *Percentage  $H_s < 1.0 m$ : 50.2%*
- *Percentage  $H_s < 1.5 m$ : 70.6%*

For a U-barge type installation vessel, the seaway behavior is assumed to be similar to a sheerleg vessel. Reference is made to Section 0.

## Time consumption

The activity times for U-barges are similar compared to sheerleg activity times. Transportation and mooring both need tug assistance and one jacket is transported at a time. Table 20 shows the estimated activity times for a preliminary U-barge design.

**Table 20: Activity times for preliminary u-barge design**

Activity	Total time [hours]
Mobilization	280
Transfer to base harbour	205
Feeder cycle	44
Installation cycle	26
Transfer to home harbour	205
Demobilization	180

### 6.4.5 Additional concepts

Regarding additional concepts, the following statements can be made:

#### Modular Jackets

- less crane capacity needed
- smaller requirements regarding the installation vessel
- easier manufacturing and onshore handling
- additional operations needed because jacket consists of at least two parts; economically not feasible
- grouted or clamped connection of parts might be difficult in water
- dimensions of 20MW jackets can still be transported as single piece
- suction buckets possible; deck area critical
- larger footprint due to suction bucket technology

#### Jacket-launching

- offshore-wind jackets not suitable for launching operation due to loads that occur while launching; material strength needs to be increased, higher material/production costs
- in general horizontal transport undesirable, jacket is not designed for horizontal storage (inclined legs)
- jackets might not be self-upending, flooding and ballast tanks are too complex and expensive

#### Floating Jacket/wet towed

- complex operation, buoyancy might not be sufficient for jacket to float
- changes to jacket design must be made in order to flood certain connections for installation
- water depth of harbour needs to be sufficient depending on the height and draught of jacket
- determination of additional transportation fatigue damage (direct exposure to seaway instead of indirect when being transported on a vessel)
- jacket is not designed for horizontal transport (other loading scenario of elements and joints); additional calculations and verifications required

## 6.5 Analysis of time consumption and installation costs

### 6.5.1 Analysis of time consumption

The total time consumption for installation and transportation can be divided by the amount of jackets in the wind park to determine a normalized parameter that allows comparison of the different installation concepts. For the analysis carried out, a wind farm of 50 turbines is taken as basis. The normalized time is shown in Figure 55 for the different vessel types presented in Section 6.4.

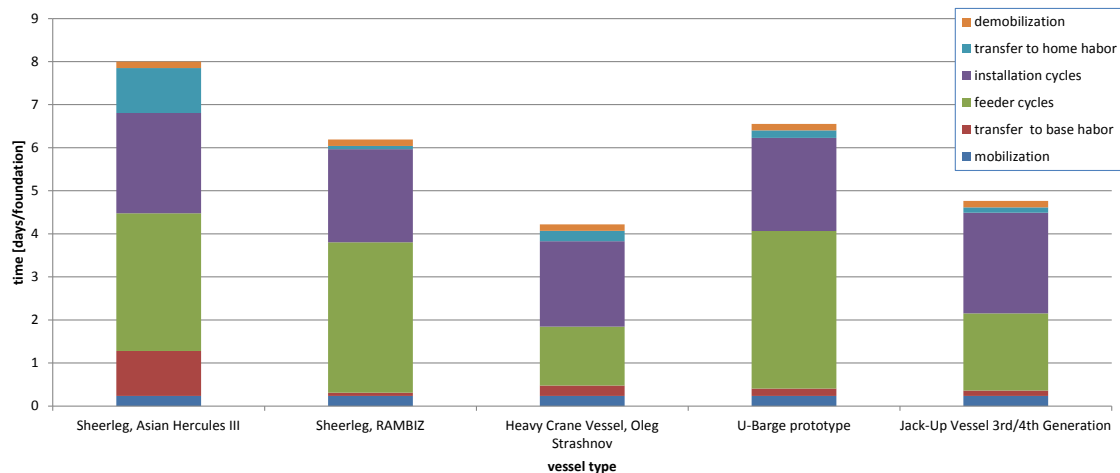


Figure 55: Installation times per foundation for different vessel types

Installation times per foundation vary between four and eight days. In general vessel types that can carry two jacket foundations need less time per foundation. Sheerlegs and the U-barge prototype represent the upper end.

The specific time shares for transfer, feeder cycle and installation cycle depend on the vessel type. Jack-up vessels and heavy crane vessels need less time for the feeder cycle as they transport two jackets simultaneously and hence the total distance travelled is half as much compared to sheerlegs and U-barges. The time for installation cycles is of similar magnitude for all vessel types as DP, spread mooring and the jack-up process are complex systems that require careful planning and execution. Additionally the duration of offshore lifting operations is comparable as the jacket needs to be slowly lowered to the ground in every case.

Mobilization and demobilization times include the set up and release of a vessel and are set to be equal for each installation method as similar consumables and equipment is loaded. It can be seen that the overall influence of mobilization and demobilization on the total time is negligible and will be even further reduced if the amount of WTG in the wind park increases.

The same applies to the transfer to and from the base harbour. As the vessels are situated in Europe the distance to the base harbour will be roughly of equal length. Exceptions are sheerlegs that are transferred to Europe for specific installation purposes. This process is only economically feasible because sheerlegs in Asia are readily available for low daily rates. With the wind park described in 6.3.5 (50 WTG) the transfer time takes up a remarkable share as seen in Figure 55, Asian Hercules III. With increased WTG in the wind park the share of the transfer time decreases which also reduces the total time per foundation. Hence continental transfers must be evaluated for every specific offshore operation and are favoured in larger projects.

## 6.5.2 Analysis of installation costs

The installation cost model described in Section 6.3.4 delivers the cost ranges per foundation for each installation concept. Figure 56 shows the results with minimum and maximum values and includes a line that represents median installation costs of 10 MW jackets for comparison. It is assumed that the 10 MW jackets are installed using a jack-up vessel (2<sup>nd</sup> Generation) and that two jackets can be transported simultaneously.

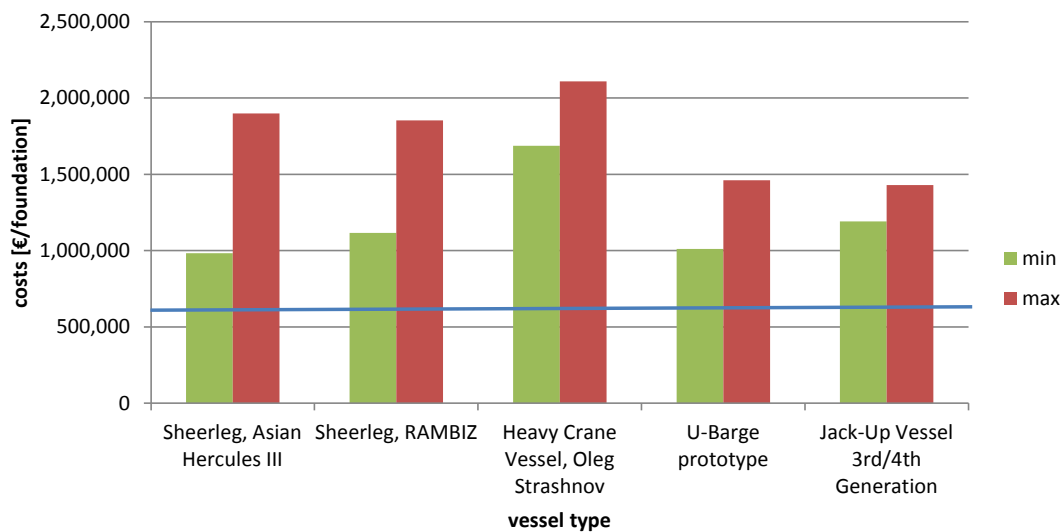


Figure 56: Costs per foundation for different vessel types

Heavy crane vessels and sheerlegs represent the highest installation costs per foundation. Heavy lift vessels, e.g. Oleg Strashnov, have a high occupancy rate which raises the charter rate. Even though the installation time per foundation is the lowest, the high costs per foundation can be explained with charter rates. The assumed maximum sea state for heavy crane vessels results in very low downtime costs.

Sheerlegs can be chartered for lower rates, especially those located in Asia. However the installation and feeder cycle require more time so that the costs per foundation are nearly equal to heavy lift vessels. Additionally the assumed maximum sea state for sheerlegs is lower which increases downtime costs. Tug costs for transport and installation are small compared to the vessel costs but also need to be considered.

Figure 57 shows the median costs per foundation for sheerlegs with home harbour in Asia in accordance to the number of WTGs in the project wind park. The median cost per foundation exponentially decreases with the number of WTG due to the lower impact of mobilization, transfer and demobilization. A break-even point can be calculated at which the costs for sheerlegs located in Asia and in Europe are identical for the same number of WTG. Consequently it can be concluded that it can be economically feasible to charter sheerlegs from Asia for larger offshore projects or multiple projects.

Jack-up vessels (3<sup>rd</sup>/4<sup>th</sup> generation) and the U-barge prototype represent the lowest installation costs. However both vessel types are not yet fully developed and the results should be interpreted with caution. Jack-up vessels are frequently used for offshore foundation and WTG installation due to their fairly low charter rate and their satisfying behavior in a seaway. The new generation must include increased crane capacities and larger deck areas to support 20 MW jackets. These properties will make them more expensive compared to present jack-up vessels. Since a shortage

of those vessels can be expected once they become available, the charter rate could increase temporarily.

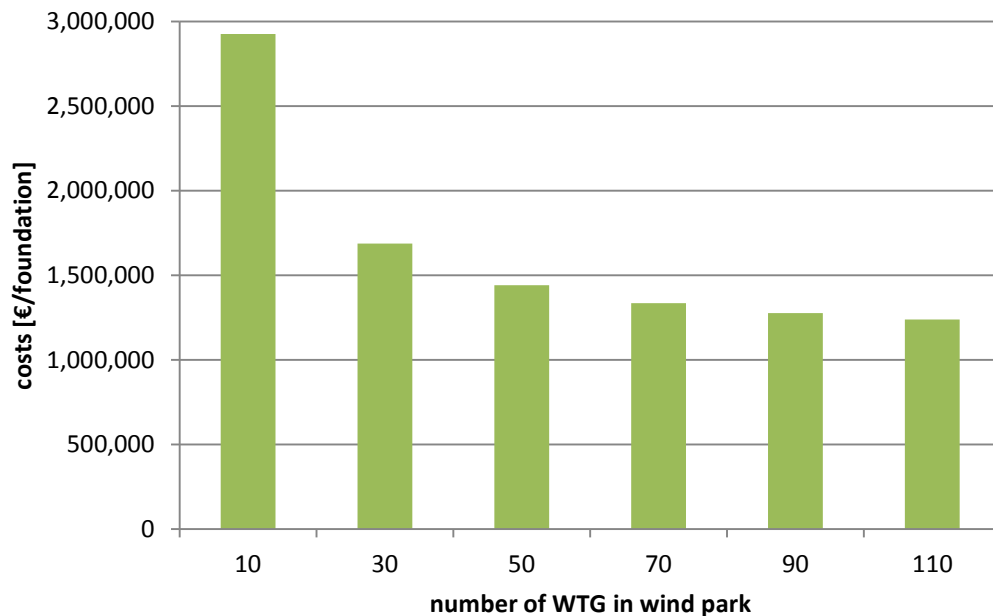


Figure 57: Median costs per foundation for sheerlegs located in Asia against number of WTG in wind park

Daily charter rates for the U-barge prototype are difficult to estimate due to development and construction. They can only be economically feasible if they are able to achieve lower installation costs than sheerlegs as they can probably not be used for multi-purpose lowering. Tug and downtime costs correlate with those of sheerlegs. An additional fee for the use of harbour cranes might apply as the U-barge cannot lift jackets on its own.

## 6.6 Evaluation and conclusion

### 6.6.1 Evaluation matrix

This section shows the different characteristics of the installation concepts suggested in section 6.4 and evaluates them with respect to each other. The aspects in Table 21 are labelled with: + for positive, 0 for neutral and - for negative.

From the evaluation matrix it can be seen that heavy lift vessels and jack-up vessels score the most positive rating. They feature fast installation times combined with enough deck area and can operate at more severe sea states. Heavy lift vessels are generally more expensive but achieve faster installation times in return.

Sheerlegs and U-barges are possible alternatives for the installation of 20MW jackets that feature great availability and simple offshore lowering operation. Time needed and installation costs are relatively high due to limited deck area and comparable low transit speeds.

**Table 21: Evaluation matrix for installation concepts, +: positive, 0: neutral, -: negative**

	Sheerleg	Heavy lift vessel	Jack-up vessel	U-barge
Costs per foundation	-	-	+	0
Time per foundation	-	+	0	-
Availability of vessel	+	-	-	+
Harbour requirements	+	+	0	-
Transit speed of vessel	-	+	0	-
Deck area (amount of jackets)	-	+	+	-
Maximum sea state	-	+	+	-
Positioning at location	-	+	0	-
Difficulty of offshore lowering operation	+	0	+	+

### 6.6.2 Conclusion

Installation and transportation costs are mainly composed of vessel type, deck capacity, installation time and maximum allowed sea state. The objective of this contribution is to detect the share of each of these cost parameters by setting up a cost model which allows finding the most cost effective solution.

From the findings gathered, 3<sup>rd</sup> and 4<sup>th</sup> generation jack-up vessels propose the most cost effective solution for installation of 20MW jackets. Vessels of this type are not available currently, so that the calculations must be regarded as provisional for now. The dimension of the jacket should be considered while finalizing the new jack-up generation, especially deck area, crane capacity and operational water depth are limiting factors for offshore installation.

Heavy crane vessels are equally suitable for the installation of 20 MW jackets and are readily available at present. Since there is a lack of availability, installation costs are higher and charter time management is even more important. Crew members are well trained for heavy offshore lifting operations as these vessels already operate for a significant time period and are able to install even heavier structures.

Sheerleg cranes and the U-barge can be regarded as suitable options for installation locations with low sea states. Their pontoon hull shape leads to larger hull motions and accelerations in heavy waves which complicate offshore operations. The U-barge can propose a worthy alternative to jack-up vessels as the design focus lies completely on installing jacket foundations. However, cost estimations for the preliminary design are difficult to predict and further investigation should be initiated when a more detailed support structure design is available.

## 6.7 References

- [6-01] INNWIND.EU project deliverable D4.34, Innovative Design of a 10MW Steel-Type Jacket, 17.06.2017
- [6-02] INNWIND.EU 10MW Reference Turbine Data Sheet. excel-sheet, version 1.04, Revision 17, 15.01.2016.
- [6-03] Homepage, Erndtebrücker Eisenwerk GmbH & Co. KG, website access 05.09.2016: <http://www.eew.de/products-services/fabrication-programme>
- [6-04] INNWIND.EU project deliverable D4.32, Innovative Concepts for Bottom-Mounted Structures, 31.07.2016, Revision 03
- [6-05] DNV-OS-J101 – Design of Offshore Wind Turbine Structures. Det Norske Veritas, May 2014.
- [6-06] Fischer, T., de Vries, W. and Schmidt, B., UpWind Design Basis, 2010
- [6-07] Carter, M., Port requirements offshore wind farm: construction and operations, 2012
- [6-08] Dalgic, Y., Lazakis, I. and Turan, O., Vessel charter rate estimation for offshore wind O&M activities, 2014
- [6-09] Herman, S., Offshore Wind Farms – Analysis of Transport and Installation Costs, 2002
- [6-010] Homepage, First Foundations Installed at Wiking OWF, website access 15.07.2016: <http://www.offshorewind.biz/2016/04/28/first-foundations-installed-at-wiking-owf/>
- [6-011] Homepage, Royal Boskalis Westminster N.V., Equipment sheet TAKLIFT 4, website access 28.07.2016: <http://boskalis.com/about-us/fleet-and-equipment/offshore-vessels/floating-sheerlegs.html>
- [6-012] Homepage, Asian Lift, Vessel specifications: Asian Hercules III, website access 20.07.2016: [http://www.asianlift.com.sg/downloads/AH%20III%20Brochure\\_updated%20April%202015.pdf](http://www.asianlift.com.sg/downloads/AH%20III%20Brochure_updated%20April%202015.pdf)
- [6-013] Homepage, Seaway Heavy Lifting, Vessel sheet: Oleg Strashnov, website access 15.07.2016: <https://www.seawayheavylifting.com.cy/vessels/oleg-strashnov>
- [6-014] OPL, Construction Vessels of the World, 7th edition, 2004
- [6-015] Homepage, Seajacks, Technical Specification: Seajacks Scylla, website access 20.07.2016: <http://www.seajacks.com/self-propelled-jack-up-vessels/seajacks-scylla/>
- [6-016] 0035/ND – Guidelines for Offshore Wind Farm Infrastructure Installation. GL Noble Denton, June 2016.

## APPENDIX A

Table 22: List of possible Crane Ships (capacity: 2000t, crane height: 84m, deck area: >1500m<sup>2</sup>) [6-014]

Vessel / Company	Flag	Crane capacity, revolving [t]	Speed [kn]	Type
Saipem 3000 / Saipem	Bahamas	2177	8	Monohull
DB 30 / J. Ray McDermott	Malaysia	2223	6	Monohull
Lan Jiang / CNOOC	China	2500	5	Monohull
Sapura 3000 / SapuraAcergy	Malaysia	2722	9	Monohull
LTS 3000 / L&T-SapuraCrest JV	India	2722	10	Monohull
DB 50 / J. Ray McDermott	Panama	3200	5	Monohull
Lan Jing / CNOOC	Hong Kong	4000	5	Monohull
Oleg Strashnov / Seaways Heavy Lifting	Cyprus	5000	9	Monohull
Balder / Heerema Marine Contractors	Panama	5000	5	Semi-submersible
Hermod / Heerema Marine Contractors	Panama	7200	6	Semi-submersible
Saipem 7000 / Saipem	Bahamas	14000	6	Semi-submersible
Thialf / Heerema Marine Contractors	Netherlands	14200	5	Semi-submersible

Table 23: List of possible floating sheerlegs (capacity: 2000t, height: ~75m) [6-014]

Vessel / Company	Flag	Capacity [t]	Crane height [m]	Speed [kn]
Kongo / Fukada Salvage & Marine Works	Japan	2050	80	
Suruga / Fukada Salvage & Marine Works	Japan	2200	97	
Rambiz / Scaldis	Belgium	2500	74	5
Fuji / Fukada Salvage & Marine Works	Japan	3000	133	
Asian Hercules II / Asian Lift	Singapore	3200	75	5
HL 5000 / Deep Offshore Technology	Iran	4500	76	
Asian Hercules III / Asian Lift	Singapore	5000	80	7
Svanen / Van Oord	Bahamas	8200	76	7